Modeling, Design, and Testing of a Microchannel Split-System Air Conditioner

A. C. Kirkwood and C. W. Bullard

ACRC TR-149 March 1999

Abstract

THE MODELING, DESIGN, AND TESTING OF A MICROCHANNEL
SPLIT-SYSTEM AIR CONDITIONER

Allen Chad Kirkwood, MS
Department of Mechanical and Industrial Engineering
University of Illinois at Urbana-Champaign, 1999
C.W. Bullard, Advisor

A steady-state microchannel split-system simulation model has been developed based on previous research at the ACRC. This model was utilized as a design tool to optimize a microchannel split system with the goal of minimizing TEWI, or total equivalent warming impact. The system components were then selected and the optimized microchannel heat exchangers were fabricated. Next, the entire system was assembled and extensive tests were run at steady state conditions over a wide range of outdoor ambient conditions in a calorimeter test facility. The experimental results have been compared to the simulations for the purpose of model refinement and its eventual validation. The full system model overpredicts the total capacity of the system with a minimum error of 0.2%, a mean error of 5%, and a maximum error of 11%. The evaporator submodel overpredicts the total capacity as well, with a minimum error of 0.7%, a mean error of 7%, and a maximum error of 11%. The condenser submodel also overpredicts with a minimum error of 0.5%, a mean error of 2%, and a maximum error of 6%. A major reason for the lower accuracy with the evaporator is because of the refrigerant maldisribution observed in the experiments. The model assumes perfect distribution, hence one reason for the overprediction of the system's capacity.

Table of contents

Chapter	Page

List of figures

List of tables

Nomenclature

a	length of top of trapezoidal port	ft
A	area	ft^2, in^2
b	tube thickness	ft
$\frac{b}{a}$	rectangular port height/port base	-
C_d	discharge coefficient	-
CF	ratio of the total air-side surface area to the total refrigerant-side area	-
D	diameter	ft, in
DeffRat	effective diameter ratio	D_{eff}/D_h
E	velocity of approach factor	-
f	friction factor	-
F_a	thermal expansion coefficient	-
Finth	fin thickness	ft
FinDns	fin density	fins/ft
h	heat transfer coefficient or trapezoidal port height	Btu/hr-ft^2-F or ft
H	horizontal tube distance	ft
Hfin	fin height	ft
Hlouv	vertical height of the louver	ft
j	Colburn j-factor dimensionless air-side heat transfer coefficient	-
k	specific heat ratio	-
K	thermal conductivity	Btu/hr-F-ft
kshape	shape factor for equivalent diameter	D_{eq}/D_h
Lweb	length of microchannel port's web	ft
Nports	number of microchannel tube's ports	#
Ntubes	number of tubes in microchannel heat exchanger	#
Nul	laminar Nusselt number	-

Nut	turbulent Nusselt number	-
Nutot	total Nusselt number	-
p, P	absolute pressure	psia
Δp, dP	heat exchanger or venturi pressure drop	psid
Pr	Prandtl number	-
Pwrfan	fan power	W
R	resistance	hr-ft^2-F/ Btu
Re	Reynolds number	$\dfrac{4w}{\pi\mu D}$
R_p	venturi pressure ratio, p_t/p_i	-
S	surface area	ft^2
S_{atp}	air-side surface density	ft^2/ft^3
S_{rtp}	Refrigerant-side surface density	ft^2/ft^3
t or T	temperature	°F
Tubelen	header to header tube length	ft
twall	microchannel tube wall thickness	ft
tweb	microchannel port web thickness	ft
U	conductance	Btu /hr-ft^2-F
V	vertical tube distance	ft
Vdota	air-side volumetric flow rate	cfm
VolExt	external volume of microchannel heat exchanger	ft^3
Wlouv	louver width	ft
Y	adiabatic gas expansion factor	-

Greek Symbols

α	thermal expansion coefficient	1/°F
β	venturi beta ratio, D_t/D_i	-
ϕ	angle used in calculating Dcircs for trapezoidal port	rads
η	efficiency	-
μ	absolute viscosity	lbm/(hr-ft)
θ	angle	deg.
ρ	venturi inlet density	lbm/in^3
σ	air-side free flow area ratio	A_{airff}/A_{front}

Subscripts and Modifiers

air	air-side
airCabinet	air-side cabinet
airCoil	air-side coil
airff	free-flow air-side
brass	brass
circs	circumscribed
C, cond	condenser
cu	copper
disc	discharge-line venturi
eff	effective
eq	equivalent
E, evap	evaporator
fan	fan

fin	fin	
front	front	
h	hydraulic	
hair	air-side hydraulic diameter	
i	inlet	
insc	inscribed	
l_p	louver pitch	
louv	fin louver	
r, ref	refrigerant-side	
sub	subcooling	
sup	superheat	
2ph	two-phase	
t	throat	
tube, t	tube	
web	web	
wlouv	louver width	

Constants

g_c	gravitational constant	32.2 lbm-ft/(lbf-s^2)
π	pi	3.14159 rad

Chapter 1

Introduction

Because of environmental and efficiency concerns, the air-conditioning industry has been forced to look for alternatives to long-standing operating fluids such as CFC's and HCFC's and examine new technologies that will allow air conditioners, using the next generation of refrigerants, to be more efficient in their energy consumption than their predecessors. This new focus in the industry has driven the development of new tools that will aid in the rapid investigation of alternative refrigerants and new technology. The Air Conditioning and Refrigeration Center (ACRC) has spent the last several years in the development of the Room Air Conditioner Model (RACMOD). Considerable effort has been expended to validate this model, and this thesis outlines one of the first applications where a form of RACMOD has been used as a tool for designing a conceptually new system that employs microchannel heat exchangers and a near azeotropic mixture of HFC refrigerants.

1.1 Background

The first iteration of RACMOD was developed by Hahn and Bullard (1993) and had its foundations based on the Oak Ridge National Laboratory (ORNL) heat pump model (Fischer and Rice, 1983) with the appropriate modifications to the equations to account for the different configurations of room air conditioners (O'Neal and Penson, 1988). The ACRC equation solver was developed so that the more flexible Newton-Raphson method for solving equations could be implemented rather than the original ORNL method using successive substitution (Bridges and Bullard, 1995). Improved refrigerant-side two-phase heat transfer coefficients developed at the ACRC (Wattlet *et al.*, 1994; Dobson and Chato, 1998) were also added to the almost 100 governing equations developed by ORNL

Mullen and Bullard (1994) developed the second version of RACMOD which consisted mainly of improving the governing equations, adding charge inventory calculations, and two-phase pressure drop correlations developed by Sousa and Pimenta (1995). Other modifications

include the implementation of a finite difference capillary tube submodel (Peixoto and Bullard, 1994) and speed enhancements to the ACRC equation solver that allowed the model to be run on a desktop computer.

Bridges and Bullard (1995) focused on validating the model by using air-side thermocouples and power measurements. This investigation was further refined when Jensen and Dunn (1996) added complete refrigerant-side instrumentation that has allowed for the further refinement and improvement of the system simulation model. During the refrigerant-side investigation, the refrigerant-side property calls where changed from the REFPROP routines over to interpolation lookup tables which provided quicker calculations and facilitated the rapid addition of alternative refrigerants (Woodall and Bullard, 1997).

1.2 Microchannel heat exchangers

Microchannel heat exchangers consist basically of extruded aluminum tubes with multiple (usually under 1 mm diameter) ports that have been sandwiched together between louvered fins and then brazed between two headers. The mobile air-conditioning industry has found significant benefits to using these heat exchangers because they are more compact for a given heat transfer capacity and pressure drop in comparison to conventional round-tube/plate-fin heat exchangers. This compactness provides savings in space, weight, and refrigerant charge. Because microchannel technology is relatively new, it has not yet been optimized. Little research has been conducted, however, to see what benefits could be gained from using the microchannel heat exchangers in residential split-system applications, which is the focus of this thesis.

Huen and Dunn (1996a, 1996b) provided a model for performing sub-optimizations of a microchannel condenser, so this was used as the blueprint for modifying the already established and validated RACMOD evaporator and condenser subroutines to simulate the new heat exchanger technology. Once a workable model had been developed, many simulation runs were performed where various parameters where varied to find the optimal design for the microchannel heat exchangers (readily available tubes were used to speed up manufacture of the heat exchangers which eliminated some of the geometry parameter variations and saved time).

2

Finally, the system was constructed, instrumented, and tested to provide further validation for the new Air Conditioner with Microchannel Heat Exchanger (ACMCHX) model.

1.3 Scope of this report

Chapter 2 provides a short summary of the experimental instrumentation and facilities used to acquire the data used for the analysis in this report.

Chapter 3 contains the analysis and discussion of the experimental results for the experimental microchannel split-system air conditioner. Both wet and dry evaporator conditions are examined over a wide range of outdoor ambient conditions. Data tables comparing experimental results against the model simulations are also inserted at the beginning of chapter 3 to facilitate ease of reference.

Chapter 4 wraps up this report with the summary and recommendations section.

Appendix A contains the methodology and the results of the simulations used for the design of the microchannel split system. It also outlines the selection of the components of the system such as the air-handler, compressor, fan motors, etc.

Appendix B provides a much more detailed explanation of the experimental instrumentation and facilities used for the data contained in this report.

Appendix C outlines the important modifications made to RACMOD and lists detailed geometric information for modeling microchannel heat exchangers as well as the correlations used in the ACMCHX model.

Finally, Appendix D simply contains the full listing of data from the simulation runs described in Chapter 3.

Chapter 2
Experimental facilities

2.1 Calorimeter test facility

The calorimeter test rooms used in this report conform to ASHRAE Standard 16-1983 (1983). The test facility consists of two thermally isolated rooms – one for simulating indoor conditions and the other for simulating the outdoor ambient environment. The indoor room has independent control of humidity and temperature, whereas, the outdoor room has only temperature control.

The facility can test air conditioners with capacities between 0.5 to 2 tons. The indoor room temperature range is between 50 to 120°F and the relative humidity range is between 5 to 95%. The outdoor room can control temperatures from 70 to 120°F. The cooling (both latent and sensible) in the outdoor room is provided by an ethylene glycol chiller which has a maximum capacity of 7 tons. A custom built evaporative humidifier provides the latent load for the indoor room, and a commercially available 10 kW electric furnace supplies the sensible load. For the higher capacity microchannel split system, the furnace fan was set to the maximum speed setting.

A Fluke 2280 Datalogger connected to a Macintosh computer provides the data acquisition for all of the instrumentation. The Fluke 2280 has the capacity to measure 100 channels at 15 channels per second. Therefore, only a subset of thermocouples could be measured during a given test because the number of thermocouples, pressure transducers, and watt transducers exceeded the available 100 channels.

A more detailed description of the indoor and outdoor rooms is provided by Fleming and Dunn (1993) and Feller and Dunn (1993), respectively. Further design information and validation of the test facilities are provided by Rugg and Dunn (1994).

2.2 Instrumentation

In order to validate the ACMCHX model, the microchannel split system was heavily instrumented on both the surface and the refrigerant sides. Figure 2.1 shows the various state points of interest within the ACMCHX model.
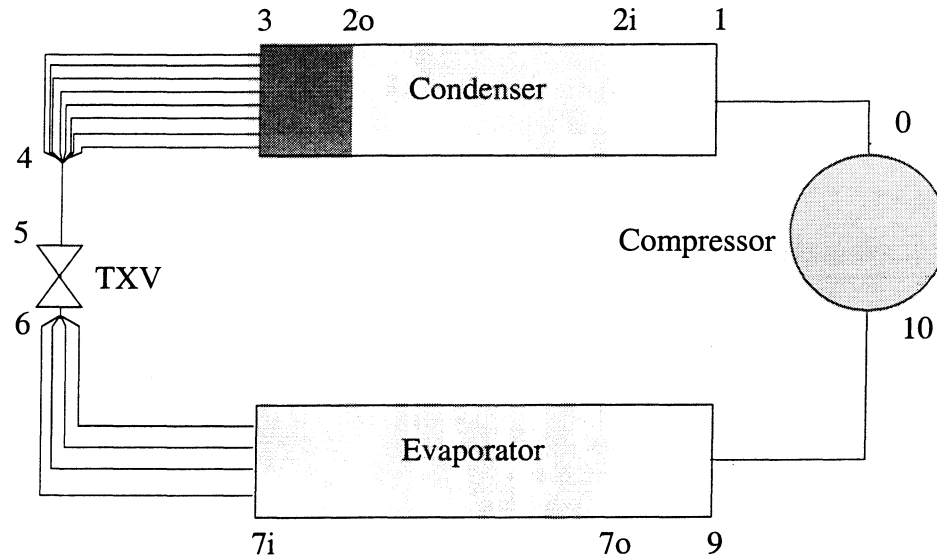
Figure 2.1 ACMCHX system state points

Table 2.1 shows the notation relating the model state points and the experimental data points shown in Chapter 3.

Table 2.1 State point correlations

Data	ACMCHX
Cond in	1
Cond sat	2o
Cond out	3
Evap sat	7i
Evap out	9

Appendix B provides details about all of the following instrumentation issues.

2.2.1 Mass flow meters

Several methods were used in this report to measure mass flow: a Micromotion mass flow sensor and two venturi meters. The Micromotion (sensor model DS025S119, and

transmitter model RFT97121RRU) was originally installed to simply calibrate the venturi meters *in situ*, but was left in place for the initial validation data presented in this thesis.

Two venturis were available from the previous RAC project (Jensen and Dunn, 1996). Because the presence of oil caused noisy readings in the suction-line, it was decided to install venturis only in the discharge and liquid lines.

Table 2.2 Venturi dimensional parameters

Size	Model	Inlet diam [in]	Throat diam [in]	β [Dt/Di]
Small	V050095-BSW	0.266	0.097	0.364
Large	V100258-BSW	0.564	0.259	0.460

From the available venturis, the small one was used in the liquid line of the microchannel split system and the large one was used in the system's discharge line. During the calibration of the two venturis, it was found that the one mounted in the discharge line was showing a significantly (0.780 as opposed to 0.937 that Jensen and Dunn measured (1996)) lower discharge coefficient. This probably was due to the troubles involved with installing the large venturi into the system. Several re-solderings were necessary which may have caused solder to collect in the venturi's throat and thereby changing the discharge coefficient. This troublesome venturi will be removed and cleaned before the next series of tests. The small venturi's discharge coefficient was identical to the 0.960 that Jensen measured. Once the Micromotion mass flow sensor is removed from the system, the small, liquid-line venturi will provide the primary mass flow measurement.

2.2.2 Pressure transducers

Again, several pressure transducers were available from previous projects. Because R410A operates at higher pressures than R22 at normal operating conditions, a new absolute pressure transducer was required for the high-side pressure measurements: a Sensotec model TJE/0713-22TJA with a maximum pressure of 1000 psia.

Table 2.3 Pressure Transducer Information (from Jensen and Dunn, 1996)

Measurement	Model	Volume (in³)	Range	Manufacturer's Accuracy	
				% Full Scale	Relative psi
High-Side Absolute	TJE/0713-22TJA	0.17	0-1000 psia	±0.10	±1.0
Low-Side Absolute	TJE/713-18	0.17	0-500 psia	±0.10	±0.5
Condenser ΔP	Z/5556-05	0.4	±10 psid	±0.25	±0.025
Discharge-line Venturi ΔP	Z/5556-01	0.4	±5 psid	±0.25	±0.013
Liquid-line Venturi ΔP	Z/5556-05	0.4	±10 psid	±0.25	±0.025

Unfortunately, due to the difficulties in instrumenting microchannel heat exchangers, the pressure taps were not located exactly at the condenser or evaporator inlets and outlets. Between the condenser exit and the liquid line there were eight header feeding tubes entering into a heat pump TXV, and between the exit of the discharge line and the entrance to the condenser was a four-way valve. The evaporator outlet measurements were taken downstream of the TXV bulb at the exit. The pressure drop observed across the condenser therefore includes the pressure drops across all of the hardware described above. This makes comparing the pressure drop across the condenser between the model and the system difficult because the model does not account for the pressure drop in the heat pump TXV, the four-way valve, or the microchannel heat exchanger's headers. The model also does not account for the pressure drop in the evaporator's headers or the TXV. Hopefully, in the next generation experimental heat exchanger this problem will be solved by brazing pressure taps directly into the aluminum inlet and outlet headers of both the condenser and evaporator.

2.2.2 Thermocouples

Four immersion, type-T, thermocouples were used for refrigerant-side temperature measurements. Each thermocouple had a stainless steel sheath that had an outer diameter of 1/16 in. with an overall length of 6 in. The type-T thermocouples had a maximum temperature of 632°F and a manufacturer's accuracy of ±0.9°F. The immersion thermocouples were placed at

the inlets and outlets of each of the condenser and evaporator. Because the original unshielded immersion thermocouples were displaying a large amount of noise, they were replaced with immersion thermocouples with shielded sheaths. The sheath was directly connected to the internal ground within the Fluke Datalogger to further reduce the noise.

Teflon coated 30 gauge Type-T thermocouple wires (from the same roll) were utilized for all of the external temperature measurement applications. The accuracy for the surface thermocouples was also ±0.9°F. Surface thermocouples were applied using an aluminum epoxy, or were attached to wire grids for air temperature measurements. Air grids were created for the entrance and exits for both the evaporator housing and the outdoor unit, and surface thermocouples were applied for critical measurements where the immersion thermocouples could not be implemented. A special section of the evaporator was left unfinned which facilitated the application and insulation of thermocouples to every other tube for some detailed distribution analysis. In all, around 96 total thermocouples (including immersion TC's) were used to characterize the performance of the microchannel split system. Appendix B has a table listing the location of all of the thermocouples as well as digital pictures of their exact installation.

Chapter 3
Experimental results and discussion

3.1 Introduction

The focus of the preliminary experiments on the microchannel split-system air conditioner was to compare the performance data of the actual system to the updated model that contained the physical dimensions of the real system. This comparison was designed to: a) identify weaknesses in the model, to serve as the basis for future improvement and validation of the model as a system design tool, and b) formulate recommendations for future investigations into the optimization of microchannel heat exchangers in residential applications. As described in Chapter 2 and Appendix B, the system has been extensively instrumented to facilitate these investigations.

3.2 Overall system performance

System data was taken both at constant indoor wet-air conditions of 80 °F dry bulb, 67 °F wet bulb and dry conditions at 80°F while the outdoor temperature varied between 69°F to 118°F. The model was then run, matching the indoor and outdoor conditions exactly. To calculate the system charge, the model's subcooling was set to match the experimental data at 9.3 °F at the 80/82 wet condition, this was done because the internal volume of the prototype system was not known exactly. This calculated charge was then used to simulate system performance at every other outdoor condition.

Table 3.1 Dry-coil performance comparison for low ambient temperatures

Point	80/68/Dry*		80/68/Dry		80/71/Dry	
Reference	Data	Model	Data	Model	Data	Model
Date	10/03/98	10/10/98	10/28/98	10/31/98	10/01/98	10/31/98
RTD indoor temp [F]	79.9	-	79.9	-	79.6	-
TC indoor temp [F]	80.1	80.1	80.1	80.1	79.8	79.8
RTD outdoor temp [F]	67.4	-	67.7	-	70.8	-
TC outdoor temp [F]	67.7	67.7	67.9	67.9	70.9	70.9
Indoor RH	21.1	21.1	19.7	19.7	20.8	20.8
Blower power [W]	120.9	120.9	119.2	119.2	122.6	122.6
RAC power (comp + blower) [W]	1583.0	1461.3	1579.4	1463.1	1651.0	1521.3
Capacity from ref.side (Tot-fanpwr) [Btu/hr]	25,985	27,164	24,764	27,148	25,130	26,774
Total capacity (ref. side) [Btu/hr]	26,398	27,577	25,171	27,555	25,548	27,192
Cond Capacity (ref. Side) [Btu/hr]	31,522	31,953	30,359	31,949	31,066	31,870
Mass flow [lbm/hr]	322.9	331	310.7	331.0	317.4	330.0
Water removal rate [lbm/hr]	-	-	-	-	-	-
Cond pressure out [psia]	269.0	255.2	264.0	255.9	282.8	268
High-side ΔP [psid]	19.2	-	22.6	-	19.0	-
Evap pressure out [psia]	128.7	138.0	124.2	138.1	127.1	138.5
Evap temperature (sat) [F]	38.2	42.4	36.1	42.4	37.5	42.6
Evap out (itc) [F]	51.9	52.2	47.6	52.2	48.6	52.4
Cond in (itc) [F]	145.5	127.9	146.4	128.2	150.5	133.7
Cond sat temp (out) [F]	85.0	81.3	83.7	81.6	88.5	84.7
Cond out (itc) [F]	77.6	71.6	76.7	71.7	78.9	74.0
Degrees of subcooling [F]	7.4	9.7	7.0	9.9	9.6	10.7
Degrees of superheat [F]	13.7	9.8	11.5	9.8	11.1	9.8

* indoor dry bulb temperature/outdoor dry bulb temperature/indoor relative humidity

Table 3.2 Dry-coil performance comparison for low ambient temperatures

Point	80/74/Dry*		80/75/Dry		80/81/Dry	
Reference	Data	Model	Data	Model	Data	Model
Date	10/06/98	10/31/98	10/23/98	10/31/98	10/23/98	10/31/98
RTD indoor temp [F]	79.7	-	80.0	-	79.9	-
TC indoor temp [F]	79.9	79.9	79.5	79.5	80.3	80.3
RTD outdoor temp [F]	74.3	-	75.4	-	81.7	-
TC outdoor temp [F]	74.0	74.0	74.9	74.9	81.4	81.4
Indoor RH	20.7	20.7	24.2	24.2	26.6	26.6
Blower power [W]	124.2	124.2	114.5	114.5	113.2	113.2
RAC power (comp + blower) [W]	1711.0	1584.0	1741.1	1593.0	1892.5	1737
Capacity from ref.side (Tot-fanpwr) [Btu/hr]	24,250	26,500	26,721	26,333	26,626	25,918
Total capacity (ref. side) [Btu/hr]	24,674	26,924	27,110	26,724	27,012	26,304
Cond Capacity (ref. Side) [Btu/hr]	30,624	31,905	32,974	31,795	33,506	32,058
Mass flow [lbm/hr]	313.0	330.6	342.6	329.2	351.3	333.1
Water removal rate [lbm/hr]	-	-	-	-	-	-
Cond pressure out [psia]	295.3	281.2	305.0	285.0	336.2	314.8
High-side ΔP [psid]	19.3	-	19.9	-	20.6	-
Evap pressure out [psia]	125.7	139.5	136.5	139.3	140.4	142.5
Evap temperature (sat) [F]	36.8	43.1	41.6	43.0	43.3	44.3
Evap out (itc) [F]	45.4	52.8	52.2	52.8	52.5	54.1
Cond in (itc) [F]	155.7	139.2	153.9	141.1	162.7	152.9
Cond sat temp (out) [F]	91.5	88.1	93.8	89.0	100.9	96.1
Cond out (itc) [F]	81.3	76.6	82.8	77.2	87.8	83.1
Degrees of subcooling [F]	10.2	11.5	10.0	11.8	13.1	13
Degrees of superheat [F]	8.6	9.7	10.6	9.8	9.2	9.8

* indoor dry bulb temperature/outdoor dry bulb temperature/indoor relative humidity

11

Table 3.3 Dry-coil performance comparison for medium ambient temperatures

Point	80/82/Dry*		80/82/Dry		80/90/Dry	
Reference	Data	Model	Data	Model	Data	Model
Date	10/08/98	10/31/98	10/23/98	10/31/98	10/24/98	10/31/98
RTD indoor temp [F]	79.9	-	80.1	-	79.9	-
TC indoor temp [F]	80.1	80.1	80.5	80.5	80.1	80.1
RTD outdoor temp [F]	82.5	-	82.8	-	90.8	-
TC outdoor temp [F]	82.2	82.2	82.5	82.5	90.4	90.4
Indoor RH	20.9	20.9	24.4	24.4	22.5	22.5
Blower power [W]	124.5	124.5	115.0	115.0	116.7	116.7
RAC power (comp + blower) [W]	1899.0	1768.3	1917.9	1765.5	2146.8	1984.7
Capacity from ref.side (Tot-fanpwr) [Btu/hr]	23,178	25,718	25,701	25,850	22,917	24,841
Total capacity (ref. side) [Btu/hr]	23,602	26,143	26,094	26,242	23,315	25,239
Cond Capacity (ref. Side) [Btu/hr]	30,558	31,985	32,662	32,117	31,286	32,046
Mass flow [lbm/hr]	311.0	332.1	339.6	333.9	317.3	333.0
Water removal rate [lbm/hr]	-	-	-	-	-	-
Cond pressure out [psia]	332.0	318.7	340.5	320.1	385.0	361.5
High-side ΔP [psid]	21.1	-	19.7	-	19.2	-
Evap pressure out [psia]	126.8	142.4	136.8	143.1	131.4	145.2
Evap temperature (sat) [F]	37.3	44.3	41.8	44.5	39.4	45.4
Evap out (itc) [F]	42.1	54.1	51.5	54.3	42.4	55.2
Cond in (itc) [F]	169.8	154.6	166.2	154.9	185.2	171.2
Cond sat temp (out) [F]	100.0	97.0	101.8	97.3	111.0	106.3
Cond out (itc) [F]	86.2	83.8	88.0	84.1	91.2	91.3
Degrees of subcooling [F]	13.8	13.2	13.8	13.2	19.8	15.0
Degrees of superheat [F]	4.8	9.8	9.7	9.8	3.0	9.8

* indoor dry bulb temperature/outdoor dry bulb temperature/indoor relative humidity

Table 3.4 Dry-coil performance comparison for medium ambient temperatures

Point	80/94/Dry*		80/95/Dry		80/95/Dry	
Reference	Data	Model	Data	Model	Data	Model
Date	10/26/98	10/31/98	10/02/98	10/10/98	10/24/98	10/31/98
RTD indoor temp [F]	79.9	-	79.8	-	79.9	-
TC indoor temp [F]	80.1	80.1	80.0	80.0	80.1	80.1
RTD outdoor temp [F]	94.1	-	94.7	-	95.6	-
TC outdoor temp [F]	93.8	93.8	94.8	94.8	95.2	95.2
Indoor RH	22.5	22.5	23.9	23.9	23.1	23.1
Blower power [W]	116.5	116.5	124.1	124.1	116.5	116.5
RAC power (comp + blower) [W]	2249.1	2091.8	2297.5	2133.4	2306.7	2138.6
Capacity from ref.side (Tot-fanpwr) [Btu/hr]	22,343	24,444	23,437	24,273	22,308	24,279
Total capacity (ref. side) [Btu/hr]	22,741	24,841	23,860	24,696	22,706	24,676
Cond Capacity (ref. Side) [Btu/hr]	31,071	32,084	31,817	32,072	31,229	32,105
Mass flow [lbm/hr]	312.9	333.3	321.1	333.1	316.6	333.5
Water removal rate [lbm/hr]	-	-	-	-	-	-
Cond pressure out [psia]	404.4	381.3	418.9	387.4	416.3	389.8
High-side ΔP [psid]	21.0	-	13.8	-	19.1	-
Evap pressure out [psia]	131.5	146.5	135.3	146.7	132.8	147.0
Evap temperature (sat) [F]	39.5	45.9	41.12	46.1	40.0	46.2
Evap out (itc) [F]	44.4	55.7	52.7	55.8	43.6	56.0
Cond in (itc) [F]	194.8	178.5	196.0	180.8	196.0	181.6
Cond sat temp (out) [F]	115.0	110.3	117.4	111.5	117.0	111.9
Cond out (itc) [F]	94.5	94.5	95.1	95.4	96.0	95.8
Degrees of subcooling [F]	20.2	15.8	22.3	16.1	21.0	16.1
Degrees of superheat [F]	5.0	9.8	11.6	9.7	3.6	9.8

* indoor dry bulb temperature/outdoor dry bulb temperature/indoor relative humidity

Table 3.5 Dry-coil performance comparison for high ambient temperatures

Point	80/96/Dry*		80/104/Dry		80/106/Dry	
Reference	Data	Model	Data	Model	Data	Model
Date	10/26/98	10/31/98	10/03/98	10/10/98	10/24/98	10/31/98
RTD indoor temp [F]	80.0	-	79.8	-	79.8	-
TC indoor temp [F]	80.2	80.2	80.0	80.0	80.1	80.1
RTD outdoor temp [F]	96.6	-	104.0	-	106.5	-
TC outdoor temp [F]	96.4	96.4	104.2	104.2	106.0	106.0
Indoor RH	22.8	22.8	26.3	26.3	25.6	25.6
Blower power [W]	116.4	116.4	124.1	124.1	118.9	118.9
RAC power (comp + blower) [W]	2336.6	2179.7	2628.7	2503.5	2724.9	2584.8
Capacity from ref.side (Tot-fanpwr) [Btu/hr]	21,982	24,165	22,444	23,102	21,338	22,907
Total capacity (ref. side) [Btu/hr]	22,379	24,562	22,868	23,525	21,744	23,313
Cond Capacity (ref. Side) [Btu/hr]	31,061	32,154	31,993	32,292	31,411	32,382
Mass flow [lbm/hr]	313.0	334.0	324.0	333.9	316.6	334.3
Water removal rate [lbm/hr]	-	-	-	-	-	-
Cond pressure out [psia]	421.5	397.2	480.3	452.9	493.3	467.7
High-side ΔP [psid]	20.2	-	15.0	-	19.5	-
Evap pressure out [psia]	132.4	147.6	139.8	150.5	137.8	151.4
Evap temperature (sat) [F]	39.9	46.4	43.1	47.6	42.2	47.9
Evap out (itc) [F]	44.3	56.2	54.8	57.4	50.9	57.7
Cond in (itc) [F]	200.3	184.2	215.5	203.5	222.4	208.3
Cond sat temp (out) [F]	118.0	113.4	128.2	123.5	130.0	126.1
Cond out (itc) [F]	97.1	97.0	104.5	104.5	106.9	106.3
Degrees of subcooling [F]	20.8	16.4	23.7	19	23.4	19.8
Degrees of superheat [F]	4.5	9.8	11.7	9.8	8.7	9.8

* indoor dry bulb temperature/outdoor dry bulb temperature/indoor relative humidity

14

Table 3.6 Dry-coil performance comparison for high ambient temperatures

Point	80/111/Dry*		80/118/Dry		80/118/Dry	
Reference	Data	Model	Data	Model	Data	Model
Date	10/25/98	10/31/98	10/04/98	10/31/98	10/26/98	10/31/98
RTD indoor temp [F]	79.9	-	79.7	-	80.3	-
TC indoor temp [F]	80.1	80.1	80.0	80.0	80.5	80.5
RTD outdoor temp [F]	111.4	-	117.4	-	118.0	-
TC outdoor temp [F]	110.9	110.9	117.6	117.6	117.8	117.8
Indoor RH	26.9	26.9	30.3	30.3	29.1	29.1
Blower power [W]	118.5	118.5	124.0	124.0	117.9	117.9
RAC power (comp + blower) [W]	2960.6	2870.7	3292.0	3490.5	3327.3	3506.8
Capacity from ref.side (Tot-fanpwr) [Btu/hr]	20,740	22,222	20,561	21,083	19,930	21,214
Total capacity (ref. side) [Btu/hr]	21,144	22,626	20,984	21,506	20,333	21,616
Cond Capacity (ref. Side) [Btu/hr]	31,517	32,643	32,395	33,351	31,944	33,538
Mass flow [lbm/hr]	314.8	334.3	323.3	332.6	316.4	334.7
Water removal rate [lbm/hr]	-	-	-	-	-	-
Cond pressure out [psia]	532.5	516.2	589.2	617.6	590.3	621.3
High-side ΔP [psid]	20.6	-	17.0	-	21.4	-
Evap pressure out [psia]	140.4	153.7	147.6	157.2	145.3	158.0
Evap temperature (sat) [F]	43.3	48.8	46.3	50.2	45.4	50.5
Evap out (itc) [F]	54.0	58.6	57.8	60.0	55.7	60.4
Cond in (itc) [F]	236.8	223.6	251.3	252.9	255.2	253.4
Cond sat temp (out) [F]	136.5	134.0	144.8	148.8	145.0	149.3
Cond out (itc) [F]	111.8	111.1	117.8	117.7	118.4	117.9
Degrees of subcooling [F]	24.7	22.9	27.0	31.1	26.6	31.4
Degrees of superheat [F]	10.7	9.8	11.5	9.8	10.3	9.9

* indoor dry bulb temperature/outdoor dry bulb temperature/indoor relative humidity

Table 3.7 Wet-coil performance comparison for low ambient temperatures

Point	80/70/50 *		80/75/50		80/82/50	
Reference	Data	Model	Data	Model	Data	Model
Date	10/06/98	10/11/98	10/07/98	10/11/98	10/07/98	10/11/98
RTD indoor temp [F]	79.4	-	80.0	-	80.0	-
TC indoor temp [F]	80.1	80.1	80.2	80.2	80.1	80.1
RTD outdoor temp [F]	70.5	-	76.2	-	82.5	-
TC outdoor temp [F]	70.5	70.5	75.8	75.8	82.4	82.4
Indoor RH	52.1	52.1	52.1	52.1	52.0	52.0
Blower power [W]	149.6	149.6	152.6	152.6	150.5	150.5
RAC power (comp + blower) [W]	1676.0	1540.4	1794.0	1642.1	1949.0	1782.6
Capacity from ref.side (Tot-fanpwr) [Btu/hr]	29,485	30,695	29,056	30,156	28,411	29,305
Total capacity (ref. side) [Btu/hr]	29,994	31,205	29,576	30,677	28,925	29,819
Cond Capacity (ref. Side) [Btu/hr]	35,503	35,770	35,540	35,777	35,598	35,638
Mass flow [lbm/hr]	377.2	389.2	381.7	387.7	381.7	384.4
Water removal rate [lbm/hr]	10.1	9.7	11.5	9.4	10.4	8.9
Cond pressure out [psia]	282.5	269	304.3	291	333.4	320.5
High-side ΔP [psid]	23.3**	-	23.3**	-	23.3**	-
Evap pressure out [psia]	147.5	158.8	149.4	159.8	150.8	160.6
Evap temperature (sat) [F]	46.3	50.9	47.0	51.3	47.6	51.6
Evap out (itc) [F]	56.9	60.7	56.4	61.1	56.1	61.4
Cond in (itc) [F]	143.4	127.5	149.5	136.5	159.7	148.3
Cond sat temp (out) [F]	88.4	85.0	93.7	90.5	100.3	97.4
Cond out (itc) [F]	82.9	81.5	87.3	84.2	91.0	88.1
Degrees of subcooling [F]	5.5	3.5	6.4	6.3	9.3	9.3
Degrees of superheat [F]	10.6	9.8	9.4	9.8	8.5	9.8

* indoor dry bulb temperature/outdoor dry bulb temperature/indoor relative humidity

** pressure transducer was at maximum differential pressure

Table 3.8 Wet-coil performance comparison for high ambient temperatures

Point	80/95/50*		80/105/50		80/118/50	
Reference	Data	Model	Data	Model	Data	Model
Date	10/9/98	10/11/98	10/9/98	10/11/98	10/12/98	10/17/98
RTD indoor temp [F]	79.7	-	79.8	-	80.0	-
TC indoor temp [F]	79.9	79.9	80.0	80.0	80.1	80.1
RTD outdoor temp [F]	95.0	-	105.3	-	118.1	-
TC outdoor temp [F]	95.0	95.0	105.4	105.4	118.3	118.3
Indoor RH	52.6	52.6	52.3	52.3	52.4	52.4
Blower power [W]	148.9	148.9	145.2	145.2	134.2	134.2
RAC power (comp + blower) [W]	2307.0	2122.1	2690.0	2492.1	3303.5	3271.7
Capacity from ref.side (Tot-fanpwr) [Btu/hr]	27,471	27,537	25,724	25,834	23,118	23,435
Total capacity (ref. side) [Btu/hr]	27,979	28,045	26,220	26,329	23,576	23,893
Cond Capacity (ref. Side) [Btu/hr]	36,124	35,407	35,733	35,196	35,175	35,421
Mass flow [lbm/hr]	386.0	380.1	375.0	375.9	368.3	369.4
Water removal rate [lbm/hr]	10.6	8.0	8.8	7.0	6.8	5.56
Cond pressure out [psia]	401.2	385.2	472.1	451.0	585.8	582.3
High-side ΔP [psid]	23.3**	-	23.3**	-	23.3**	-
Evap pressure out [psia]	156.3	163.1	157.2	165.4	162.6	169.1
Evap temperature (sat) [F]	49.8	52.5	50.1	53.4	52.2	54.7
Evap out (itc) [F]	58.3	62.3	59.9	63.2	60.7	64.6
Cond in (itc) [F]	182.0	172.7	206.2	195.7	237.8	236
Cond sat temp (out) [F]	114.1	111.1	126.8	123.2	144.4	143.9
Cond out (itc) [F]	99.3	97.5	106.1	106.5	118.9	118.6
Degrees of subcooling [F]	14.8	13.6	20.7	16.7	25.5	25.3
Degrees of superheat [F]	8.5	9.8	9.8	9.8	8.5	9.9

* indoor dry bulb temperature/outdoor dry bulb temperature/indoor relative humidity

** pressure transducer was at maximum differential pressure

3.2.1 Total capacity

Figure 3.1 shows the total system capacity, comparing the measured data with the system simulation results for the 18 dry points taken.

17
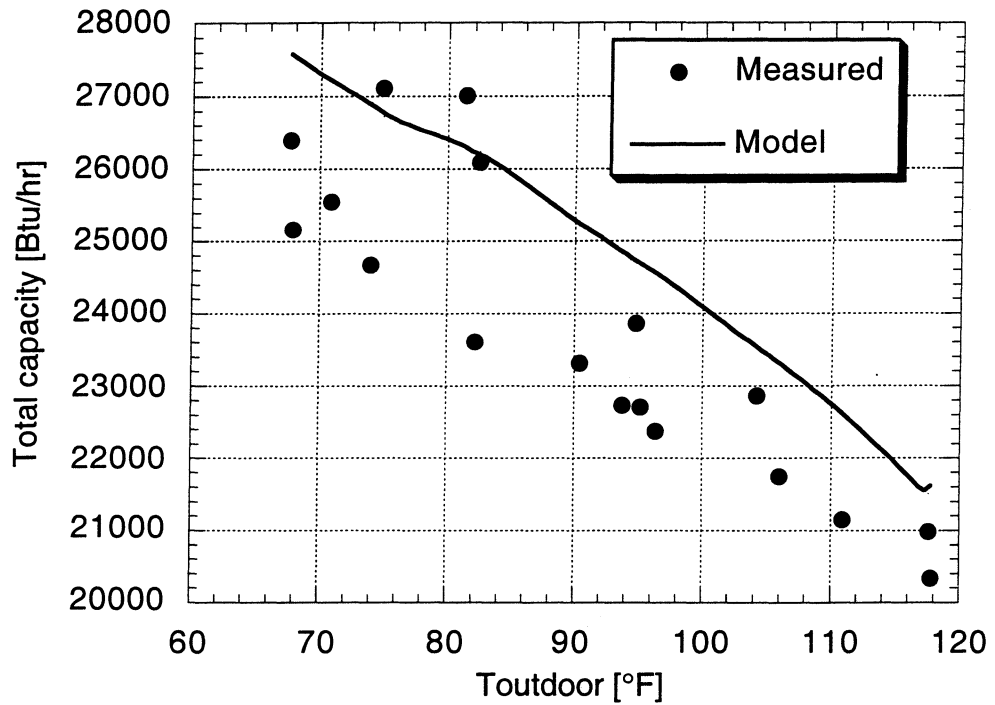
Figure 3.1 Dry-coil total capacity comparison for the system model

As can be seen above, the model overpredicts the actual capacity by around 10.9% at its

worst. A certain amount of scatter and repeatability problems were present in the experimental

data. Upon observing this scatter in the dry data, the entire unfinned section (see Figure 3.2)

thermocouples were attached for all data sets after the 20th of October in order to gather data on

maldistribution.
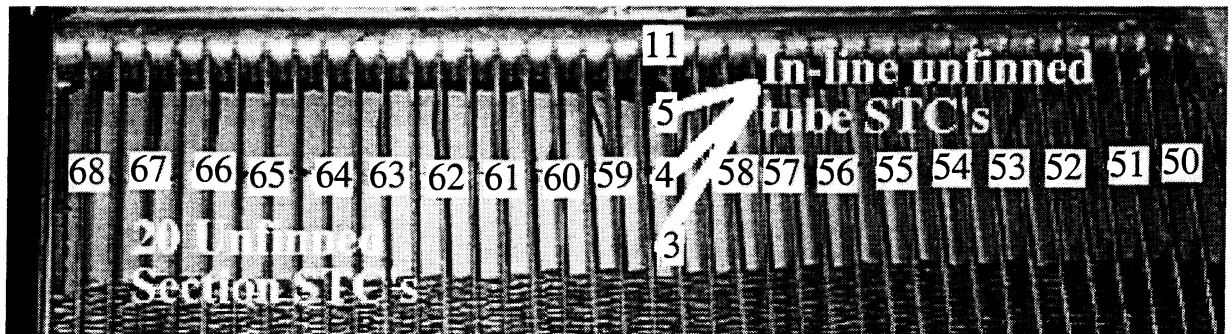
Figure 3.2 Evaporator unfinned section surface thermocouples

Some interesting observations can be made from this maldistribution data. As can be observed in Figure 3.1, most of the dry points follow a somewhat linear trend beneath the predicted total capacity curve. Figure 3.3 shows a common maldistribution pattern across the unfinned section for the points that follow that linear trend.
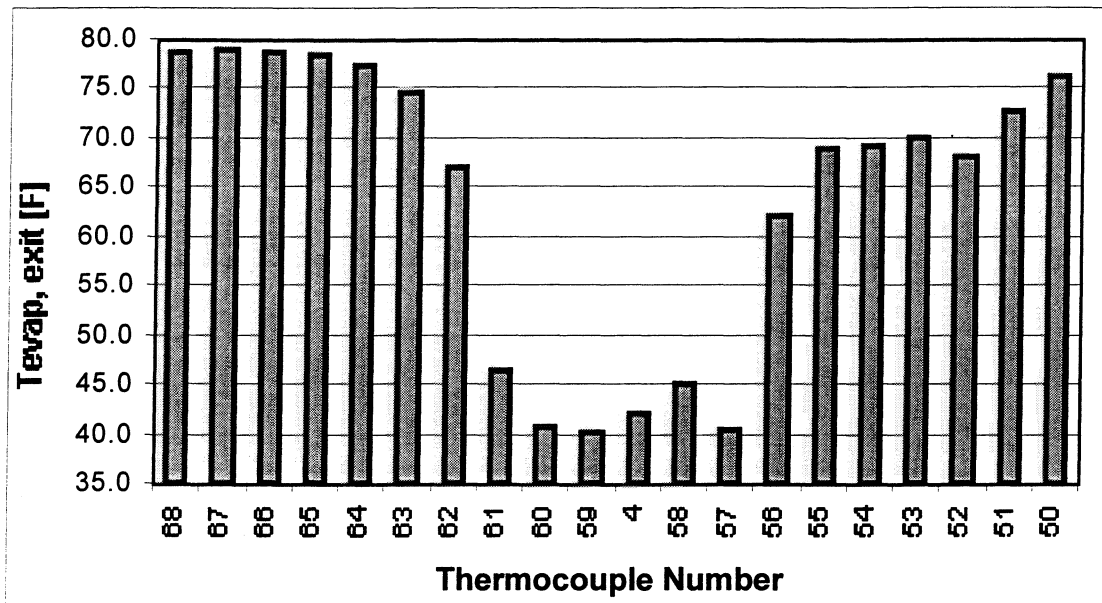
Figure 3.3 Evaporator unfinned section maldistribution (80/90 condition, 10-24-98)

Significant amounts of maldistribution can be observed from Figure 3.3. The tubes towards either end of the evaporator see large amounts of highly superheated vapor, while the middle tubes exit from the evaporator close to the saturated evaporating temperature of around 42°F. The reason for this distribution pattern can be observed by examining the refrigerant distributor in Figures 3.4 and 3.5.

Figure 3.5 shows the orientation of the header feeder tubes as they come out of the distributor as well as the corresponding header feeder tube number. Header feeding tube 3 sits at the lowest point on the distributor, so it would receive the most liquid of the four feeding tubes and it feeds into the section between thermocouple #60 and #61 which corresponds to the two-phase section. Because the other three header feeding tubes are at higher elevations they will see correspondingly more vapor under maldistribution conditions and that is why the superheat

regions are higher at either end of the heat exchanger. Of course, assuming that there are no baffles in between the header inlet sections, some mixing will occur within the evaporator inlet header.
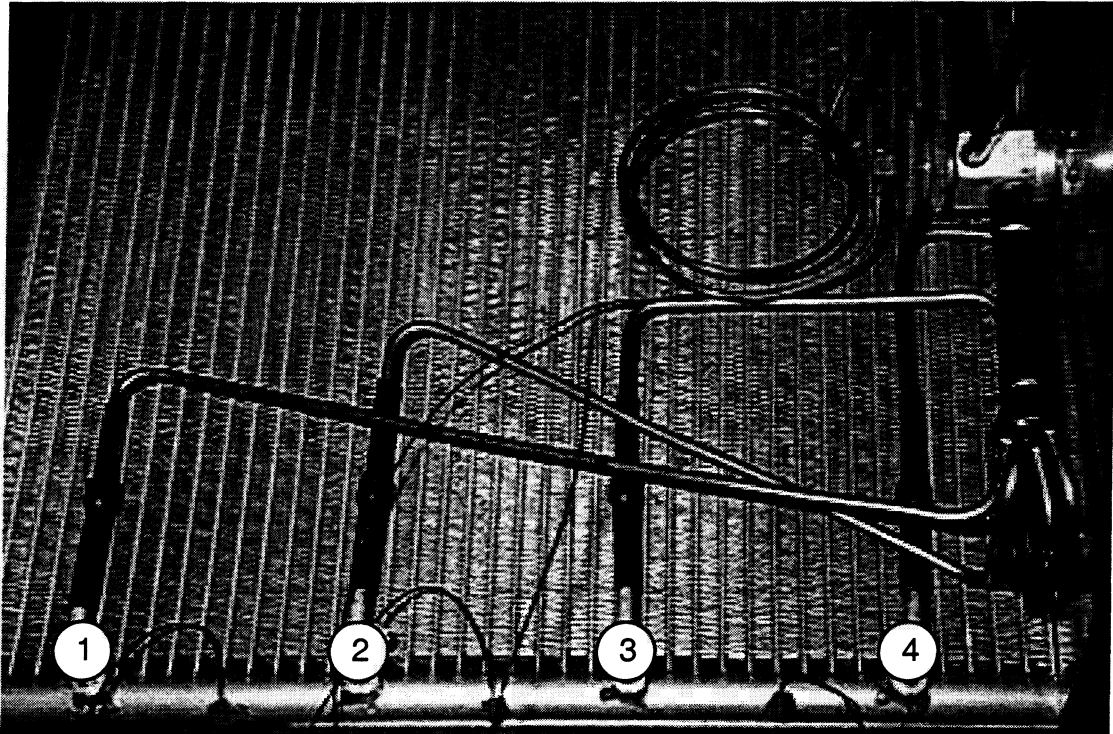
Figure 3.4 Evaporator inlet distribution system
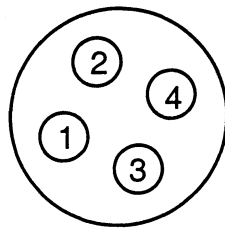
Figure 3.5 Evaporator distributor orientation

The three points that lie the closest to the predicted curve in Figure 3.1 also provide insight into the effects of maldstribution on the system.

Figure 3.6 shows the general distribution pattern for one of the three points that were closest to the predicted curve. Generally, the distribution was much better than the other fifteen dry evaporator points. The resulting total capacity for the 80/82 dry point observed was

approximately 10% higher than the corresponding 80/82 point that suffered severe maldistribution similar to Figure 3.5.
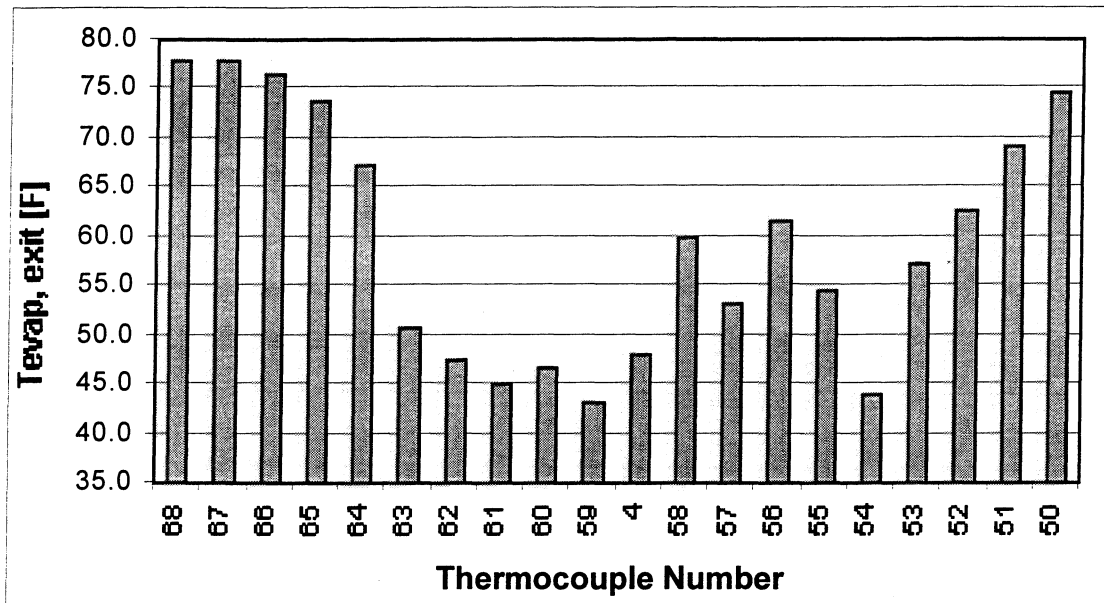
Figure 3.6 Evaporator unfinned section maldistribution (80/82 condition, 10-23-98)

A possible explanation for the repeatability problems in the system's capacity could be that, at the lower ambient temperatures, the evaporator distributor experiences a lower volumetric flow rate (hence a lower refrigerant velocity) which lowers the pressure drop through the header feeding tubes and thereby increases the maldisribution as gravity pulls the heavier liquid towards the lower tube (since the distributor was mounted horizontally) which causes the TXV to perform poorly (Sporlan, 1975), hence the steady but unpredictable superheat results observed. Because higher outdoor ambient temperatures would result in higher volumetric flow rates in the evaporator distributor causing improved distribution, the general improvement in the model's prediction at higher ambient conditions would also be explained. Many of these repeatability issues will be addressed in a forthcoming ACRC Technical Report (Stott, 1999).

The difference between the measured and the calculated saturated evaporating temperature provided an accurate predictor of the errors between the actual and predicted system capacity. In general, the evaporating temperature was overpredicted, which caused the model to predict higher mass flow rates because the compressor mass flow rate was very sensitive to the

21

suction pressure. Having a higher saturated evaporating temperature would reduce the overall pressure ratio, which raises the mass flow rate.
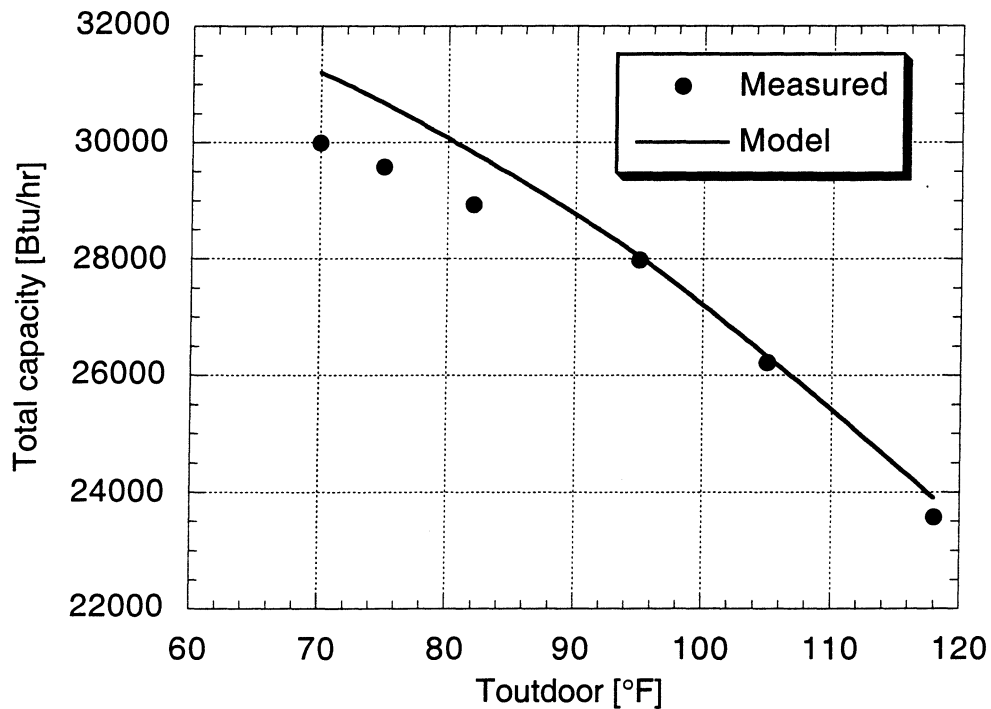
Figure 3.7 Wet-coil total capacity comparison

Again, due to time constraints, fewer wet points were taken for comparison to the overall system model predictions. Figure 3.7 shows that the predicted capacity exceeded the actual system's capacity by only about 4% at the low outdoor temperatures, and matched within less than 1% for the high outdoor temperatures. Again, the improvement in the model's predicted total capacity at the higher outdoor ambient conditions would suggest that the distribution was improved due to the increased volumetric flow rate at the evaporator distributor. Since the actual evaporator surface was colder than the system model predicted, the water removal rate for the actual system was higher. This increased latent heat transfer may account for the improvement in the prediction of the total capacity relative to the dry-evaporator case.

A possible factor in the general overestimation of the capacity was also the air-side heat transfer coefficient. An overestimation in the air-side heat transfer coefficient would result in the

predicted condensing pressure being lower than what would be observed experimentally and the predicted evaporating pressure would be higher than the actual system. This can be observed in the Tables 3.1 through 3.8 for the wet and dry indoor conditions.

To investigate the air-side error, the evaporator and condenser were analyzed using component simulation models. The entering enthalpy, temperature, and mass flow rate from the measured data were input into the de-coupled evaporator model and then the exit conditions were obtained. The result should then be independent of modeling errors in the rest of the system and should reveal if the air-side heat transfer coefficient was overestimated.

Figure 3.8 shows that the evaporator submodel overpredicts the total capacity by more than 5% throughout the outdoor ambient temperature range of 68 to 118°F. In microchannel heat exchangers, the refrigerant-side resistances only amount to about 11% of the total because of the relatively large refrigerant-side area. Therefore, the modeling error is more likely attributable to the air-side correlations than the refrigerant-side heat transfer coefficients. Maldistribution would also be a significant penalty that would result in differences between the predicted and experimental data for Figure 3.8. This overestimation in the air-side heat transfer coefficient suggests the need for testing other correlations available in literature besides the Chang and Wang correlation (1996) used currently in the model.

Other possible factors for the difference in the predicted and measured values for the total capacity could also be due to the model not accounting for the forty-five degree change in the air-flow path of the actual system (because of its "arrowhead" shape) or oil circulation effects.

Tables 3.9 and 3.10 show that the evaporator submodel, when given the experimental inlet conditions, overpredicts evaporator superheat as well as capacity. Because the two-phase region should be identical for both model and the experimental system at the measured evaporating pressure and temperature, this overprediction of the evaporator superheat again strongly suggests that either: a) the air-side heat transfer coefficient is overestimated, or, b) significant maldsitribution resulted in capacity penalties. Future investigations will attempt to quantify the magnitude of these two effects. Note that the model also predicted the water removal rates within 7%, once the discrepancy in the evaporating temperature was eliminated.
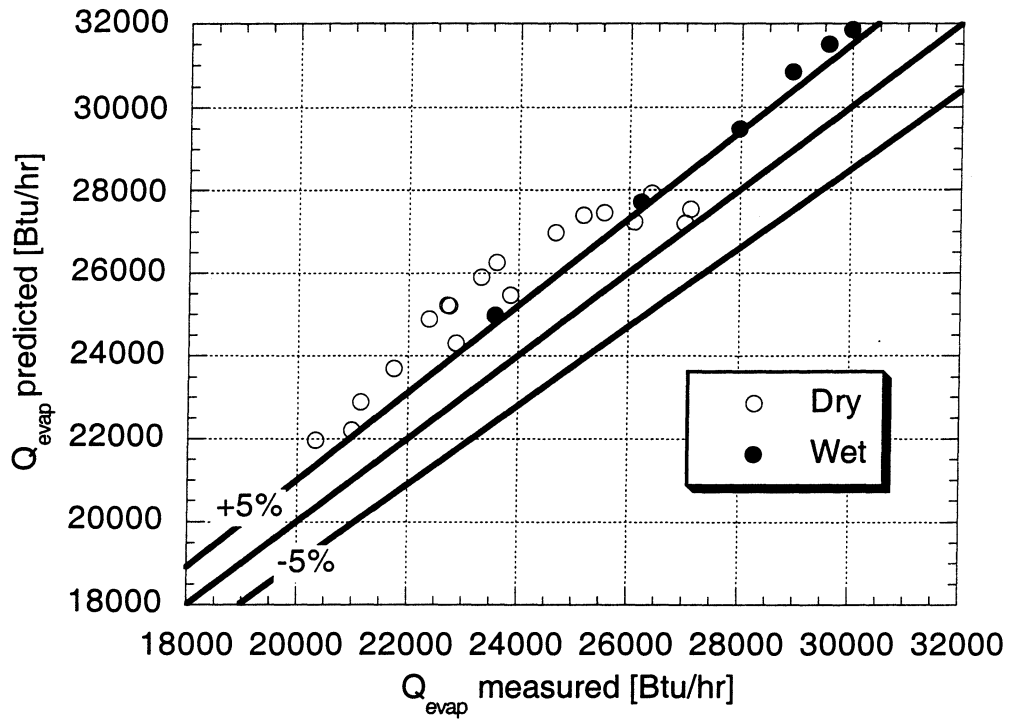
Figure 3.8 Accuracy of total capacity submodel predictions

Table 3.9 Evaporator submodel superheat predictions for dry indoor conditions

Dry evap points	$\Delta T_{superheat}$ [°F]	
	Data	Model
80/68	14	32
80/68	12	39
80/71	11	35
80/74	9	37
80/75	11	15
80/81	9	12
80/82	5	38
80/82	10	23
80/90	3	34
80/94	5	35
80/95	12	31
80/95	4	34
80/96	5	35
80/104	12	29
80/106	9	32
80/111	11	32
80/118	12	26
80/118	10	30

Table 3.10 Evaporator submodel superheat and water removal rate predictions for wet indoor condition

	$\Delta T_{superheat}$ [°F]		Water removal rate [lbm/hr]	
Wet evap points	Data	Model	Data	Model
80/70/50	11	29	10.1	10.9
80/75/50	9	28	11.5	10.7
80/82/50	9	27	10.4	10.2
80/95/50	9	23	10.6	9.4
80/105/50	10	24	8.8	8.5
80/118/50	9	22	6.8	7.0

As mentioned in Chapter 2, several difficulties in the instrumentation of the system have made certain comparisons to the model considerably more difficult. The pressure taps and immersion thermocouples were not located exactly at the condenser or evaporator inlets and outlets. Between the condenser exit and the liquid line there were eight header feeding tubes entering into a heat pump TXV, and between the exit of the discharge line and the entrance to the condenser was a four-way valve. The evaporator outlet measurements were taken downstream of the TXV bulb at the exit, and there was only a surface thermocouple at the entrance header feeding tubes. The pressure drop observed across the condenser then includes the pressure drops across all of the hardware described above. This makes comparing the pressure drop across the condenser between the model and the system difficult because the model does not account for the pressure drop in the heat pump TXV, the four-way valve, or the microchannel heat exchanger's headers. The model also does not account for the pressure drop in the evaporator's headers or the TXV. A pressure drop of around 23 psid amounted to only around 5°F error in the condensing temperature. It was not possible to determine how much of the additional pressure drop occurred immediately upstream or downstream of the condenser. Therefore the actual penalty on the saturated condensing temperature would be some fraction of the previously mentioned 5°F.

3.2.2 Condenser heat rejected

The condenser submodel was also de-coupled to investigate possible overpredictions in the air-side heat transfer coefficient. The measured input conditions were used in the model and then the outlet conditions were solved for.

Figure 3.9 shows that the condenser heat transfer over both the wet and dry tests was usually predicted within 5% by the condenser submodel. Because the condenser was being fed superheated vapor, it should not be affected by the two-phase distribution problems that plagued the evaporator. Since the predicted capacities were significantly better for the condenser, this could suggest that maldistribution, rather than the air-side heat transfer coefficient, may be the significant factor in the overprediction of the evaporator's capacity.
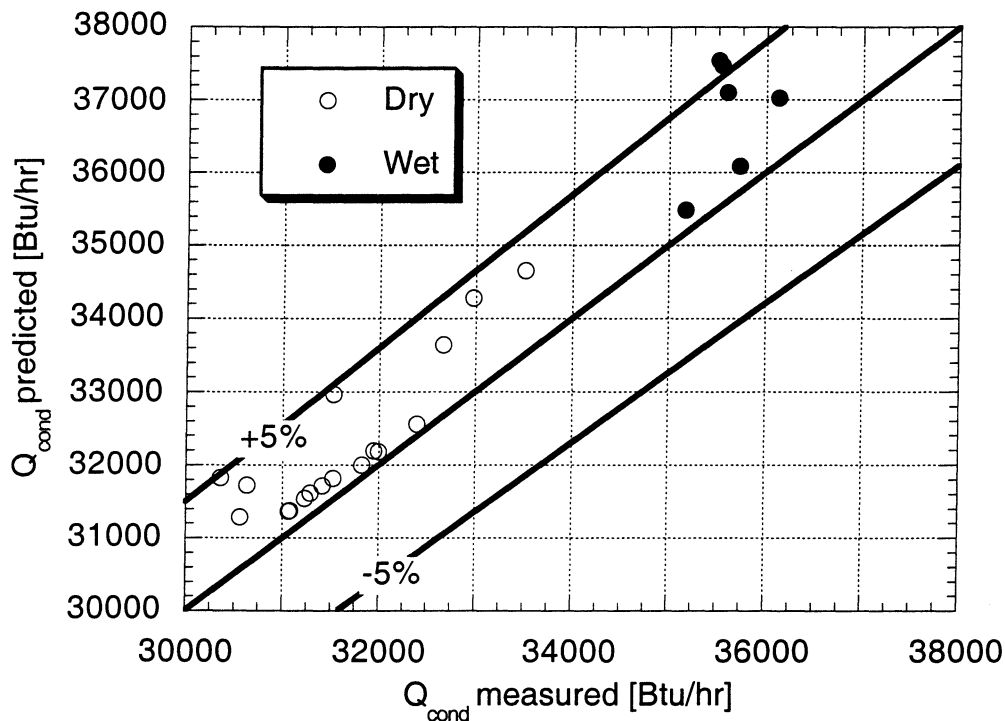
Figure 3.9 Accuracy of condenser submodel predictions

26

Table 3.11 Condenser submodel exit temperature predictions for dry indoor condtions

	$T_{condout}$ [°F]	
Dry evap points	Data	Model
80/68	78	68
80/68	77	68
80/71	79	71
80/74	81	74
80/75	83	75
80/81	88	82
80/82	86	82
80/82	88	83
80/90	91	91
80/94	95	94
80/95	95	95
80/95	96	95
80/96	97	97
80/104	105	104
80/106	107	106
80/111	112	111
80/118	118	118
80/118	118	118

Table 3.12 Condenser submodel exit temperature predictions for wet indoor condtions

	$T_{condout}$ [°F]	
Wet evap points	Data	Model
80/70/50	83	71
80/75/50	87	77
80/82/50	91	84
80/95/50	99	96
80/105/50	106	106
80/118/50	119	119

Tables 3.11 and 3.12 show that the condenser submodel overpredicts the heat transfer from the condenser generally within less than 5%. An interesting trend with the subcooling was that the model's predictions generally improved with increasing outdoor temperatures, especially after around 95°F outdoor ambient temperatures.

Currently the model predicts a pressure drop across the condenser that is less than 1 psid (header pressure drop is not included). The total high-side pressure drop from the experimental data is on the order of 20 psid so it is difficult to estimate a condenser inlet pressure for the model, so the exit pressure was used as the input pressure for the previous comparison because

there is considerably less pressure drop in the liquid phase and the pressure read at the outlet is probably closer to the actual two-phase pressure than the compressor exit pressure minus the pressure drop experienced by the superheated vapor.

3.2.3 Charge

Another major difference between the actual system and the model's predictions was the total charge of the system. In order to reach approximately 10°F subcooling at the 80/82 wet condition, it was necessary to charge with 7.2 lbm of R410A, whereas the model predicted that a total charge of 5.9 lbm would be required. This is an underestimation of 18%.

Table 3.13 Predicted charge distribution throughout system (80/82 wet)

Component	Charge [lbm]	%Total	Volume [ft³]
Condenser charge (total)	**2.349**	**39.7**	**0.07458**
Inlet header	0.039	0.7	0.00779
Superheat	0.052	0.9	0.00702
Two-phase	1.422	24.1	0.04708
Subcooling	0.337	5.7	0.00490
Outlet header	0.498	8.4	0.00779
Evaporator charge (total)	**0.385**	**6.5**	**0.02540**
Inlet header	0.056	1.0	0.00395
Two-phase	0.314	5.3	0.01614
Superheat	0.004	0.1	0.00137
Outlet header	0.011	0.2	0.00395
Other charge (Total)	**3.176**	**53.7**	**0.15854**
Cond exit header tubes	0.332	5.6	0.00524
Liquid line	1.181	20.0	0.01867
Evap inlet header feeding tubes	0.02	0.3	0.00014
Suction line	0.096	1.6	0.03021
Comp	0.159	2.7	0.07430
Ref in oil	0.506	8.6	-
Discharge line	0.078	1.3	0.01728
Filter/Dryer	0.800	13.5	0.01270

Table 3.13 shows the largest contributors to the charge in the system to be the condenser, liquid line, and the filter/dryer as would be expected since they contain dense liquid refrigerant. The charge in the condenser would have to increase by around 50% in order to match the 7.2 used in the actual experiments. It is also important to remember that the charge estimates in the model do not include either of the two TXVs (and their distributors), the four-way valve, or any

of the additional volumes required for the instrumentation of the system (pressure transducers, lines, mass flow meter, etc.).

Table 3.14 shows rather convincingly that the high-side instrumentation, even if filled completely with liquid refrigerant, could not account for the almost 1.2 lbm difference in the predicted and the experimentally measured charge.

Table 3.14 Predicted charge for additional instrumentation

Component	Charge [lbm]	Volume [ft³]
Liquid line venturi entrance pressure tap line	0.010	0.0001575
Liquid line venturi throat pressure tap line	0.010	0.0001613
Liquid line venturi diff. press. transducer	0.015	0.0002315
High-side abs press. transducer	0.006	0.00009838
Micromotion mass flow sensor	0.033	0.005294
Low-side abs press. transducer tap line	0.002	0.000804
Low-side abs press. transducer	0.0002	0.00009838
Discharge line venturi entrance pressure tap line	0.005	0.0009892
Discharge line venturi throat pressure tap line	0.005	0.0009342
Discharge line venturi diff. press. transducer	0.001	0.00002315
High-side diff press. transducer tap line liquid side	0.005	0.0007489
High-side diff press. transducer tap line discharge side	0.0001	0.00002112
High-side diff press. transducer	0.008	0.00002315
Total	**0.1003**	**0.00958478**

A possible explanation for the increased charge required in the actual system could be that some of the ports in the condenser were clogged and filled with liquid. Both the evaporator and the condenser heat exchanger tubes were bent along their major axes, which could: a) be a cause for this blockage of certain tubes or b) result in maldistribution and pressure drop. As mentioned previously, a forthcoming technical report will address the significant differences between the model's predicted performance, and the experimental system's actual performance.

Chapter 4
Summary and recommendations

A steady-state microchannel split-system simulation model was developed from the firm foundations of previous research at the ACRC. This model was then used as a design tool to optimize a microchannel split system with the goal of minimizing TEWI, or total equivalent warming impact. The system components were then selected and the optimized microchannel heat exchangers were fabricated. The entire system was then assembled and extensive tests were run at steady state conditions over a wide range of outdoor ambient conditions in a calorimeter test facility. Experimental results were compared to the simulations for the purpose of model validation and refinement. The full system model overpredicted the total capacity of the system with a minimum error of 0.2%, a mean error of 5%, and a maximum error of 11%. The evaporator submodel overpredicted the total capacity as well, with a minimum error of 0.7%, a mean error of 7%, and a maximum error of 11%. The condensing capacity was also overpredicted with a minimum error of 0.5%, a mean error of 2%, and a maximum error of 6%. A major reason for the lower accuracy with the evaporator was because of the refrigerant maldisribution observed in the experiments. Since the model simulates perfect distribution among the 40 parallel circuits, it overpredicts the cooling capacity.

This report gives a general overview of the model's performance in comparison to the actual system. More experimental data must be obtained before the model can be fully validated. For example, the range of refrigerant-side mass flow rates can be extended by testing over a wide range of indoor temperatures and humidities to validate heat transfer and pressure drop correlations. Likewise, the variable speed fan and blower also allow for the validation of air-side correlations. The present version of the model does not account for pressure drop within the headers and the pressures drop measured for the condenser was considerably larger than what the model predicted. If this uncertainty cannot be resolved by more data, instrumentation improvements may be needed in the next generation microchannel heat exchangers: e.g. pressure

taps built into the headers. The charge inventory calculations are another major source of uncertainty that will require further investigation.

References

ASHRAE, "Method of Testing for Rating Room Air Conditioners and Packaged Terminal Air Conditioners." ANSI/ASHRAE Standard 16-1983, 1983.

Bridges, B.D. and C.W. Bullard, "Simulation of Room Air Conditioner Performance." *University of Illinois at Urbana-Champaign*, ACRC TR-79, 1995.

Chang, Y.J. and C.C. Wang, "A Generalized Heat Transfer Correlation for Louver Fin Geometry." *Int. J. Heat Mass Transfer*, vol. 40, no. 3, pp. 533-544, 1997.

Dobson, M.K. and J.C. Chato, "Condensation in Smooth Horizontal Tubes," *Journal of Heat Transfer*, 120:2, pp. 193-213, 1998.

Feller, S.D. and W.E. Dunn, "Design of the Outdoor Environmental Chamber of a Room Air Conditioner Test Facility." *University of Illinois at Urbana-Champaign*, ACRC TR-43, 1993.

Fischer, S.K. and C.K. Rice, "The Oak Ridge Heat Pump Models." *Oak Ridge National Laboratory*, ORNL/CON-90/R1, 1983.

Fleming, J.E. and W.E. Dunn, "Design of the Psychrometric Calorimeter Chamber of a Room Air Conditioner Test Facility." *University of Illinois at Urbana-Champaign*, ACRC TR-44, 1993.

Hahn, G.W. and C.W. Bullard, "Modeling Room Air Conditioner Performance." *University of Illinois at Urbana-Champaign*, ACRC TR-40, 1993.

Heun, M.K. and W.E. Dunn, "Principles of Refrigerant Circuiting with Application to Microchannel Condensers: Part I-Problem Formulation and the Effects of Port Diameter and Port Shape," *ASHRAE Transactions*, 102:2, pp. 373-381, 1996.

Heun, M.K. and W.E. Dunn, "Principles of Refrigerant Circuiting with Application to Microchannel Condensers: Part II-The Pressure-Drop Effect and the Cross-Flow Heat Exchanger Effect," *ASHRAE Transactions*, 102:2, pp. 382-393, 1996.

Jensen, A.C. and W.E. Dunn, "Refrigerant-Side Instrumentation in Room Air Conditioners." *University of Illinois at Urbana-Champaign*, ACRC TR-101, 1996.

Mullen, C.E. and C.W. Bullard, "Room Air Conditioner System Modeling." *University of Illinois at Urbana-Champaign*, ACRC TR-61, 1994.

O'Neal, D.L. and S.B. Penson, "An Analysis of Efficiency Improvements In Room Air Conditioners." *Texas A&M University*, ESL/88-04, 1988.

Peixoto, R. and C.W. Bullard, "A Design Model for Capillary Tube-Suction Line Heat Exchangers." *Proceedings of 1994 International Refrigeration Conference-Purdue University*, July, 1994.

Rugg, S.M. and W.E. Dunn, "Design, Testing, and Validation of a Room Air Conditioner Test Facility." *University of Illinois at Urbana-Champaign*, ACRC TR-59, 1994.

Souza, A.L. and M.M. Pimenta, "Prediction of Pressure Drop During Horizontal Two-Phase Flow of Pure and Mixed Refrigerants," *ASME Conf. Cavitation and Multiphase Flow*, S. Carolina, FED Vol. 210, pp. 161-71, 1995.

Sporlan Valve Company, *Refrigerant Distributors*, June Bulletin 20-10, 1975.

Stott, S.L. and C.W. Bullard, Future Technical Report, *University of Illinois at Urbana-Champaign*, ACRC, 1999.

Wattelet, J.P., J.C. Chato, A.L. Souza, and B.R. Christoffersen, "Evaporative Characteristics of R-12, R-134a, and MP-39 at Low Mass Fluxes," *ASHRAE Transactions*, 100:1, pp. 603-615, 1994.

Woodall, R.J. and C.W. Bullard, "Simulating Effects of Multispeed Compressors on Refrigerator/Freezer Performance," *Transactions of the American Society of Heating, Refrigeration, and Air Conditioning Engineers*, 103:2, pp. 630-639, 1997.

Appendix A
Microchannel system design

A.1 Introduction

An important factor in selecting the final design for the condenser and evaporator micro-channel heat exchangers was the effect of the design on TEWI, or total equivalent warming impact (Sand et al., 1997). TEWI analyses were performed using a systems approach that considered the global warming impact over the unit's lifetime of both the release of the refrigerant into the atmosphere and the indirect component that resulted from the carbon dioxide emissions associated with the energy consumption of the system. The TEWI calculations were performed assuming a 20 year lifetime, 4% loss of charge per year, 900 hours per year running time (Illinois), and a 0% loss at end of lifetime.

The optimizations were performed at the ARI standard test B condition (80,67 indoor and 82,65 outdoor). Additional simulation runs were conducted at the ARI standard test A condition (80,67 indoor and 95,75 outdoor) to ensure that the constraint limiting the sensible heat ratio to 0.75 on the evaporator was met at that condition. The split system air conditioner model utilized R410A refrigerant properties and a compressor map that simulated a two-ton capacity scroll compressor (Bridges and Bullard, 1995).

The objective function to be minimized for this design investigation was TEWI/Qload which has units of $kgCO_2$/ton-hr of cooling capacity. This objective function considers the amount of charge in the system, the overall efficiency of the unit, and finally the cooling capacity supplied by the system. Because the direct effect of refrigerant loss is only around 10% of the total, the objective function was relatively insensitive to assumptions about the unit's lifetime and its running time per year. However, it does not follow that the optimal tradeoff between direct and indirect TEWI contributions is insensitive to such assumptions. One thing not considered in this objective function and in the analysis that follows was the cost of both materials and manufacturing for the heat exchangers and other components that could contribute

to minimizing TEWI/Qload. Care was taken to ensure that the sensible heat ratio never exceeded 75% at the ARI A test condition.

The triangular port tube with a hydraulic diameter of 0.67 mm and 19 ports was selected as being the best candidate for the final design of the minimum TEWI system because they offered a balance between compactness and internal surface area, and were also readily available. The effects of varying the length of the tubes and the number of tubes from the ultra-compact design (see Table A.1) were then examined on both the condenser and the evaporator to finalize their designs. The ultra-compact system was based on dimensions of an existing microchannel split-system that utilized R22 instead of R410A, except the modeled condenser had only one pass to allow for later heat pump applications, whereas the actual R22 heat exchanger had two passes. This ultra-compact split-system provided the baseline system for comparison to the minimum-TEWI system. The focus of this optimization was on the core length and core width that would minimize the objective function (TEWI/Qload). The effects of fan power and compressor power were also investigated to provide recommendations for components to focus on for further improvements. The simulations, unless otherwise noted, were performed at the ARI standard test B (80/67 indoor and 82/65 outdoor) with the evaporator superheat set at 10°F and the condenser subcooling at 10°F.

The optimization described in both the condenser and evaporator sections utilized a univariate search technique, which involved changing one parameter at a time in order to gain insights into the nature of the physical tradeoffs involved.

Table A.1 Ultra-compact design for condenser and evaporator

Parameter	Ultra-compact condenser	Ultra-compact evaporator
Port geometry	Triangles	Triangles
Number of tubes	65	45
Vertical tube thickness [in]	0.075	0.075
Horizontal tube width [in]	0.74	0.74
Core length [ft]	4.81	3.06
Core width [ft]	2.10	1.49
Face area [ft^2]	10.08	4.52
Fin density [fins/ft]	240	240
Volumetric flow rate [cfm]	2755	993
Housing height [ft]	2.13	1.58
Housing width [ft]	1.81	1.33
Housing depth [ft]	1.81	1.50
System charge [lbm]	3.7	
TEWI/Qload [kgCO$_2$/ton-hr] system (@80/82)	0.63	

A.2 Condenser design

A.2.1 Effects of face area variation

The proposed design for the outdoor (a/c condenser) bends the tubes along their major axis into a "V" shape (see Fig. A.1), which would facilitate refrigerant distribution and defrost drainage from the outdoor coil in heat pump mode. The placing of various components in the outdoor condenser cabinet created additional constraints to the final design besides those of the actual housing dimensions themselves (see Table A.1). The coil was pushed to the maximum height of 2.82 ft so that the compressor would have clearance beneath it (in case the coil is inverted from its "V" design to an "A" for a/c applications). The bend radius for the "V" coil was set at 2 inches, which was similar to the base case design. For these design runs, the core width was varied with core length so that the resulting combination would have a "square footprint" (i.e. the core width = the front width) within the rectangular footprint of the housing. This "square" design was selected so that the largest condenser fan could be utilized for a given

35

condenser configuration. The compressor would then be placed in the space remaining in the rectangular housing in a configuration that would later facilitate the conversion of the system to a heat pump. The outdoor housing dimensions provide a reasonable size and layout for the condenser coil and the compressor. More flexibility exists for the dimensions on the outdoor unit because a custom cabinet will be built for it; however, the indoor cabinet will most likely be selected from commercially available furnaces and air handlers so the interior housing constraints are more rigorously binding.

Front View   Side View
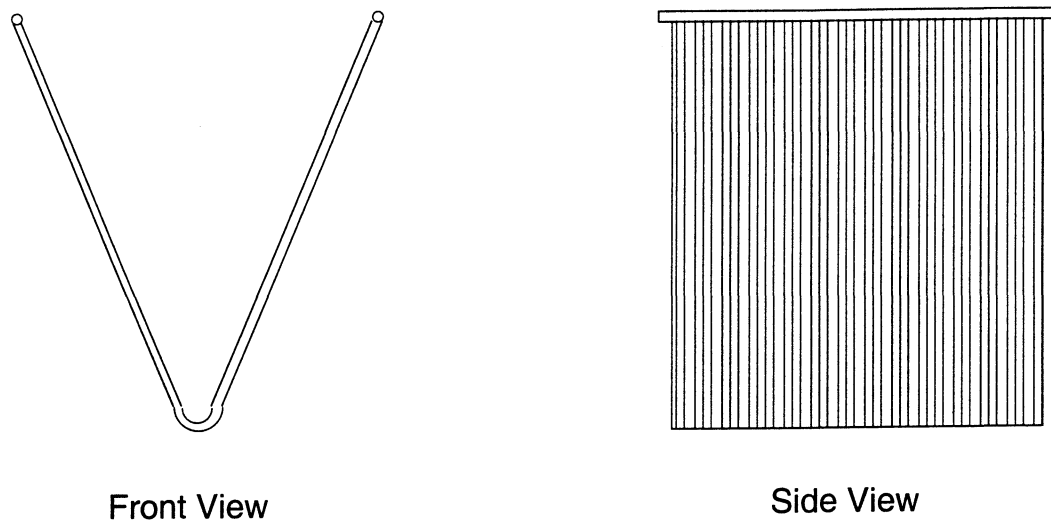
Figure A.1 "V" coil design

This full utilization of cabinet dimensions yielded a face area almost twice that of the ultra-compact condenser. Initial simulations held the volumetric flow rate and subcooling constant at the base value of 2755 cfm and 10°F respectively, for these "square footprint" constraints. The evaporator parameters were held constant at the ultra-compact values while the outdoor optimization was performed. The fan power was calculated using Eq. A.1 from the volumetric flow rate and the pressure drop through the outdoor unit, using a fan/motor efficiency determined from the ultra-compact system's measured power.

$$PwrFanC = 3.2532 \cdot VdotaC \cdot \left[\frac{dP_{airCoil} + dP_{airCabinet} \cdot \left(\frac{VdotaC}{2755} \right)^2}{\eta_{fanC}} \right]$$

(A.1)

The factor of 3.2532 converts the power to watts. The pressure drop across the cabinet was calculated using data from the ultra-compact system and the fan laws were used to calculate this pressure drop for varying volumetric flow rates. The pressure drop across the coil was calculated from the friction factor from Eq. A.2 developed by Davenport (1983).

$$f = 0.494 \cdot Re_{lp}^{-0.39} \cdot \left[\frac{l_h}{H} \right]^{-0.33} \cdot \left[\frac{l_l}{H} \right]^{1.1} \cdot H^{0.46}$$

(A.2)

Where:

Re_{lp} = Reynolds number based on louver pitch [-]
l_h = louver height [mm]
H = fin height [mm]
l_l = louver length [mm]

This correlation is good over a range of $1000 < Re < 4000$, where Re is the Reynolds number based on the hydraulic diameter (this is not the same Reynolds number as is used in the correlation, which is based on the louver pitch of the fins). Also note that the fin height dimension must be in mm in order for the correlation to give the correct friction factor.

The results of these initial simulations are shown in Fig. A.2.
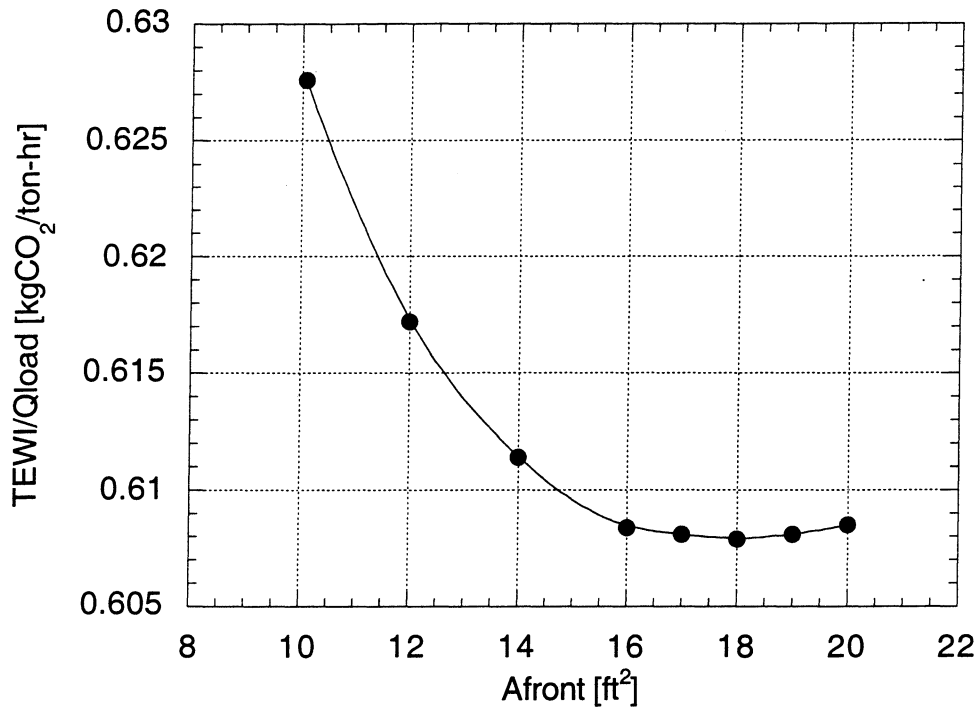
Figure A.2 TEWI/Qload for square footprint (Vdotac = 2755)

A general decreasing trend was observed with increasing face area because the free flow velocity was decreasing due to the constant volumetric flow rate and increasing face area. This decreasing face velocity lowered the air-side pressure drop and thereby decreased the fan power required for a constant volumetric flow rate. A face area of 16 ft^2 (and its "square footprint" of 6.5 ft^2) was selected as being the optimal face area because it balanced the effects of decreasing the condenser fan power with the negative effects of increasing the charge due to the increased internal volume of larger condensers without exceeding the housing constraints. The 60% increased area resulted in an objective function decrease of 3.5% over the ultra-compact design mainly due to a 28% decrease in the condenser fan power. The dimensions of the "square" condenser for the flattened out 16 ft^2 face area are shown in Fig. A.3 below. This coil would require a bend angle of 45 degrees once it was bent into the "V" configuration.
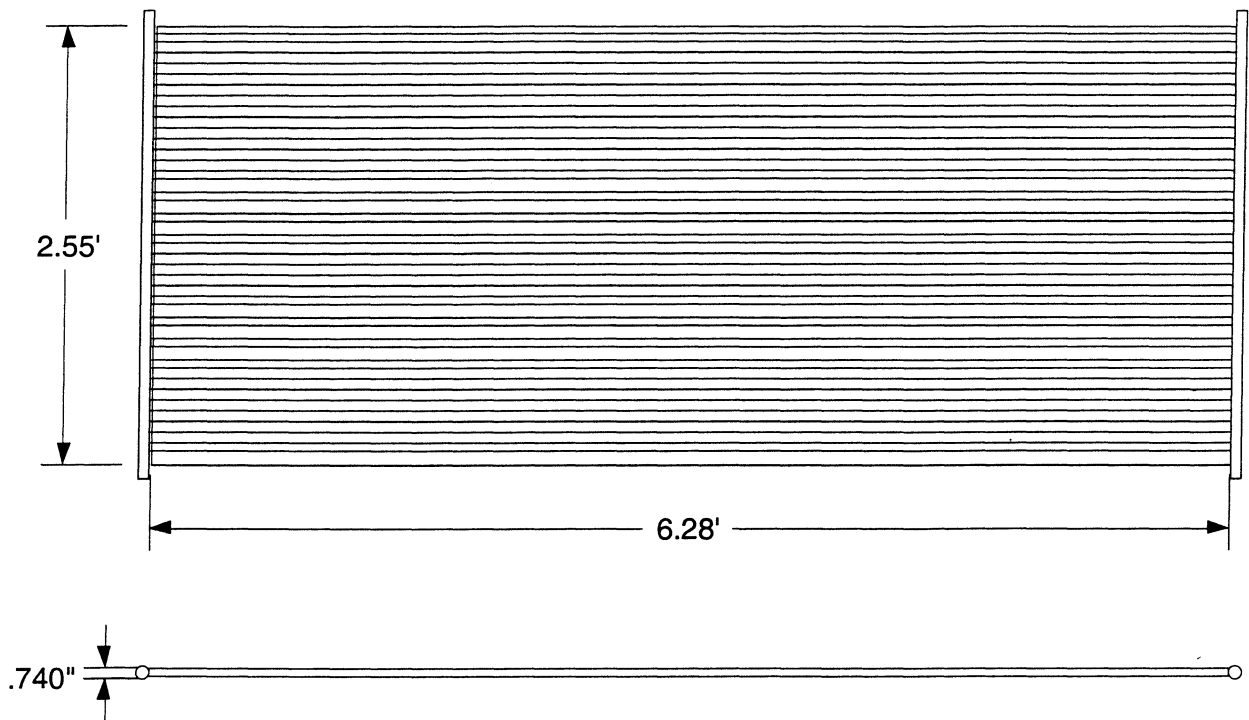
Figure A.3 Dimensions of 2.55 ft square footprint condenser design

The binding constraints were the housing width and height; however, there still was room to have a larger core width in the housing depth constraint, but increasing the number of tubes would have an adverse effect on the objective function because of the additional charge in both the headers and the tubes.

This design, compared to the ultra-compact system, increased the core length from 4.81 ft to 6.28 ft and also increased the number of tubes from 65 to 79. This increased volume increased system charge about 19%, but this was offset in the objective function by both the reduced power consumption of the fan due to the lowered free flow velocities associated with increased face area and also the increased heat transfer surface area. For both the ultra-compact condenser coil and the 60% larger one, the refrigerant-side pressure drop was between 0.4 to 1.0 psi and therefore negligible.

A.2.2 Effects of condenser volumetric flow rate variation

Next, the volumetric air flow rate was varied between 2400 and 4200 cfm. Fig. A.4 shows the results of the simulation runs.
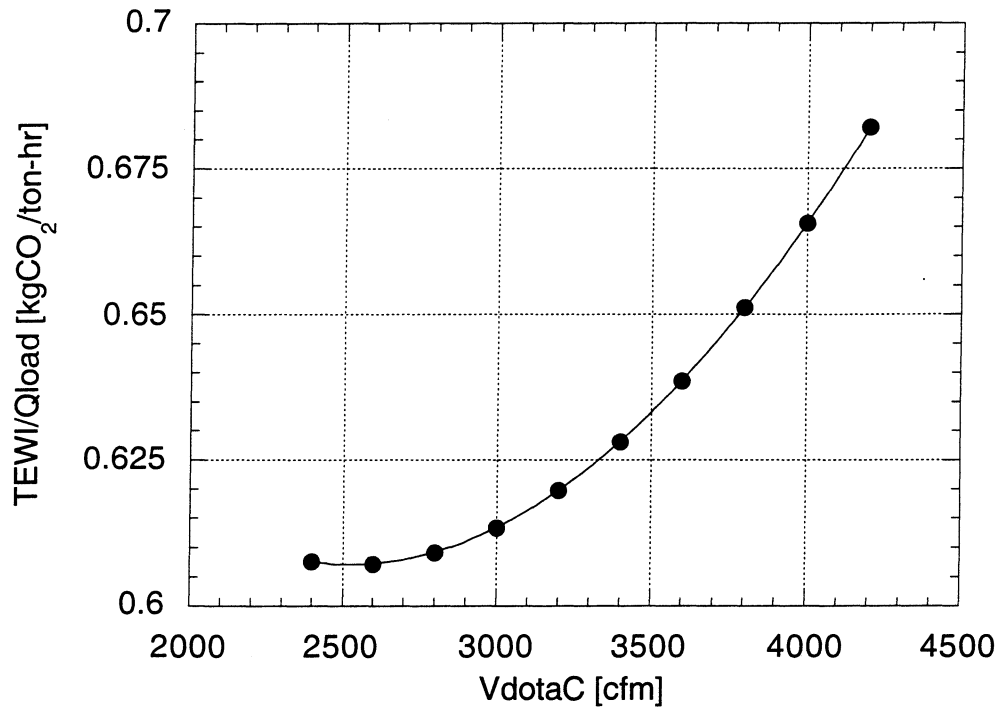
Figure A.4 TEWI/Qload vs. VdotaC for condenser (AfrontC = 16 ft^2)

From around 2400 to 2600 cfm, the objective function was observed to level off because the increasing air-flow rates provided increased heat transfer that improved the system's efficiency and overcame the increased power consumption required by the fans due to the increasing air-side pressure drop across the condenser coil. Above 2600 cfm, the increasing power requirements for the fan exceeded the benefits of increased heat transfer acquired through the higher free-flow velocities in the coil. Running the condenser fan at 2600 cfm resulted in a 3.7% improvement in TEWI/Qload over the ultra-compact system, which is only a 0.2% improvement over the 16 ft^2 face area condenser running at the base volumetric flow rate of 2755 cfm.

A.2.3 Effects of subcooling

The subcooling was then varied between 2° and 20 ° F and the effect of this variation on the objective function was investigated in Fig. A.5.
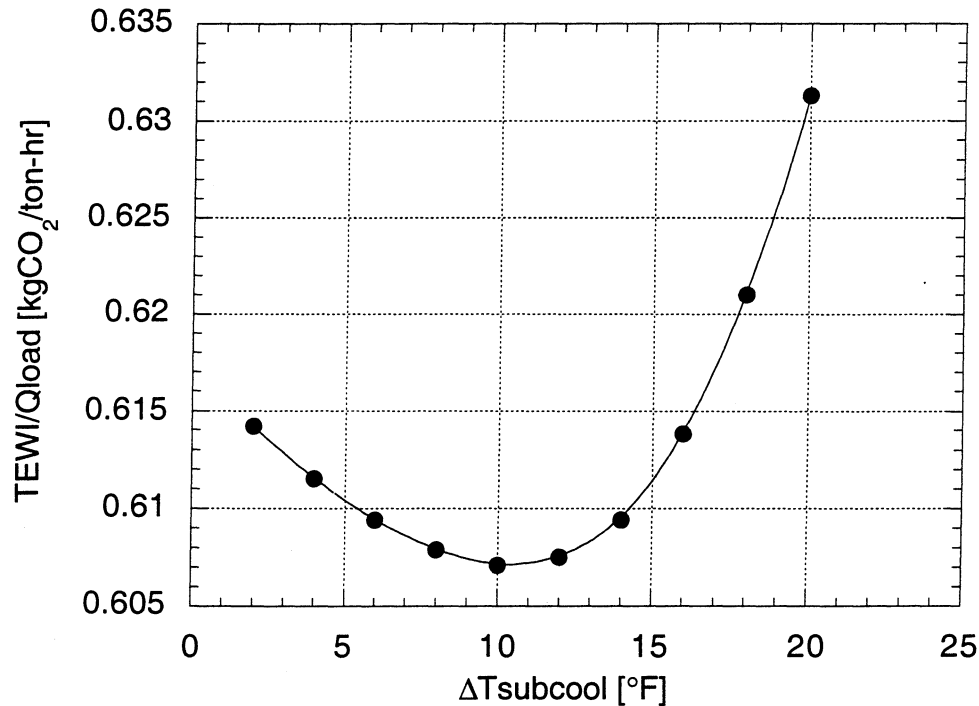
Figure A.5 TEWI/Qload vs. ΔTsubcool for condenser

(AfrontC=16 ft², VdotaC=2600 cfm)

Fig. A.5 revealed a minimum TEWI/Qload in the region around 10° F. The reason that the points to the left of this region show a generally decreasing trend was that the inlet quality to the evaporator was decreasing, and the resulting increase in evaporator capacity outweighed the effects of increasing charge and condensing temperature. Above 10° F subcooling, the inlet quality showed no real signs of decreasing with increasing subcooling because the condensing pressure was also rising simultaneously, so the benefits of increasing subcooling were lost and the system's refrigerant charge was also increasing. In order for the optimal subcooling to decrease, the volumetric flow rate would need to be increased to considerably larger values so that the heat could be rejected at a much lower temperature difference. This higher flow rate created more of penalty on the efficiency of the system due to its increased fan power consumption, and this effect was found to outweigh the benefits of decreasing the subcooling and the condensing pressure slightly for large increases in the fan volumetric flow rate.

Basically, 10° F subcooling was optimal because it balanced the benefits of lower evaporator inlet quality with lower compressor power consumption and charge. The objective function decreased by the same 3.7% relative to the ultra-compact system as in the previous design run because this was the same subcooling that was set initially in the design runs.

A.2.4 Condenser design summary

Table A.2 summarizes and compares the minimum-TEWI condenser design geometry to that of the ultra-compact condenser design

Table A.2 Minimum-TEWI condenser design comparison

Parameter	Ultra-compact condenser	Min.-TEWI condenser
Port geometry	Triangles	Triangles
Number of tubes	65	79
Vertical tube thickness [in]	0.075	0.075
Horizontal tube width [in]	0.74	0.74
Core length [ft]	4.81	6.28
Core width [ft]	2.10	2.55
Face area [ft^2]	10.08	16.00
Fin density [fins/ft]	240	240
Volumetric flow rate [cfm]	2755	2600
Housing height [ft]	2.13	2.82*
Housing width [ft]	1.81	2.6*
Housing depth [ft]	1.81	2.91*
System charge [lbm]	3.7	4.4
TEWI/Qload [kgCO$_2$/ton-hr] system (@80/82)	0.63	0.61

* (Carrier, 1996) 2-ton system components

A.3 Evaporator design

<u>A.3.1 Effects of face area variation</u>

For the evaporator geometry selection, the face area was varied by increasing the number of tubes and the length of the tubes while holding the volumetric flow rate constant. The condenser parameters were held constant for the minimum-TEWI condenser outlined above. The evaporator had an additional constraint over the condenser in that the sensible heat ratio also had to be monitored at the ARI A test condition (80/95). As a rule of thumb, the upper limit for a comfortable sensible heat ratio is around 0.75 at this condition, so that became a binding constraint for the evaporator design simulations shown in Fig. A.6.
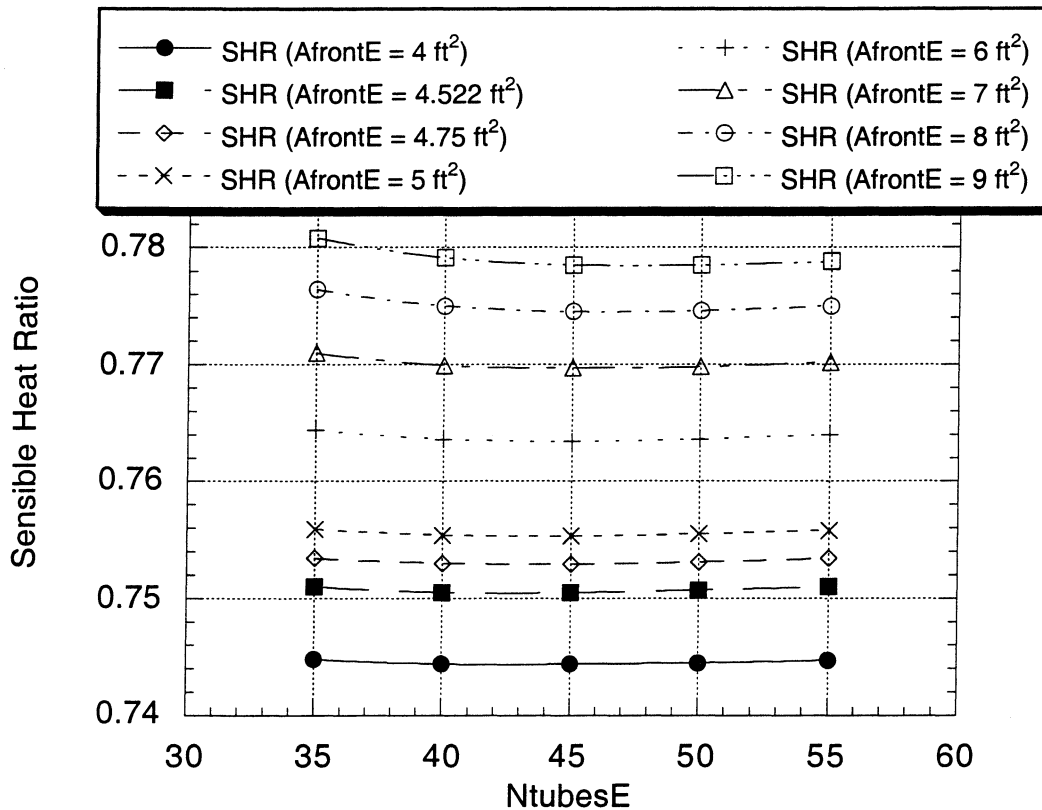
Figure A.6 SHR vs. NtubesE at 80/95 condition (const. VdotaE = 993 cfm)

Fig. A.6 shows that face areas above 4.5 ft² exceeded the sensible heat ratio limitation of 0.75 at the ultra-compact volumetric flow rate of 993 cfm. Although the 4.75 ft² face area exceeded the sensible heat ratio by around 0.3%, it was selected as being the optimal design

because it was the largest heat exchanger design that would fit within the housing constraints. As would be expected, the sensible heat ratio for the larger heat exchangers was increasing because the corresponding increase in the heat transfer surface area increased the fin surface temperature and thus less water was removed.

Next, the effect of the face area variation on the objective function was examined at the 80/82 condition.
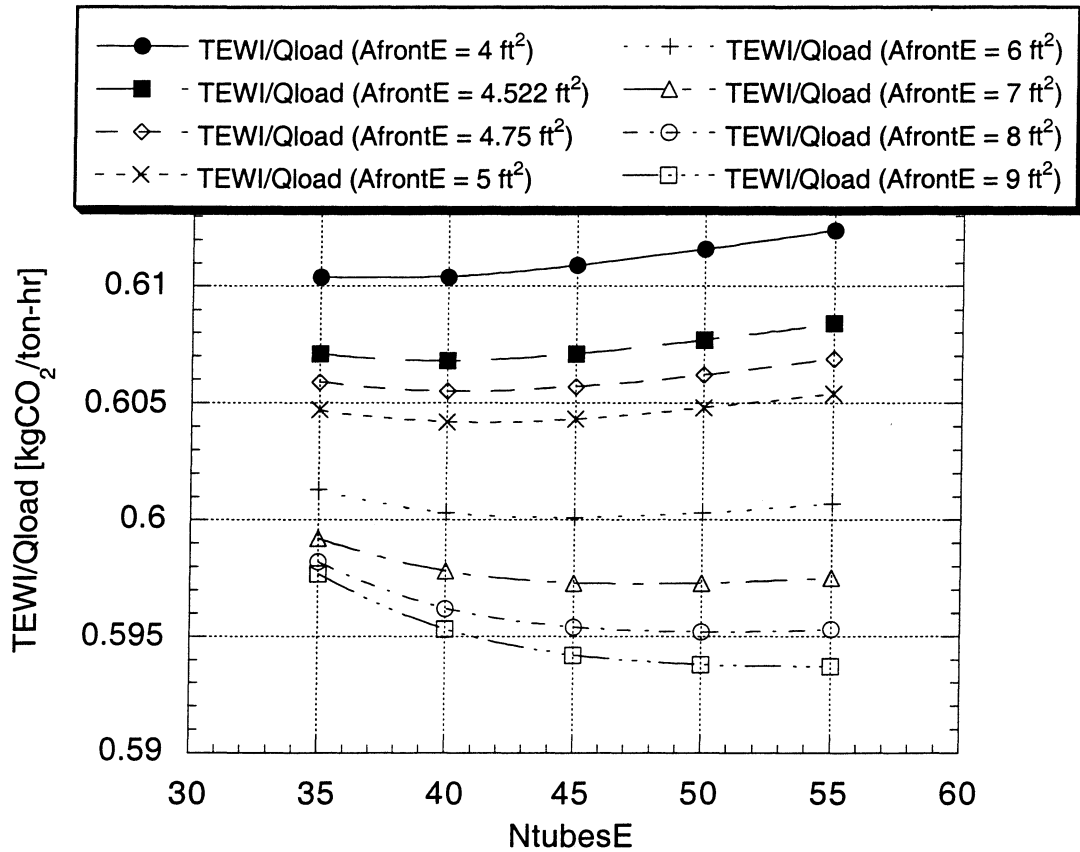
Figure A.7 TEWI/Qload vs. NtubesE at 80/82 condition (const. VdotaE = 993 cfm)

The larger face areas were included in Fig. A.7 to illustrate the small 1.9% savings obtainable by ignoring the sensible heat ratio and selecting a face area that was almost twice as large as the ultra-compact heat exchanger (and also exceeded the housing constraints).

Achieving greater benefit from a larger evaporator would require substantial increases in air-flow rate, which itself would be costly due to the high pressure drops experienced in typical residential ductwork. The 4.75 ft^2 face area evaporator was selected as being the best heat

exchanger because it was close to the 0.75 sensible heat ratio constraint and reduced TEWI/Qload from the ultra-compact design by around 0.25% (for a 5.6% face area increase). The minimum objective function for this face area occurred with 40 tubes (a core width of 1.29 ft) and a core length of 3.6 ft. This balanced the benefits of increasing heat transfer area against the negative effects of increasing charge in the headers and tubes. The major dimensions of the flattened evaporator are shown in Fig. A.8 below. To fit the cabinet constraint, a bend angle of 49 degrees was used for the "V" configuration of this coil.
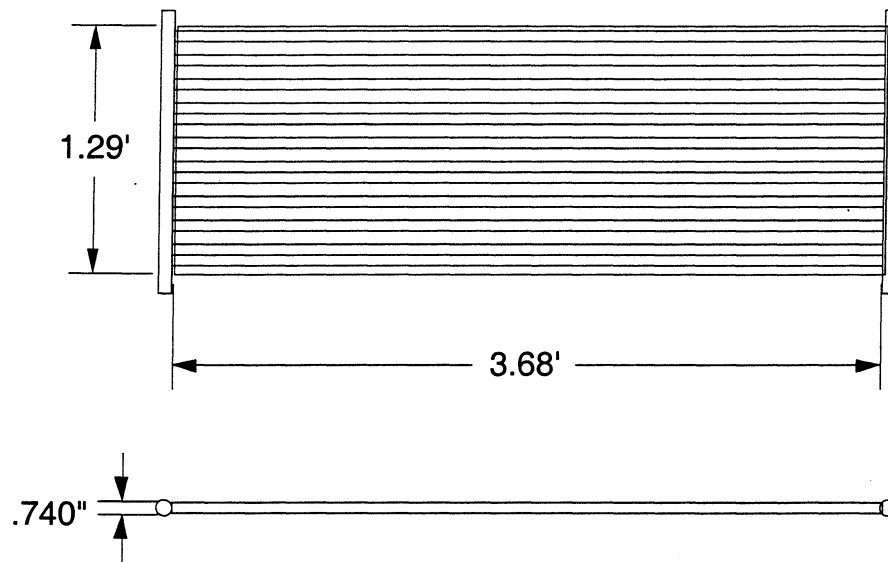
Figure A.8 Dimensions of flattened evaporator coil for 4.75 ft^2 face area design

The dimensions listed in Table A.1 for the evaporator housing have had clearances for headers and other mounting hardware factored in so that the design will have a small degree of freedom for mounting position and other unforeseen fittings and hardware that may be necessary.

The design for the evaporator was not limited to having a "square footprint" as the condenser coil was, however the simulations pushed the design in certain directions. The number of tubes that minimized the objective function over the range of reasonable face areas was around 40 tubes, so this set the core width at around 1.29 ft, within the interior housing constraint of 1.3 ft. The interior housing constraints of 1.66 ft on the width and 1.6 ft on the height were also binding for this coil design. Increasing the face area beyond 4.75 ft^2 increased

the "V-coil" height beyond that of the interior housing, so this limited the investigation to face areas less than 4.75 ft^2.

A.3.2 Effects of evaporator volumetric flow rate variation

The effects of varying the evaporator fan volumetric flow rate between 200 and 2000 cfm are summarized in Fig. A.9.
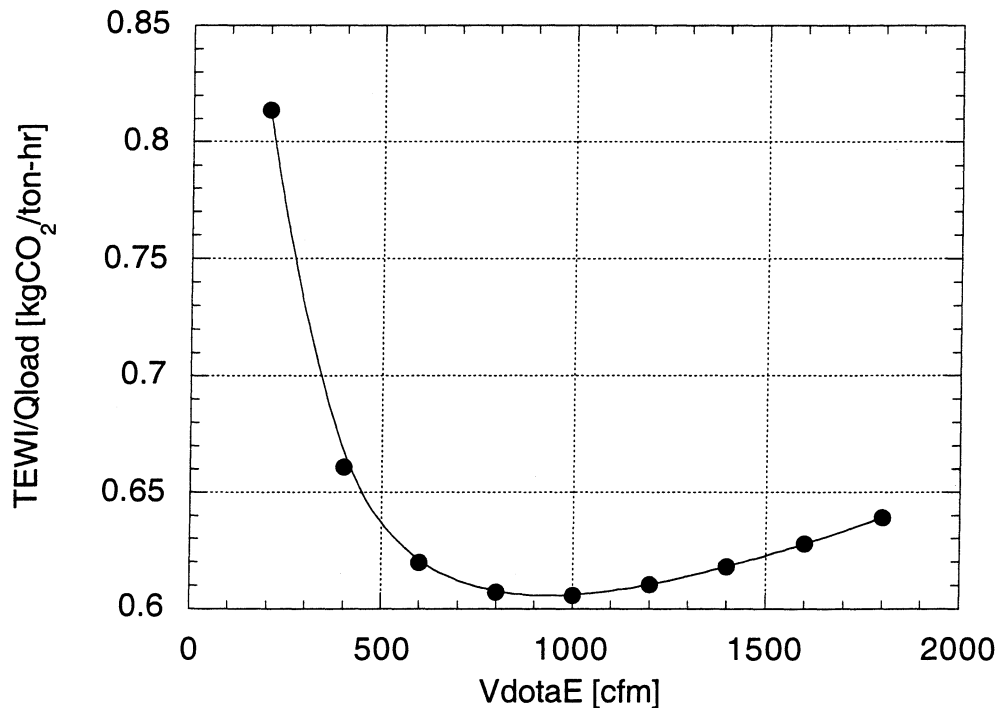
Figure A.9 TEWI/Qload vs. VdotaE at the 80/82 condition for 4.75 ft^2 face area design

A relatively flat region was observed between 800 and 1000 cfm which was due to the opposing effects of increasing the flow rate over the coil and the increased power consumption associated with the faster fan speeds. The fan power for the evaporator was calculated based on the ARI default value of 365 watts per 1000 cfm. This assumption was used because of uncertainties in the design and pressure drop of the duct work used for this new system. The 800 cfm volumetric flow rate was selected as being the optimal point because it would provide a lower sensible heat ratio while still reducing the objective function. This 800 cfm volumetric flow rate for a face area of 4.75 ft^2 resulted in a face velocity of 2.8 ft/s which was 23% less than

46

the ultra-compact evaporator. The sensible heat ratio at the 80/95 condition was therefore reduced to around 70%, down from 75% for the 993 cfm air flow rate. Simulations were also run at the 800 cfm volumetric flow rate for various face areas and the result was that the coils that were somewhat larger than the 4.75 ft^2 face area design did not exceed the sensible heat ratio at 80/95 as they did previously, however these larger designs also exceed the housing height constraint and therefore were not used.

A.3.3 Evaporator design summary

Table A.3 compares the minimum-TEWI evaporator geometry to the ultra-compact.

Table A.3 Minimum-TEWI evaporator design comparison

Parameter	Ultra-compact evaporator	Min.-TEWI evaporator
Port geometry	Triangles	Triangles
Number of tubes	45	40
Vertical tube thickness [in]	0.075	0.075
Horizontal tube width [in]	0.74	0.74
Core length [ft]	3.06	3.68
Core width [ft]	1.49	1.29
Face area [ft^2]	4.52	4.75
Fin density [fins/ft]	240	240
Volumetric flow rate [cfm]	993	800
Housing height [ft]	1.58	1.60*
Housing width [ft]	1.33	1.66*
Housing depth [ft]	1.5	1.30*
System charge [lbm]	3.7	4.4
TEWI/Qload [kgCO$_2$/ton-hr] system (@80/82)	0.63	0.61

* (Carrier, 1996) 2-ton system components

A.4 Minimum-TEWI system performance summary

A.4.1 System performance at 80/82

The overall system performance comparisons for the ultra-compact and optimal system are summarized in Table A.4.

Table A.4 Performance comparison of minimum-TEWI system at 80/82

	Ultra-compact System	Min.-TEWI System
EER [Btu/W-hr]	13.32	14.26
Qevap [Btu/hr]	31,371	30,534
Charge [lbm]	3.7	4.4
Indirect TEWI [kgCO$_2$]	27,370	25,045
Direct TEWI [kgCO$_2$]	2307	2758
TEWI [kgCO$_2$]	29,677	27,803
TEWI/Qload [kgCO$_2$/ton-hr]	0.63	0.61

$$TEWI = \text{Indirect Effect} + \text{Direct Effect} \qquad (A.3)$$

$$\text{Indirect Effect} = \text{UnitPower} \cdot \text{RunTime} \cdot \text{Life} \cdot \text{MassCO}_2 \qquad (A.4)$$

Where:

UnitPower = A/C unit power consumed [kW$_e$]

RunTime = Amount of time unit runs per year [900 hr/yr, Illinois]

Life = Life of the unit [20 yr]

MassCO$_2$ = Fraction of mass of CO$_2$ produced per kWh$_e$ [kgCO$_2$/kW$_e$]

$$\text{Direct Effect} = \text{Charge} \cdot \text{LossRate} \cdot \text{Life} \cdot \text{GWP} \qquad (A.5)$$

Where:

Charge = Total charge of the A/C [kg]

LossRate = Rate of loss of charge per year (4%/yr)

Life = Life of the unit [20 yr]

GWP = Global warming potential R410A [1730 kgCO$_2$/kg]

$$Qload = Capacity \bullet RunTime \bullet Life \qquad (A.6)$$

Where:

Capacity = Cooling capacity of A/C [tons]

RunTime = Amount of time unit runs per year [900 hr/yr, Illinois]

Life = Life of the unit [20 yr]

The objective function decreased by a total of 3.8% for the minimum-TEWI condenser and evaporator due primarily to the 7% increase in EER (formulation for equations from Bivens, 1996). For the optimal design, the direct contribution to TEWI (Eq. A.5) from the refrigerant accounted for only around 10% of the total TEWI. Because the evaporator air-flow rate was reduced from 993 to 800 cfm there was also a 2.8% decrease in the optimal system capacity. All these results, of course, were calculated using the compressor performance maps for the ZP23K3E--PFV compressor (Copeland, 1996), which was not optimized for such a highly efficient system having such a low temperature lift.

Surprisingly, little TEWI reduction was obtained through this optimization. Significant increases in energy efficiency were achieved, but at the expense of greater charge inventory.

A.4.2 Sensitivity analysis

Since the efficiency of the system dominates the overall TEWI, another possibility for improving the system's performance would be to focus on the efficiency of the compressor at the design condition. The isentropic efficiency of the actual compressor at the 80/82 condition was around 0.58, probably because it was optimized for a more typical (higher) pressure ratio. Because the scroll compressor is a constant volume-ratio device, this particular unit would incur significant penalties for overcompression. After several discussions with the compressor manufacturer, it was suggested that a compressor operating around an isentropic efficiency of 0.7 could be developed for the more efficient microchannel system. In the following analysis, the efficiency has been improved to reflect this "ideal" compressor.

A sensitivity analysis was performed on the minimum-TEWI design to examine what the effects of the more efficient compressor would have on the design algorithm detailed previously. Since the 16 ft^2 condenser face area was bound by the housing constraint, the condenser could not be increased beyond that, although the idealized compressor would allow more area if the

constraints were not binding. The reduced compressor power did not alter the choice for the optimal condenser fan air flow rate of 2600 cfm, or optimal subcooling of around 10°F, as was found in the previous simulations. Again the evaporator coil was bounded by the housing constraints so the face area was kept at 4.75 ft^2, and the optimal volumetric flow rate stayed the same as the compressor with an isentropic efficiency of 0.58. The additional savings for using this idealized compressor in the system was around 14.5% over the system with a compressor operating at the lower isentropic efficiency.

The effects of using a fan that was 10% more efficient on the optimal design were examined in the next sensitivity analysis. The condenser optimal volumetric flow rate remained at 2600 cfm and the optimal subcooling was again 10°F. The savings in the objective function for the more efficient fan was around 0.6% over the minimum-TEWI system.

A.4.3 Robustness of the minimum-TEWI system

Finally the robustness of the final design for the system using the actual compressor (not the hypothetical system outlined in the preceding sensitivity analysis) was examined between outdoor temperature extremes of 55°F and 115°F, while holding the indoor temperature constant at 80°F. The efficiency of the compressor was held at the original values because of uncertainties about how the optimized compressor would perform over the spectrum of outdoor temperatures. Fig. A.10 reveals the results of these simulation runs on the overall system efficiency for both the minimum-TEWI system and the ultra-compact design.
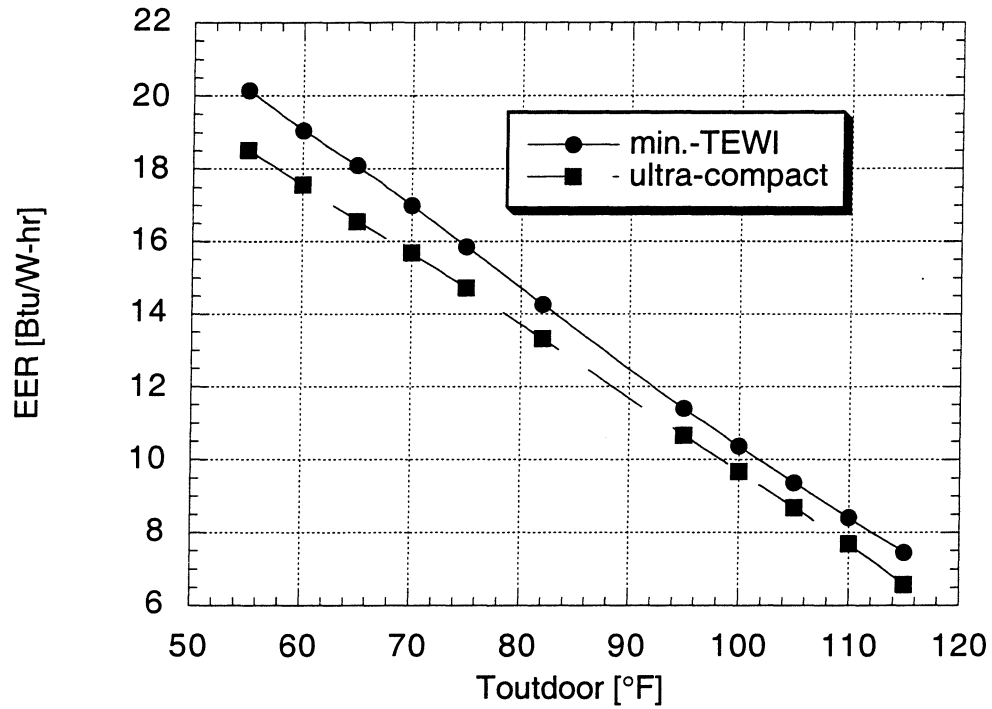
Figure A.10 EER vs Toutdoor for the min.-TEWI system

A very linear EER relationship was observed for both the minimum-TEWI and ultra-compact systems. The condenser exit for the minimum-TEWI system became two-phase just at the very lowest outdoor temperature of 60°F, whereas the ultra-compact system became two-phase at around 65°F. Over the whole range of outdoor temperatures, the minimum-TEWI system was more efficient than the ultra-compact design.
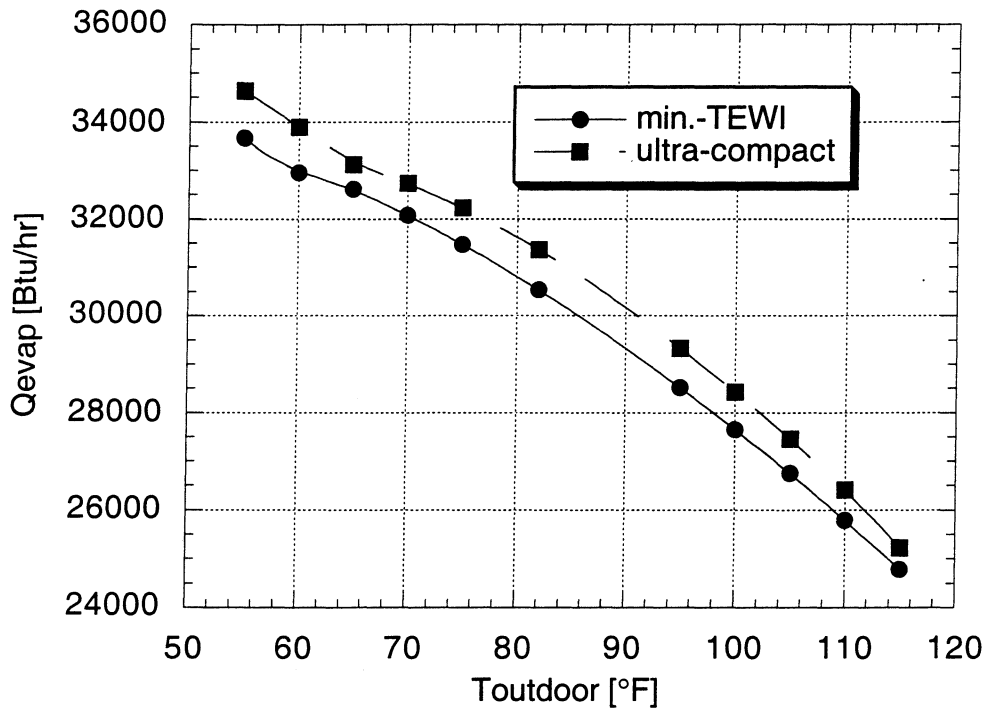
Figure A.11 Capacity vs Toutdoor for the min.-TEWI system

As would be expected, an overall decreasing capacity trend for was observed for both designs as the outdoor temperature increased. Because the minimum-TEWI and the ultra-compact system's condenser exit becomes two-phase at an outdoor temperature of around 60°F and 65°F respectively, there is a visible kink in the curve for the transition and then the curve rises fairly linearly. The capacity was also higher for the ultra-compact design because of the higher air-side volumetric flow rate on the evaporator.

A.5 Component selection

A.5.1 Evaporator housing

The housing for a Bryant FK4CNF003 Direct Expansion Fan Coil was selected for the indoor unit because its dimensions contained enough clearance for the microchannel heat exchanger designed previously. It also had the added advantage of programmable integrated

controls and a blower motor (ICM2) that would allow evaporator air flow to be set at prescribed rates. The integrated controls allowed this motor to deliver a set cfm independent of the duct system's static load.
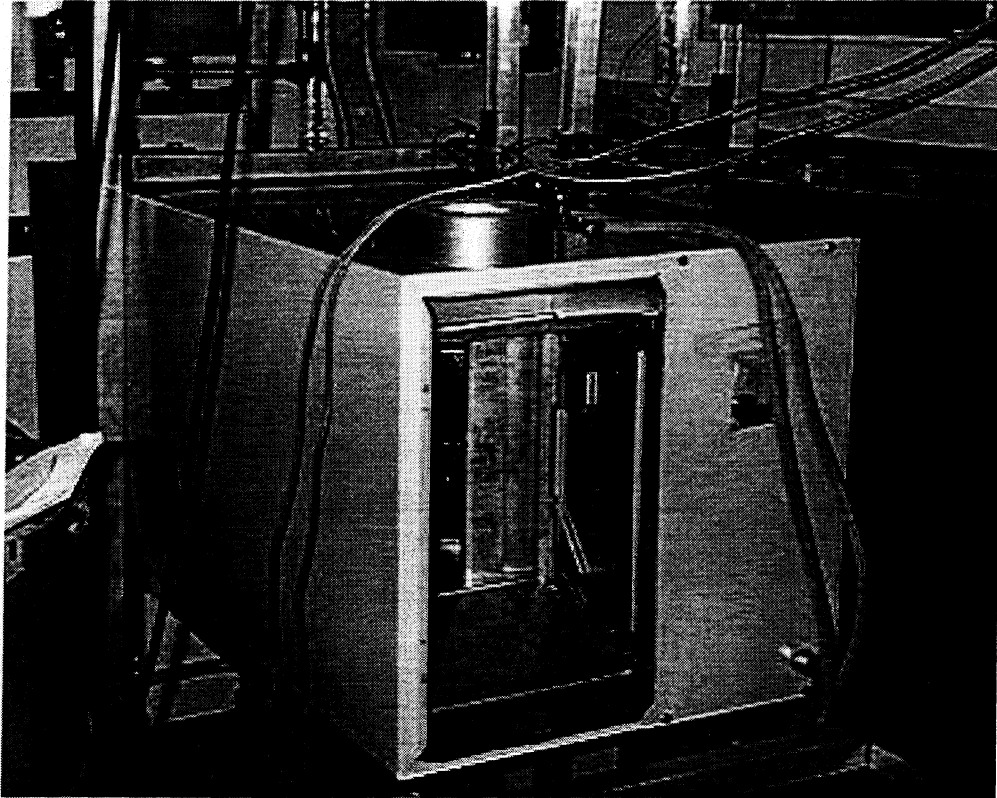
Figure A.12 Evaporator housing in horizontal configuration

Figure A.12 shows how the actual evaporator coil was mounted within the housing. Since the housing was mounted horizontally, the coil was mounted in an "arrowhead" configuration instead of the "V" configuration suggested in the preceding design exercise. Mounting the coil in this "arrowhead" configuration aided in water-shedding and refrigerant distribution for the microchannel evaporator.
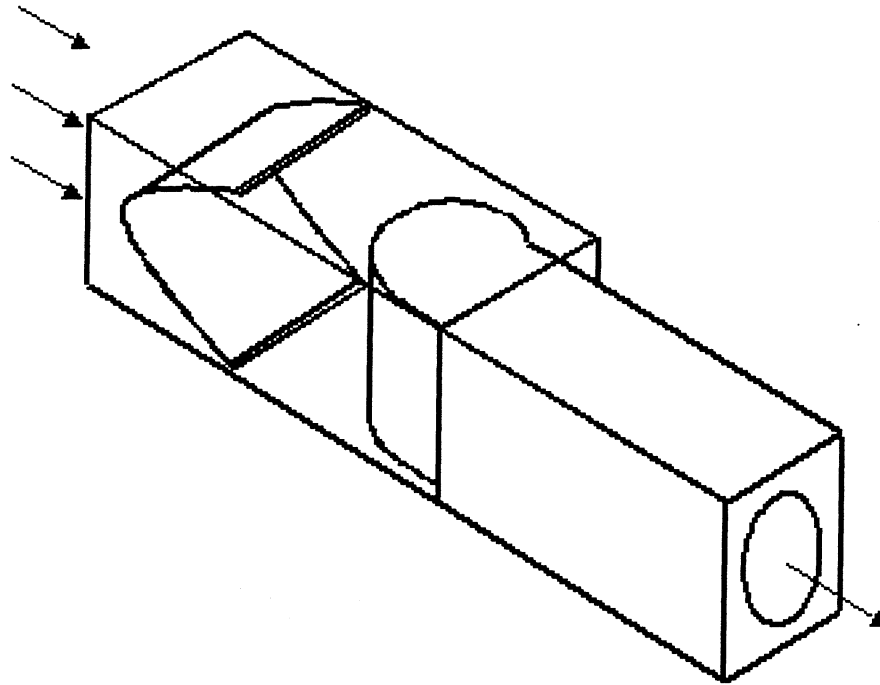
Figure A.13 Orientation of evaporator coil within housing

The blower motor was controlled via the 'Easy Select™ Board' that was attached to the interior of the evaporator housing (see Fig. A.14). For the experimental system, however, this board was removed from the housing and mounted in the outdoor chamber so that the motor control was easily accessible. Another attractive feature of the housing was that it could be configured in a horizontal position, which was necessary due to the limited ceiling height of the indoor chamber. A 40 in. duct with an outlet orifice of 98.1 in^2 was fitted to the outlet of the housing to provide a pressure drop load of around 0.15 in-H_2O at an air-flow rate not to exceed 37.5 SCFM per 1,000 Btu/hr of rated capacity. Finally a Sporlan R410A TXV, model Y113-CBBIZE-2-GA, with a screw adjustment for superheat levels was selected as the microchannel system's expansion device.
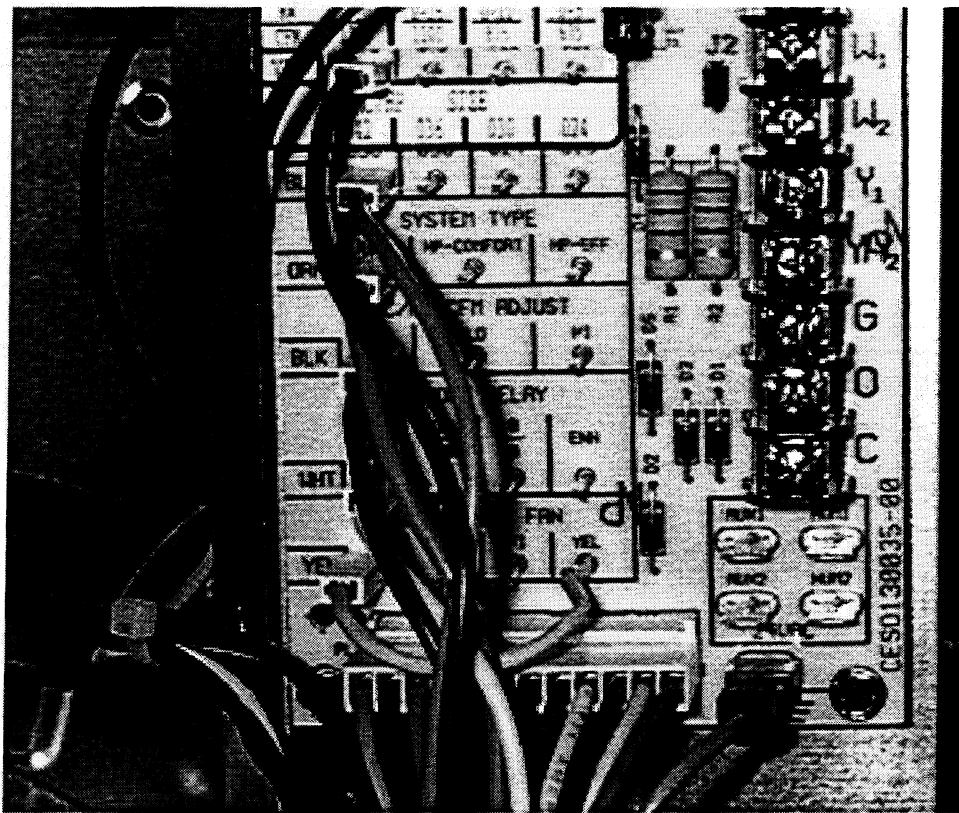
Figure A.14 Easy Select™ Board

A.5.2 Blower motor

The blower motor that came with the Bryant housing was the GE Model 5SME39HL0140, rated at 1/2 hp at a maximum of 1400 rpm. The integrated controls discussed earlier were built into the motor and the control algorithm was based on feedback from the motor's torque. The motor was capable of a wide range of volumetric flow rates depending on the settings in the 'Easy Select™ Board' as seen in Table A.6. A logarithmic spiral blower housing was used in this particular indoor unit.

Table A.5 General Electric ECM Programmable motor

Model	5SME39HL0140
Phase	single
Volts	120/240
Horsepower	1/2
Speed	0-1400 rpm
Frequency	60 Hz
Rotation	CCW
Type	ECM
Enclosure	open

Table A.6 'Easy Select™ Board' settings with corresponding volumetric flow rates from Modine Calibration

Settings	cfm
G-Low	723
G-Med	903
G-Hi	1232
Y1-24	620
Y1-30	665
Y1-36-Lo	705
Y1-36	795
Y1-42-Lo	826
Y1-42	886
Y1-42-Hi	1005

A.5.3 Indoor unit calibration

The following curve details the pressure drop calibration of the final coil, fan, and housing combination. The calibration was performed by Modine with the objective of sizing an orifice plate and outlet duct combination that would provide approximately 0.15 iwc at the blower setting that supplied around 800 acfm to the evaporator coil. The tests were performed at an ambient temperature of 60°F. The orifice area was 98.1 in^2 and the duct dimensions were 40 in. long by 19 1/4 in. high by 11 in. wide. All of these tests were performed with the coil dry.

Another orifice plate (124.2 in^2) was also supplied. It was used to achieve around 0.15 iwc for a volumetric flow rate around 1,000 acfm. Modine also tested the Y1-36 setting with the larger orifice, which had a pressure drop that was approximately half that of the smaller orifice but the ICM motor was able to hold the volumetric flow rate within 0.5% of the air flow rate

observed with the smaller orifice plate, thus confidence in the blower motor's ability to maintain

a fairly constant volumetric flow rate for different pressure drops was established.
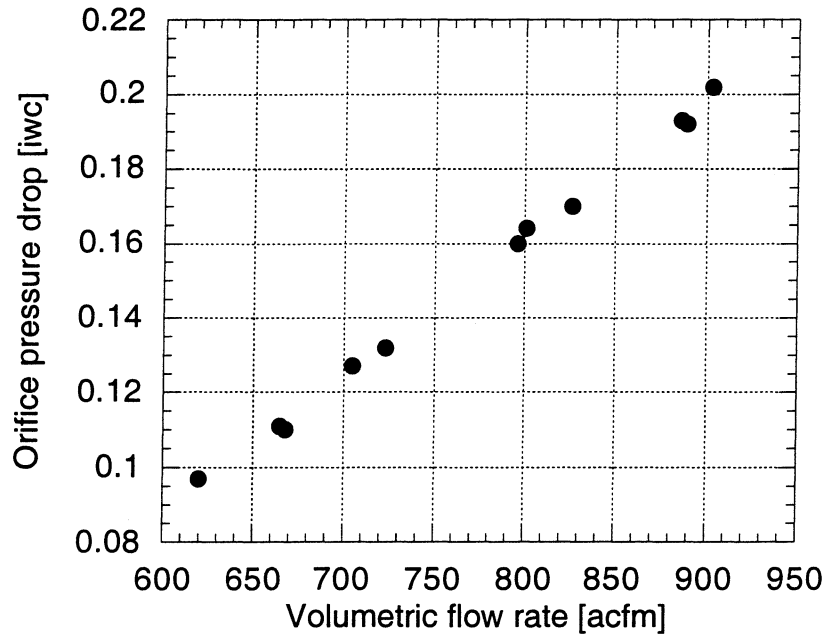
Figure A.15 Orifice pressure drop for the FK4C air handler, microchannel evaporator, and outlet

duct with 98.1 in² orifice plate from Modine calibration
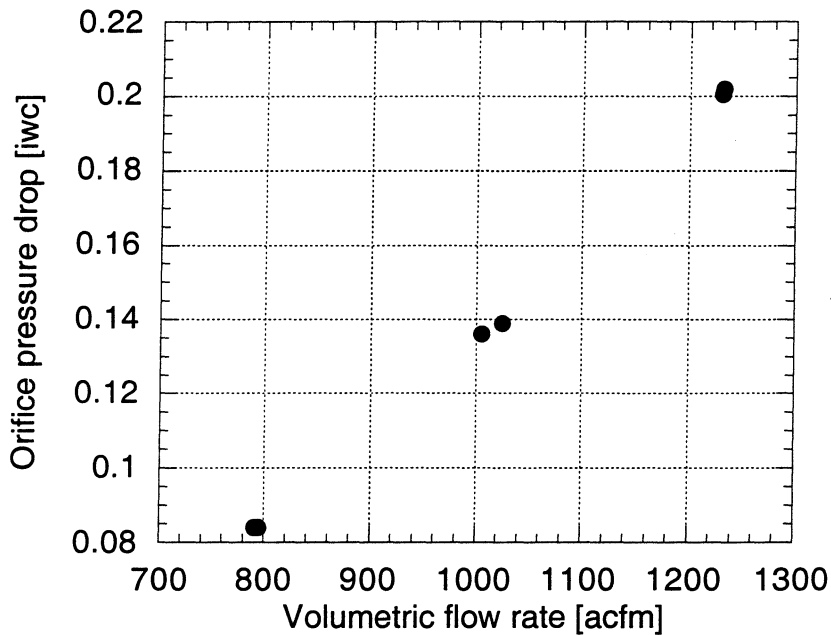
Figure A.16 Orifice pressure drop for the FK4C air handler, microchannel evaporator, and outlet

duct with 124.2 in^2 orifice plate Modine calibration

A.5.4 Condenser housing

A custom outdoor housing was designed and constructed by Modine Manufacturing Company for our the microchannel condenser coil. The housing has a separate chamber for the compressor and the condenser "V"-coil. The supporting structure was built entirely out of aluminum. A Sporlan Y113-CBBIZE-2-GA TXV and an ALCO RV4F46 four-way valve were also mounted in the outdoor housing to facilitate future heat pump investigations.
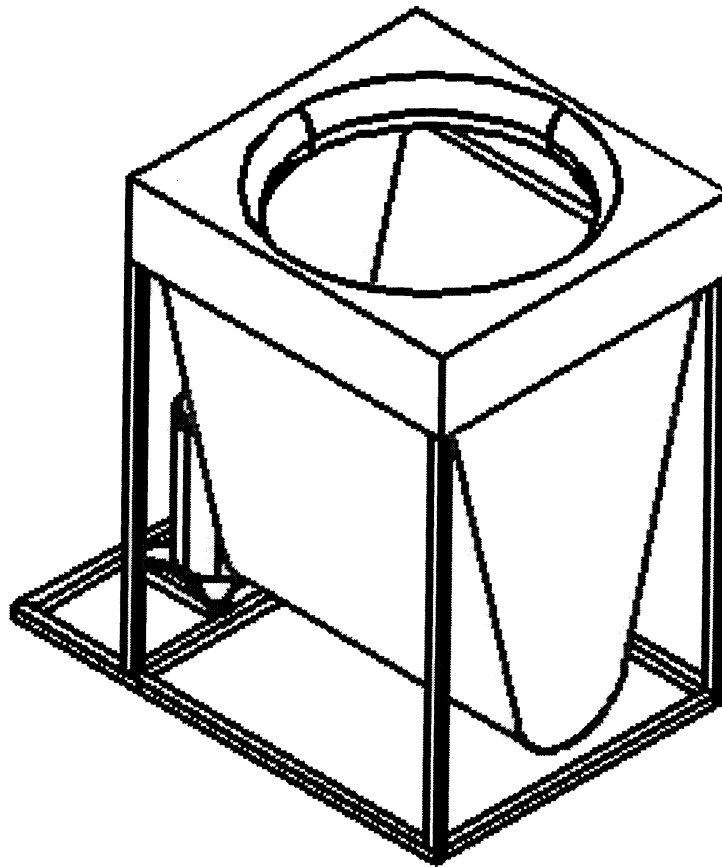
Figure A.17 Condenser housing framework

A.5.5 Outdoor fan

A custom 22 in. bell orifice was constructed by Memphis Metal out of 18 gauge galvanized steel for the outdoor housing. A three-phase motor was selected for use in the outdoor housing because it could be controlled by a variable speed drive which would be used to vary fan speeds in future air-flow optimization investigations. The three-phase motor selected for this application was a 1/3 hp Franklin (model 1331630101). This motor was selected because it had a nominal speed of around 1140 rpm, which was a speed high enough that it would allow for a significant range of air-flow rate variations (the lowest calibrated speed was 692 rpm, and the tests were run at 810 rpm). The three-phase motor was approximately two inches longer than stock single-phase motors so it was also necessary to raise the motor mountings on the grille the same distance so that the fan would line up with the bell orifice. The fan blade selected for the outdoor unit had a 22" diameter, a 15° pitch angle, and three blades.

Table A.7 Franklin three-phase motor

Model	1331630101
Phase	three
Volts	200-230/460
Horsepower	1/3
Speed	1140 rpm
Frequency	60/3 Hz
Rotation	CCW
Type	three-phase
Enclosure	totally enclosed

A.5.6 Compressor

A Copeland scroll compressor, model ZP23K3E--PFV, was chosen because, at the time of the system design, it was the compressor that would yield the smallest capacity for our system. Compressor maps generated for this model from manufacturer's data were utilized in the design of the microchannel heat exchangers, and the compressor was donated by Copeland.

A.5.7 Outdoor unit calibration

The following curves detail the calibration of the final coil, fan, and housing combination that were performed by Modine Manufacturing Company. The tests were performed at an ambient temperature between 95.3 and 97.7°F and the flow rate was varied continuously between 2000 and 3600 cfm by using the variable speed drive described previously.
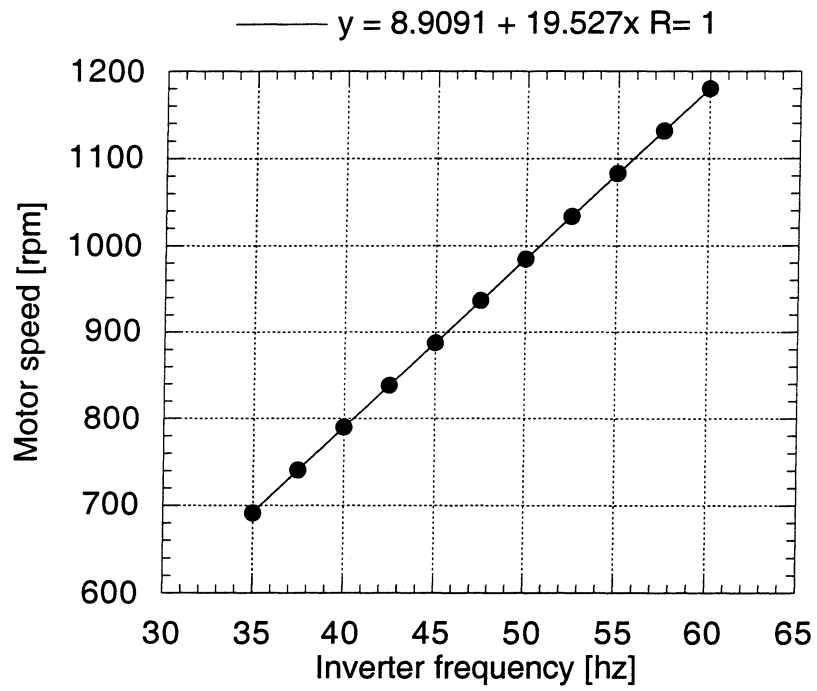
Figure A.18 Resulting motor speeds for different frequency settings from Modine calibration
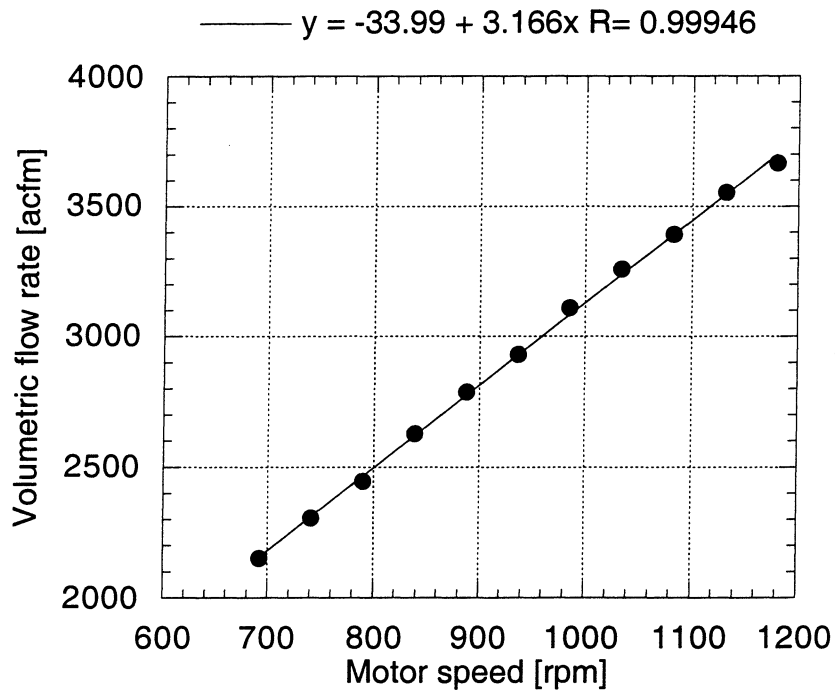
Figure A.19 Volumetric air flow rate for different motor speed settings from Modine calibration

References

Bivens, D.B., DuPont Fluorochemicals, personal communication, 1997.

Bridges, B.D. and C.W. Bullard, "Simulation of Room Air Conditioner Performance." *University of Illinois at Urbana-Champaign*, ACRC TR-79, 1995.

Carrier Corporation, *FK4C Direct Expansion Fan Coil*, Product Data Sheet, 1996.

Carrier Corporation, *38TXA (60 Hz) Air Conditioner with R-410A*, Product Data Sheet, 1996.

Copeland Corporation, *ZP23K3E 1 phase Copeland® Compliant Scroll Compressor*, Product Data Sheet, 1996.

Davenport, C.J., "Correlations for Heat Transfer and Flow Friction Characteristics of Louvered Fin." *AIChE Symposium Series, Heat Transfer-Seattle*, pp. 19-27, 1983.

Sand, J.R., S.K. Fischer, V.D. Baxter, "Energy and global warming impact of HFC refrigerants and emerging technologies." A report sponsored by the Alternative Fluorocarbons Environmental Acceptability Study (AFEAS) and the U.S. Department of Energy, 1997.

Appendix B

Instrumentation and experimental facility

B.1 Introduction

This appendix covers in detail the extensive instrumentation that has been utilized in the microchannel split system to aid in the acquisition of experimental data for both short and long term investigations. In total, 96 thermocouples (4 immersion) were utilized to characterize and observe various phenomena in the current and future test conditions. Because the data acquisition system was only capable of reading 64 channels at a time, care was given to decide which thermocouples were necessary for each test. Two venturis were installed in the liquid and discharge lines of the system and were calibrated using a micromotion mass flow meter that was later removed from the system. Five pressure transducers were also added to the system for accurate pressure measurements.

Extensive modifications were also made to the room air-conditioner psychrometric room facilities (Rugg and Dunn, 1994) in order to accommodate the microchannel split system. An aluminum bracket was constructed to elevate the indoor air handler, and baffles were added both to the outdoor and indoor room facilities to reduce air stratification as much as possible. The indoor room furnace fan was also put on high speed to handle the increased evaporating capacity of the split system.

B.2 Instrumentation

B.2.1 Pressure transducers

Several pressure transducers were available for use from previous projects. All of the pressure transducers from Table B.1, except the high-side absolute, were selected from those currently accessible to the current microchannel split-system project. Manufacturer's data confirmed that these transducers would be appropriate for the higher pressure (than the previous R22 system in which the transducers were used) R410A system. However, simulation analyses revealed that the condensing pressure at an outdoor temperature of around 115°F was around 567

psia which would exceed the limits of both of the available absolute pressure transducers, so a new transducer would need to be purchased. The manufacturer was contacted and a Sensotec model TJE/0713-22TJA with a maximum pressure of 1000 psia was selected because it was a stock product and it easily exceeded the maximum condensing pressures that this system would be exposed to.

Table B.1 Pressure Transducer Information (from Jensen and Dunn, 1996)

Measurement	Model	Volume (in^3)	Range	Manufacturer's Accuracy	
				% Full Scale	Relative psi
High-Side Absolute	TJE/0713-22TJA	0.17	0-1000 psia	±0.10	±1.0
Low-Side Absolute	TJE/713-18	0.17	0-500 psia	±0.10	±0.5
Condenser ΔP	Z/5556-05	0.4	±10 psid	±0.25	±0.025
Discharge-line Venturi ΔP	Z/5556-01	0.4	±5 psid	±0.25	±0.013
Liquid-line Venturi ΔP	Z/5556-05	0.4	±10 psid	±0.25	±0.025

The positioning of the refrigerant-side instrumentation is illustrated in Fig. B.1. A ±10 psid differential pressure transducer spanned between the high-side absolute measurement and the exit of the discharge-line venturi. An immersion thermocouple at the exit of the discharge-line venturi, along with the calculated condenser entrance pressure (absolute pressure at condenser exit plus ±10 psid differential across the condenser), defined the condenser entrance state point just before the condenser entrance (also including the heat transfer and pressure drop of the ALCO -ay valve). The high-side absolute pressure transducer was placed at the entrance of the liquid-line venturi (or at the exit of the condenser after the condenser header tubes and the heating mode TXV) to allow for the measurement of the subcooled pressure and a dedicated refrigerant-side thermocouple was also placed there to characterize the refrigerant state pint at that location. However, it should be noted that the previous two state points were not at the immediate entrance or exit of the heat exchanger so five heavily insulated surface thermocouples were attached to both the inlet and outlet headers to characterize those conditions. The pressure drop across the liquid line was calculated across a wide range of anticipated extreme operating

conditions using the system simulation model, and it was found to be, at most, around 1.3 psid, which was within the ±0.9 °F error associated with the immersion thermocouple that would be at the end of the liquid line. Thus, it was decided that a calculated adjustment to the pressure measured at the exit of the liquid-line venturi would be adequate for setting down the evaporator entrance properties, and that a differential pressure transducer across the liquid line would not be necessary. However, a pressure tap was installed and capped at the end of the liquid line in case of future need. The immersion thermocouple was then mounted 1.5 in. (to avoid bending) in a 3/8 in. "T" just 1 in. upstream from the pressure tap. Around 10 in. of liquid line after the immersion thermocouple and before the TXV was tightly wrapped in insulation to prevent any additional heat transfer and to guarantee that the immersion thermocouple accurately measured the refrigerant temperature just prior to the TXV. Because the inlet header feeding tubes had ID's of 0.1275 inches, immersion thermocouples were not an option for measuring the evaporator inlet temperature so a surface thermocouple placed in the middle of 8.5 in. of insulated length was utilized, so this temperature, along with the inlet enthalpy, allowed for the calculation of the inlet quality. This thermocouple also defined the entrance evaporating pressure, which could be confirmed by the three insulated surface thermocouples mounted on the header. A 500 psia max. absolute pressure transducer and an immersion thermocouple were utilized at the entrance to the suction line, which facilitated an evaporator pressure drop calculation and defined the evaporator exit conditions. The pressure tap was installed with a 0.5 in. section of undisturbed flow in the location where the suction line exits from the air handler. The immersion thermocouple was then mounted upstream in a 3/4 in. "T" and was extended about 1.5 in. into the suction line to a point downstream of the pressure tap. Finally, a heavily insulated surface thermocouple was installed prior to the compressor entrance.
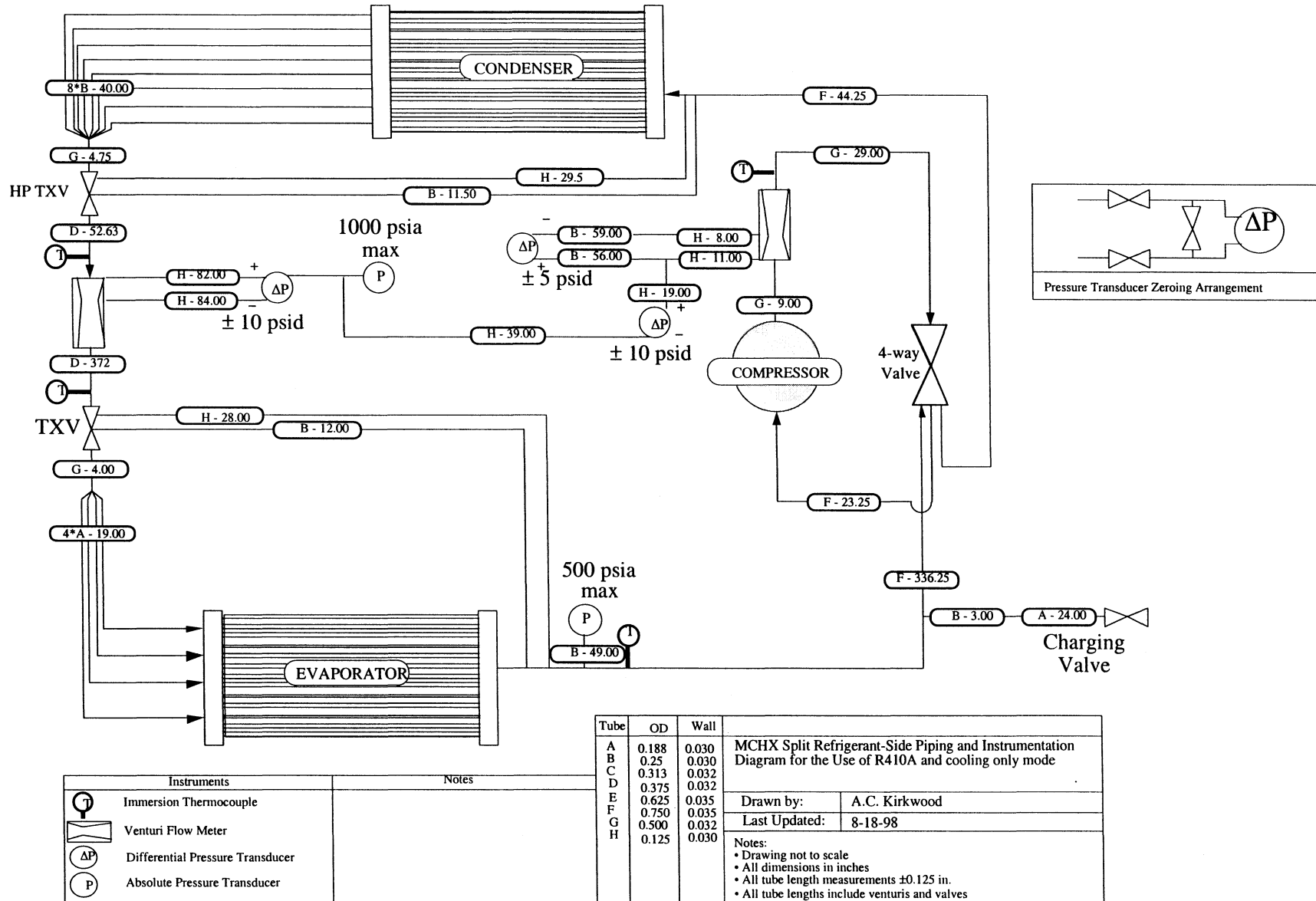
Figure B.1 Piping and instrument diagram for the microchannel refrigerant-side instrumentation system

B.2.2 Venturis

Three different venturis were available from the RAC project: one each for the discharge, liquid, and suction lines. Because of oil clogging in the suction-line venturi and differential pressure transducer, it was decided to install venturis only on the discharge and liquid lines (Jensen and Dunn, 1996). The simulated condenser exit transitioned to two-phase under certain extreme indoor and outdoor conditions (range of 115/110 to 80/70) which would cause the liquid line venturi to lose accuracy in mass flow measurement. However, it would provide a nice secondary mass flow measurement under normal operating conditions to compare to the discharge-line venturi, and to monitor charge migration under certain off-cycle conditions.

Table B.2 Venturi dimensional parameters for available venturis

Size	Model	Inlet diam [in]	Throat diam [in]	β [Dt/Di]
Small	V050095-BSW	0.266	0.097	0.364
Medium	V060175-BSW	0.316	0.175	0.555
Large	V100258-BSW	0.564	0.259	0.460

From the three available venturis, the small one was used in the liquid line of the room air conditioner, the medium was used on the discharge line, and, finally, the largest was used on the suction line. Because the room air-conditioning system used R22 and had a smaller capacity, some analysis was required to decide whether these venturis could be applied to the current 2.5 ton system running R410A.

The primary equation used for converting the pressure drop across the venturi to an actual mass flow rate (which was thoroughly discussed in Jensen and Dunn, 1996) was Eq. B.1. For ideal, inviscid flow, the parameters C_d, Fa_i, and Y_i would all equal unity.

$$w = C_d Fa_i Y_i EA_i \sqrt{2 \Delta p \rho_i g_c} \qquad (B.1)$$

Where:

C_d = Discharge coefficient [-], calibrated *in situ*

Fa_i = Thermal expansion coefficient [-]

67

Y_i = Inlet adiabatic gas exp. factor [-], ref. dependent

E = Velocity of approach factor [-] = $\sqrt{\dfrac{\beta^4}{1-\beta^4}}$

β = Area reduction ratio [-] = D_t/D_i

A_i = Inlet area [in^2] = $\dfrac{\pi D_i^2}{4}$

Δp = venturi diff. pressure [psid] = $p_i - p_t$

ρ_I = inlet density [lbm/in^3]

g_c = gravitational const. [lbm-in/lbf-h^2]
  = 32.174*12*3600^2

The discharge coefficients were dependent on the inlet Reynolds number. In order to get an accurate measurement of mass flow to verify the discharge coefficients, a MicroMotion (sensor model DS025S119, and transmitter model RFT97121RRU) mass flow meter was temporarily added to the system and each venturi was calibrated. Figures B.3 and B.4 show the calibrated discharge coefficients for discharge-line and liquid-line venturis.
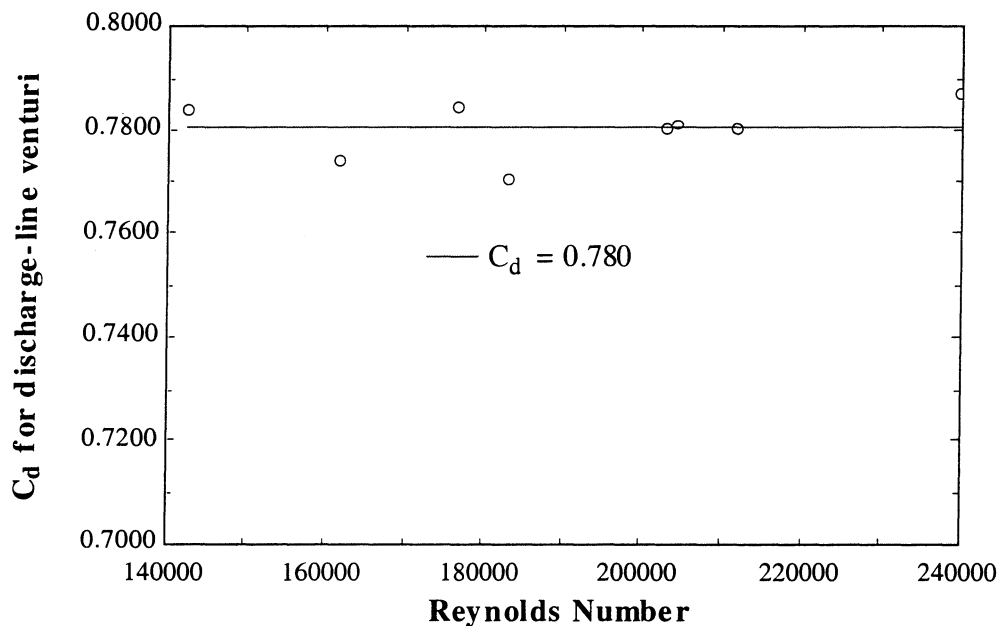
Figure B.2 Discharge-line venturi calibration

Fig. B.3 shows a calibrated C_d of 0.780, which falls significantly below the previously calibrated value of 0.937 (Jensen and Dunn, 1996). The reason for this discrepancy probably resulted from the difficulties involved with installing and mounting the discharge-line venturi. The pressure taps into the venturi were re-soldered numerous time due to leaks observed, which may have introduced solder into the venturi's throat thus changing its dimensions and giving an erroneous discharge coefficient. Fortunately, a liquid-line venturi was also installed and was used for the primary mass flow measurements.
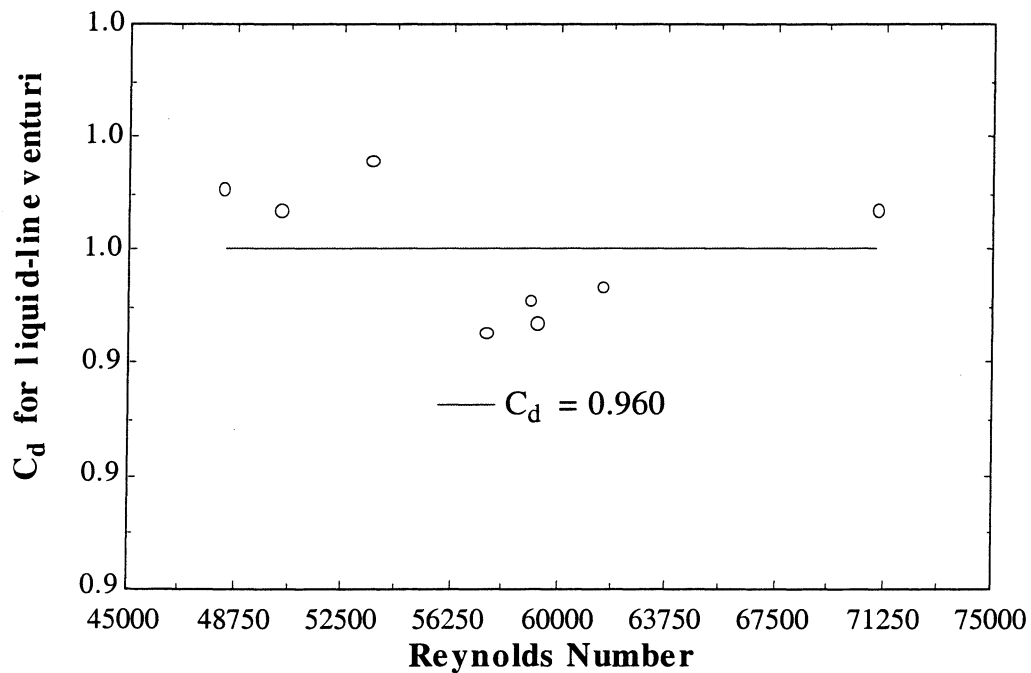
Figure B.3 Liquid-line venturi calibration

The liquid-line venturi calibration was identical to the 0.960 Jensen and Dunn observed in his calibration of the venturi in an R22 window room air-conditioner system, so confidence in this venturi was established.

The thermal expansion coefficient is dependent on: the area reduction ratio, β, the thermal expansion coefficients of the venturi materials, the inlet temperature, and a reference temperature as shown in Eq. B.2. For the simulations performed, Fa_i was always very close to

unity (see Table B.3 below). T0 was the reference temperature for the diameter measurements of the venturis.

$$Fa_i = 1 + \left[\left(\frac{2}{1-\beta^4} \right) \cdot (\alpha_{brass} - \beta^4 \cdot \alpha_{cu}) \right] \cdot (T_i - T0)$$

(B.2)

Finally, for converting venturi pressure drops to mass flow rates, the inlet adiabatic gas expansion factor must be determined. Y_i is dependent on: the specific heat ratios (k_i) of the refrigerant at the inlet, the pressure ratio (Rp) of the venturi, and β (Eq. B.3).

$$Y_i = \sqrt{ \frac{\left[(1-\beta^4) \cdot \left(\frac{k_i}{k_i - 1} \right) \right] \cdot Rp^{\left[\frac{2}{k_i} \right]} \cdot (1 - Rp^{\left[\frac{k_i - 1}{k_i} \right]})}{(1 - \beta^4 \cdot Rp^{\left[\frac{2}{k_i} \right]}) \cdot (1 - Rp)} }$$

(B.3)

After evaluating the refrigerant specific heat ratio data using the simulation temperatures and pressures for each venturi inlet, Y_i was re-calculated for the R410A discharge line. Again, for the range of 115/110 to 80/70 indoor and outdoor temperatures, Y_i was insensitive to changes in k_i so a linear curve fit was made as a function of the pressure ratio to facilitate rapid data reduction. Y_i was, by definition, 1 for the liquid line (Jensen and Dunn, 1996).

$$Y_{i,disc} = Rp*0.41973432 + 0.58027256$$

(B.4)

The mass flow rates, temperatures, and pressures from the extreme range of indoor and outdoor conditions was then fed into Eq. B.1 to solve for the pressure drop across venturis and it was revealed that the original discharge venturi (the medium one) would be seeing a differential pressure as high as 15 psid inside the new 2.5 ton, R410A system. Since no suction-line venturi would be installed in this application, the largest venturi could be used in the discharge line. This reduced the pressure drop to well below 5 psid (see Table B.3 below). This allowed the use of an available differential pressure transducer. The liquid-line venturi (the smallest) observed

nearly a 9 psid differential pressure drop before transitioning to two-phase at the 115°F conditions, which required a pressure transducer with a higher differential range than what was used previously. Using the medium venturi in the liquid line resulted in a reduction of pressure drop to less than 1 psid which would require the purchase of a smaller differential pressure transducer. Fig. B.2 shows the locations of each pressure transducer and venturi.

Table B.3 Venturi simulation analyses

Dry conditions [°F]	Mass flow [lbm/hr]	Re_{dis} [-]	Re_{liq} [-]	$Fa_{i.dis}$ [-]	$Fa_{i,liq}$ [-]	$Y_{i,dis}$ [-]	$Y_{i,liq}$ [-]	Δp_{dis} [psid]	Δp_{liq} [psid]
115/110	520.1	275,081	-	1.002	-	0.9977	-	2.528	-
115/95	506.1	294,850	-	1.002	-	0.997	-	2.82	-
115/85	498.8	309,984	-	1.001	-	0.9962	-	3.081	-
95/95	399.9	221,218	72,899	1.002	1	0.998	1	1.854	8.755
95/75	395.7	254,586	67,370	1.001	1	0.9966	1	2.329	8.188
80/95	335.9	176,415	60,454	1.002	1	0.9985	1	1.35	6.124
80/82	333.9	196,353	56,875	1.002	1	0.9979	1	1.571	5.837
80/70	332.1	215,068	53,677	1.001	0.9999	0.9971	1	1.816	5.612

B.2.3 Immersion thermocouples

Four immersion, type-T, thermocouples were used for refrigerant-side temperature measurements. Each thermocouple had a stainless steel sheath that had an outer diameter of 1/16 in. with an overall length of 6 in. The type-T thermocouples had a maximum temperature of 632°F and a manufacturer's accuracy of ±0.9°F. Care was taken on installation to insert the stainless steel thermocouple sheath 1.5 inches into the tube, and to keep it away from the tube wall in order to avoid conduction errors. Fig. B.6 illustrates the installation method for the immersion thermocouples.
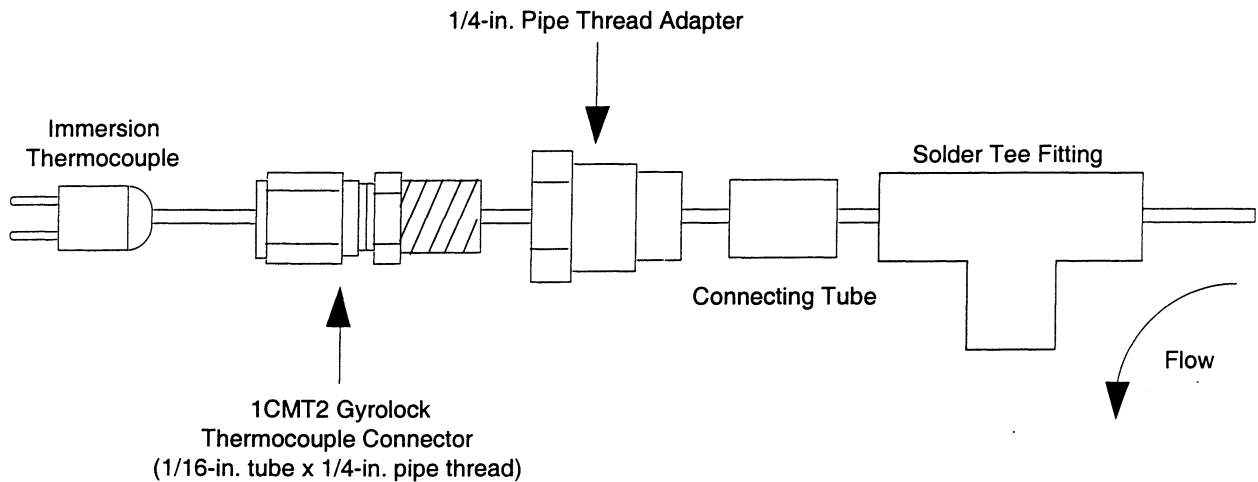
Figure B.4 Installation Method for Refrigerant-Side Thermocouples

(from Jensen and Dunn, 1996)

The same methodology used by Jensen and Dunn (1996) was followed for this microchannel split-system application. All of the immersion thermocouples were installed in the above manner in place of a pre-existing elbow near the desired temperature measurement location. Every connection was soldered, including the threaded connection between the Gyrolock fitting and the adapter, excepting the Gyrolock nut-to-thermocouple connection which facilitated the easy replacement of the immersion thermocouples. As can be seen in Fig. B.2 previously, the thermocouples were placed at the inlets and outlets of each of the four main components.

B.2.4 Surface thermocouples

Teflon coated 30 gauge Type-T thermocouple wires (from the same roll) were utilized for all of the external temperature measurement applications. The accuracy for the surface thermocouples was also ±0.9°F.

Table B.4 Thermocouple Descriptions

T.C. #	Location	Length [ft]
1	STC suction line	9
2	STC evap. liquid header feeding tube	9
3	STC evap. coil unfinned, middle MC, 3 series: closest to fins	9
4	STC evap. coil unfinned, middle MC, 3 series: middle	9
5	STC evap. coil unfinned, middle MC, 3 series: closest to header	8
6	STC evap coil, entrance header, 3 series: left	8
7	STC evap coil, entrance header, 3 series: middle	8
8	STC evap coil, entrance header, 3 series: right	8
9	ITC liquid line exit (indoor room)	5
10	ITC suction line (indoor room)	5
11	STC evap coil, exit header, middle (20th tube from left)	8
12	ITC liquid line entrance (outdoor room)	14*
13	ITC discharge line (outdoor room)	14*
14	STC compressor , middle of shell	12
15	STC suction line, beneith ALCO valve	12
16	STC cond inlet header 5 series: closest to compressor	12
17	STC cond inlet header 5 series: 2nd closest to comp.	12
18	STC cond inlet header 5 series: middle	12
19	STC cond inlet header 5 series: 2nd closest to wall	12
20	STC cond inlet header 5 series: closest to wall	12
21	STC cond exit header 5 series: closest to compressor	14*
22	STC cond exit header 5 series: 2nd closest to comp.	14*
23	STC cond exit header 5series: middle	14*
24	STC cond exit header 5 series: 2nd closest to wall	14*
25	STC cond exit header 5 series: closest to wall	12
26	ASTC cond air in 1, (looking at coil, 3X3 grid) upper right corner	12
27	ASTC cond air in 1, upper center	12
28	ASTC cond air in 1, upper left corner	14*
29	ASTC cond air in 1, middle right	12
30	ASTC cond air in 1, middle center	14*
31	ASTC cond air in 1, middle left	15
32	ASTC cond air in 1, lower right corner	15
33	ASTC cond air in 1, lower center	15
34	ASTC cond air in 1, lower left corner	15
35	ASTC cond air in 2, (looking at coil, 3X3 grid) upper left corner	15
36	ASTC cond air in 2, upper center	15
37	ASTC cond air in 2, upper right corner	15
38	ASTC cond air in 2, middle left	15
39	ASTC cond air in 2, middle center	15
40	ASTC cond air in 2, middle right	15
41	ASTC cond air in 2, lower left corner	15
42	ASTC cond air in 2, lower center	15
43	ASTC cond air in 2, lower right corner	17*
44	ASTC cond exit, west, outer circle (looking from top, SW = comp)	12
45	ASTC cond exit, west, inner circle (closest to motor)	12
46	ASTC cond exit, north, outer circle	13
47	ASTC cond exit, north, inner circle	14*

48	ASTC cond exit, east, outer circle	14*
49	ASTC cond exit, east , inner circle	14*
50	STC evap, unfinned MC, 2nd tube from left (looking into coil)	8
51	STC evap, unfinned MC, 4th tube from left	8
52	STC evap, unfinned MC, 6th tube from left	8
53	STC evap, unfinned MC, 8th tube from left	8
54	STC evap, unfinned MC, 10th tube from left	8
55	STC evap, unfinned MC, 12th tube from left	8
56	STC evap, unfinned MC, 14th tube from left	8
57	STC evap, unfinned MC, 16th tube from left	8
58	STC evap, unfinned MC, 18th tube from left	8
59	STC evap, unfinned MC, 22nd tube from left	8
60	STC evap, unfinned MC, 24th tube from left	8
61	STC evap, unfinned MC, 26th tube from left	8
62	STC evap, unfinned MC, 28th tube from left	8
63	STC evap, unfinned MC, 30th tube from left	8
64	STC evap, unfinned MC, 32nd tube from left	7.5
65	STC evap, unfinned MC, 34th tube from left	7.5
66	STC evap, unfinned MC, 36th tube from left	7.5
67	STC evap, unfinned MC, 38th tube from left	7.5
68	STC evap, unfinned MC, 40th tube from left	7.5
69	ASTC evap inlet, 1st row (top), left corner (looking at filter)	8
70	ASTC evap inlet, 1st row, 2nd from left	8
71	ASTC evap inlet, 1st row, 3rd from left	8
72	ASTC evap inlet, 1st row, 4th from left	8
73	ASTC evap inlet, 2nd row, leftmost	8
74	ASTC evap inlet, 2nd row, 2nd from left	8
75	ASTC evap inlet, 2nd row, 3rd from left	8
76	ASTC evap inlet, 2nd row, 4th from left	8
77	ASTC evap inlet, 3rd row, leftmost	8
78	ASTC evap inlet, 3rd row, 2nd from left	8
79	ASTC evap inlet, 3rd row, 3rd from left	8
80	ASTC evap inlet, 3rd row, 4th from left	8
81	ASTC evap inlet, 4th row (bottom), leftmost	8
82	ASTC evap inlet, 4th row, 2nd from left	8
83	ASTC evap inlet, 4th row, 3rd from left	8
84	ASTC evap inlet, 4th row, 4th from left	8
85	ASTC evap exit, (looking at duct, 3X3 grid) upper left corner	7.5
86	ASTC evap exit, upper center	7.5
87	ASTC evap exit, upper right corner	7.5
88	ASTC evap exit, middle left	7.5
89	ASTC evap exit, middle center	7.5
90	ASTC evap exit, middle right	7.5
91	ASTC evap exit, lower left	7.5
92	ASTC evap exit, lower center	7.5
93	ASTC evap exit, lower right	7.5

94	ASTC cond exit, south, outer circle	12
95	ASTC cond exit, south, inner circle	12
96	STC middle of evap exit header	8

STC: surface thermocouple
ITC: immersion thermocouple
ASTC: air-side thermocouple
cond air in 1: air grid below inlet header (closest to wall)
cond air in 2: air grid below exit header (closest to door)
*: 2 ft. extension included
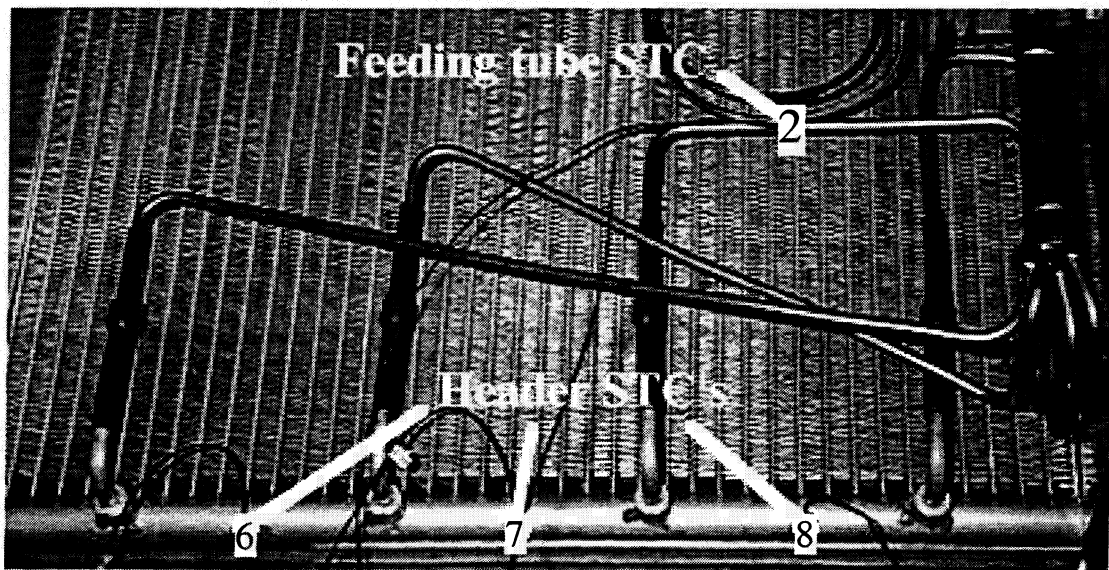
Figure B.5 Evaporator refrigerant inlet surface thermocouples
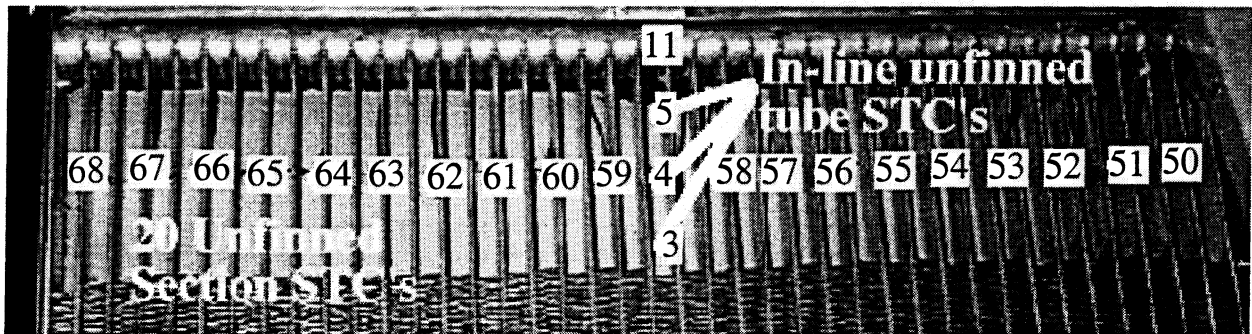
Figure B.6 Evaporator unfinned section surface thermocouples
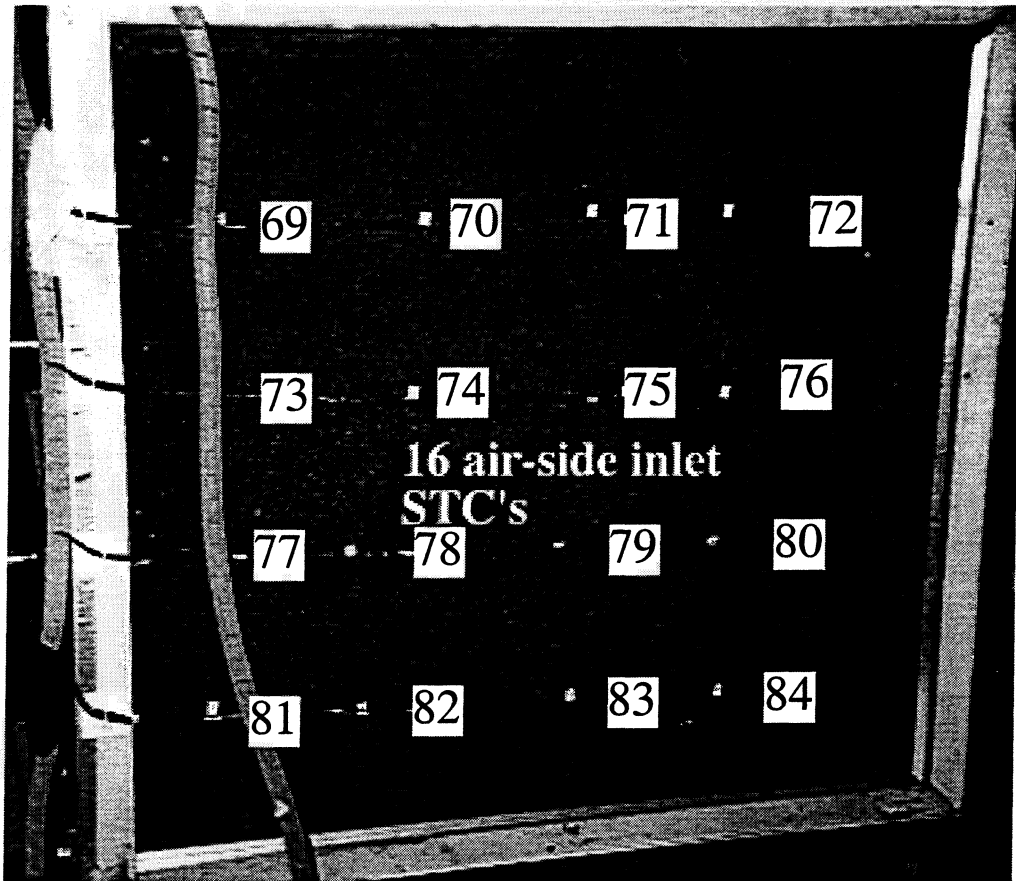
Figure B.7 Evaporator air-side outlet thermocouples
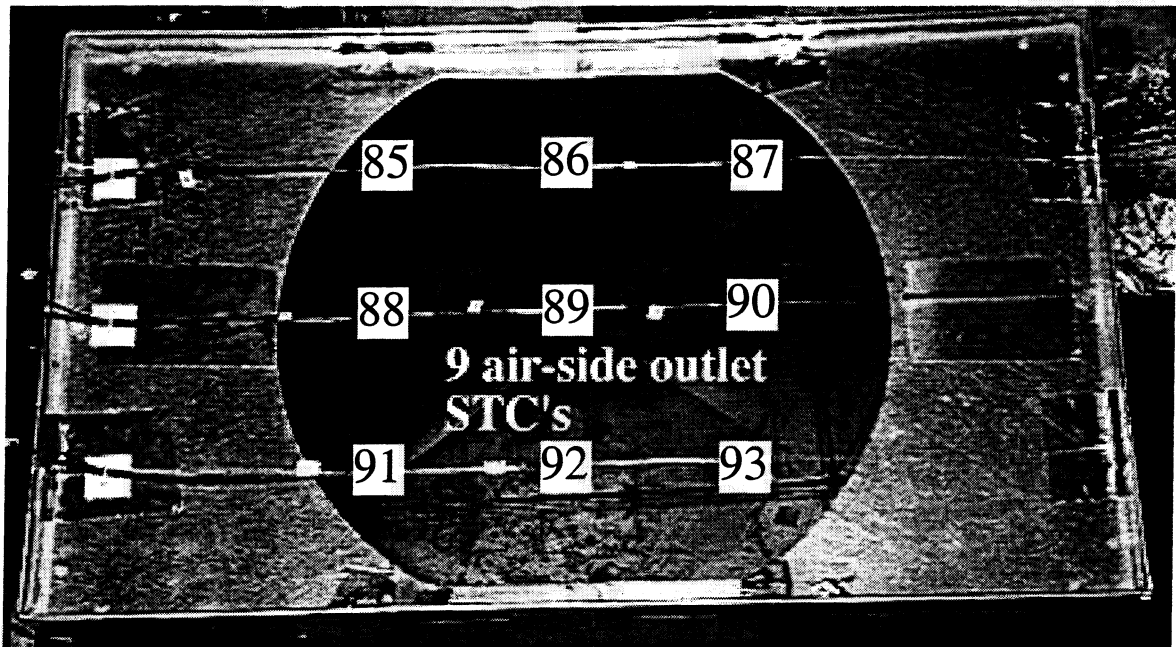
Figure B.8 Evaporator air-side outlet thermocouples

Figure B.9 Condenser inlet header surface thermocouples
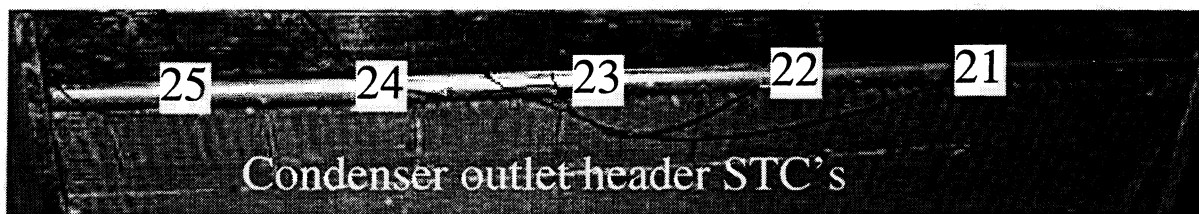
Figure B.10 Condenser outlet header surface thermocouples
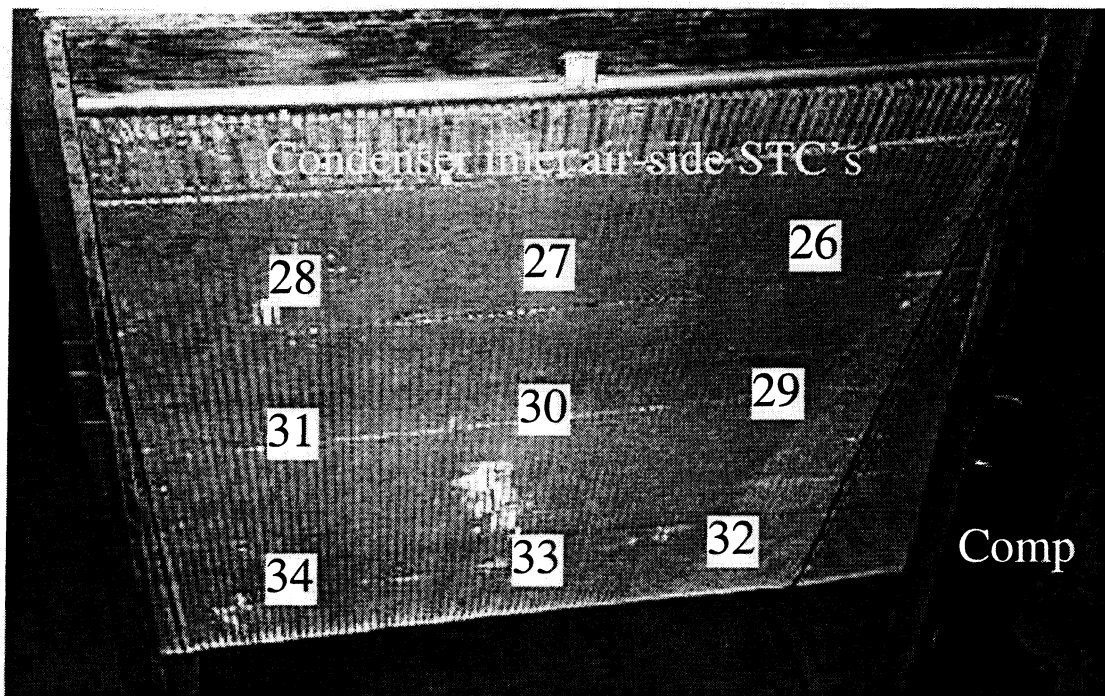
Figure B.11 Condenser left air-side inlet thermocouples
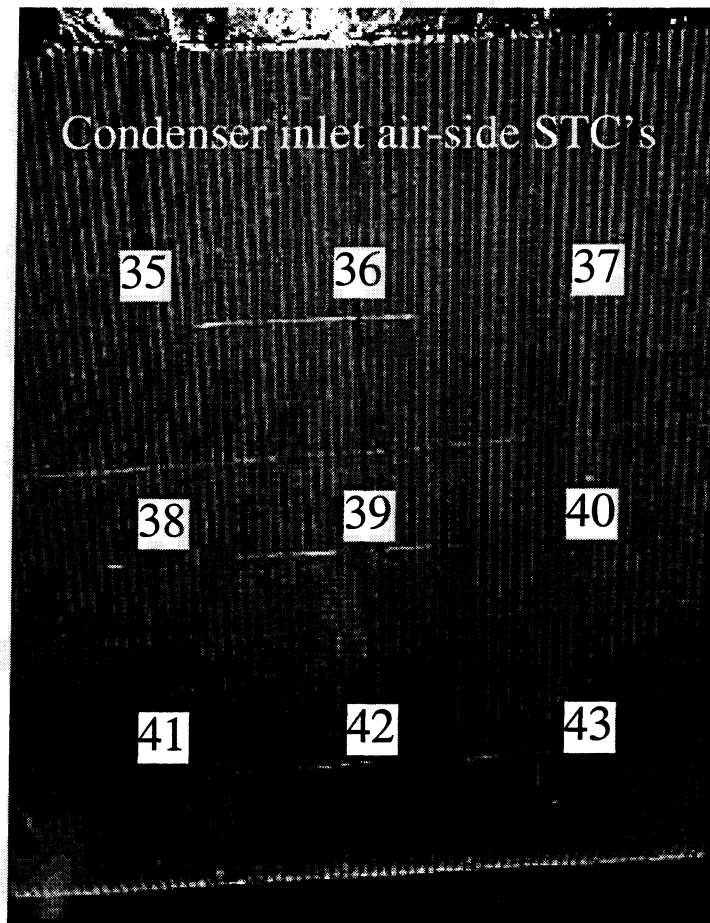
Figure B.12 Condenser right air-side inlet thermocouples
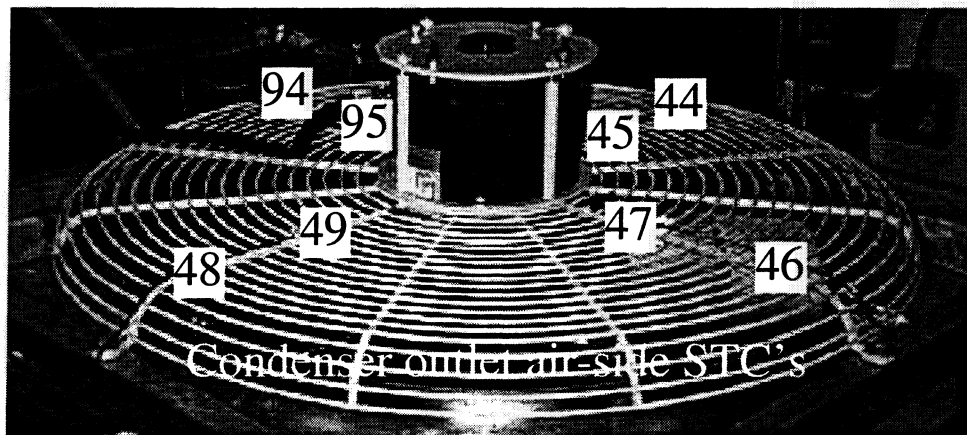
Figure B.13 Condenser air-side outlet thermocouples

B.3 Facility

B.3.1 Indoor room furnace settings

The indoor room was designed to accommodate room air conditioners ranging in sizes from 0.5 to 2.5 tons (Fleming and Dunn, 1993). The furnace selected for the facility had a maximum energy input of 10 kW and had low, medium, and high settings that could be adjusted as needed for each system tested (Rugg and Dunn, 1994). Because the microchannel split-system was at the high end of the indoor room's capabilities, the high furnace fan speed was selected which provided a volumetric flow rate of around 1860 cfm, to minimize the nonuniformities introduced by the approximately 800 cfm flow over the split-system's indoor coil.

B.3.2 Indoor room layout and modifications

Because of the space limitations in the indoor room facility, the evaporator housing was mounted horizontally. In order to reduce vibrations and mount the housing securely, an aluminum bracket was designed and built into the structure of the indoor room. Figure B.16 shows the extreme limitations in floor space, which required the housing to be elevated in order for access to all portions of the indoor room.
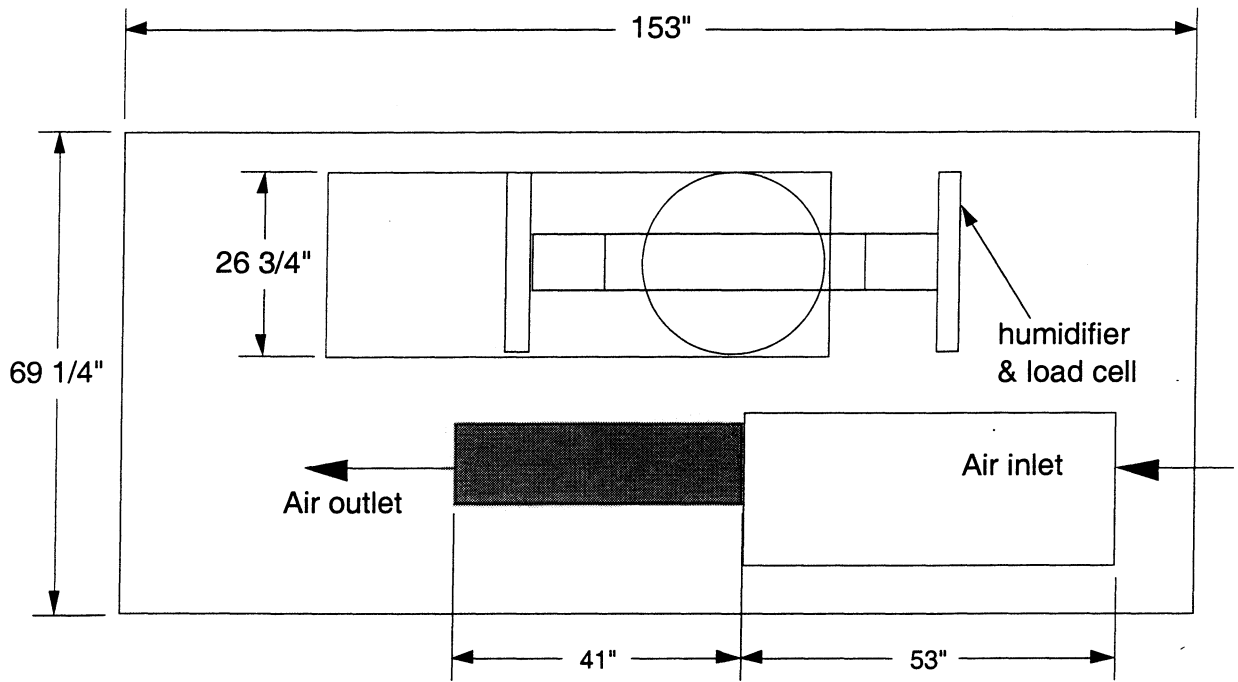
Figure B.14 Overhead view of indoor room

Figure B.15 shows the basic dimensions of the mounting bracket and the clearances for major portions of the indoor room that may need to be accessed such as the thermocouple junction boz. Also having the housing mounted in this fashion allows for the easy opening of the housing's access panel through the plug opening in the test facility's outdoor room.
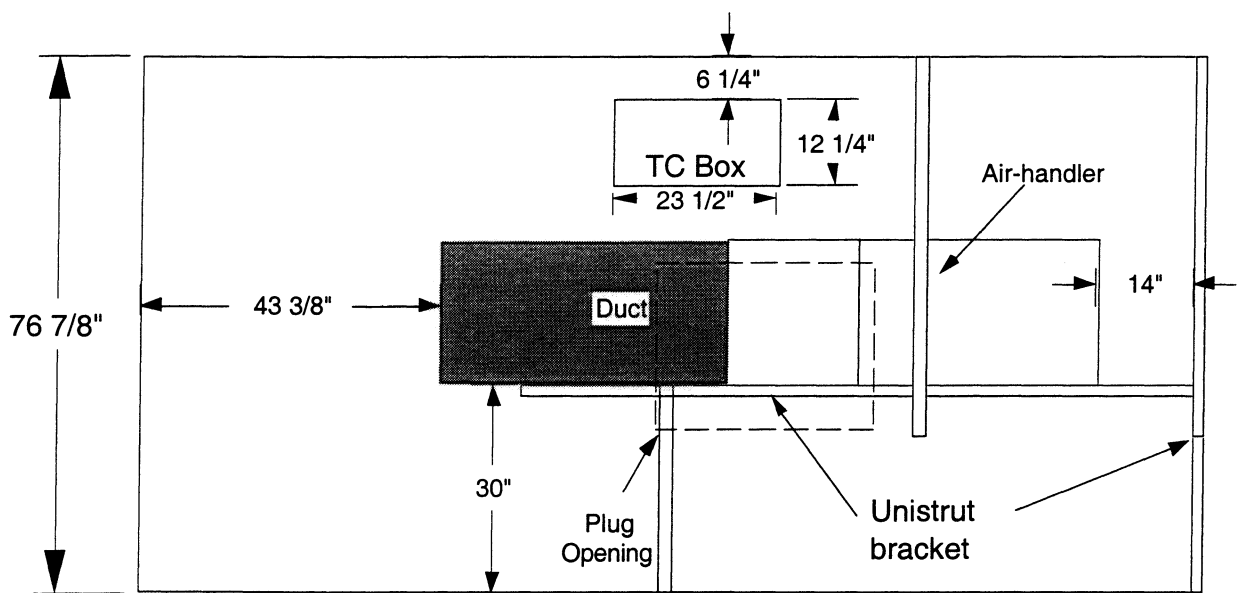
Figure B.15 Side view of air housing and unistrut mounting bracket

References

Rugg, S.M. and W.E. Dunn, "Design, Testing, and Validation of a Room Air Conditioner Test Facility." *University of Illinois at Urbana-Champaign*, ACRC TR-59, 1994.

Jensen, A.C. and W.E. Dunn, "Refrigerant-Side Instrumentation in Room Air Conditioners." *University of Illinois at Urbana-Champaign*, ACRC TR-101, 1996.

Fleming, J.E. and W.E. Dunn, "Design of the Psychrometric Calorimeter Chamber of a Room Air Conditioner Test Facility." *University of Illinois at Urbana-Champaign*, ACRC TR-44, 1993.

Appendix C
ACMCHX model documentation

C.1 Introduction

The air-conditioner with microchannel heat exchangers, or, ACMCHX model was the hybridization of two ACRC models: RACMOD, a room air-conditioner system model (Bridges and Bullard, 1995), and the microchannel condenser submodel developed by Heun and Dunn (1996a, 1996b). RACMOD provided the overall foundation for the ACMCHX system model, while Heun's condenser submodel provided the key geometry equations and some references for the refrigerant-side correlations. This appendix will describe the fundamental equations and correlations that are used by ACMCHX and are different from those utilized in the RACMOD simulation model. The structure and solver of RACMOD outlined in appendices D, I, J, and K of Bridges' thesis remain intact and so will not be reiterated in this appendix.

C.2 Overall conductances

The evaporator conductance is split into two separate zones: the two-phase region and the superheated region. The subroutine used in ACMCHX for the evaporator overall conductance calculation was USEVAPMCHX which is included (along with all of the other microchannel specific functions and subroutines) in the MCHX.f file. The equations used for these regions are outlined below:

$$U_{2phE} = \frac{1}{R_{air} + R_{r2phE}}$$

(C.1)

$$U_{supE} = \frac{1}{R_{air} + R_{rsupE}}$$

(C.2)

These equations are the same formulation that Heun used. The tube resistance does not appear in the conductance equations because it was accounted for in the refrigerant-side resistance equation as a web efficiency.

The air-side resistance was calculated using the following equation:

82

$$R_{air} = \frac{1}{CF \cdot \eta_{air} \cdot h_{air}}$$

(C.3)

Where CF is the coil factor (ratio of the total air-side area to the total refrigerant-side area), η_{air} is the air-side surface efficiency, and h_{air} is the air-side heat transfer coefficient. The details of calculating these values will be discussed in more detail later.

Equation C.4 shows the general form of the equation used to calculate the refrigerant-side resistance.

$$R_{ref} = \frac{1}{\eta_{ref} \cdot h_{ref}}$$

(C.4)

η_{ref} is simply the efficiency of the web between adjacent microchannel ports and h_{ref} is the appropriate refrigerant-side heat transfer coefficient for the given region.

Finally, the condenser conductances were calculated in the USCONDMCHX subroutine in the MCHX.f file of the ACMCHX model. The condenser was split into three separate zones: the superheat region, the two-phase region, and finally the subcooled exit region. The equations for these conductances follow:

$$U_{supC} = \frac{1}{R_{air} + R_{rsupC}}$$

(C.5)

$$U_{2phC} = \frac{1}{R_{air} + R_{r2phC}}$$

(C.6)

$$U_{subC} = \frac{1}{R_{air} + R_{rsubC}}$$

(C.7)
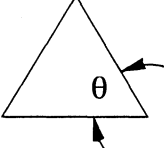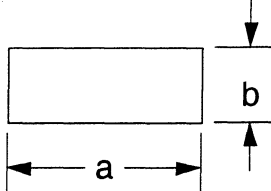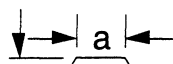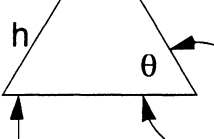
C.3 Heat exchanger geometry

Because the microchannel heat exchangers have the capability of utilizing various port shapes, the ACMCHX model is capable of modeling four different port geometries: triangular ports, circular ports, rectangular ports, and finally trapezoidal ports. The majority of the geometry calculations were taken from Heun and Dunn (1995), with some added corrections and

83

refinements that enable greater flexibility in selecting the port shape (e.g. isosceles triangular ports versus equilateral ports or rectangular ports versus square ports).

Because of the variety of port geometries, two to four parameters are necessary to characterize the geometry for other geometry calculations. These parameters are assigned different values depending on the port geometry selected. Table C.1 lists these parameters and how they relate to the port geometries.

Table C.1 Port geometry parameters

Port geometry	Short form	Program form	Description	Units
All	D_h	Dh_t	Hydraulic diameter $$D_h = 4 \cdot \frac{A_{port}}{P_{port}}$$	[ft]
Triangular	θ	geodes	Repeated angle in isosceles triangle	[deg.]
Rectangular	$\dfrac{b}{a}$	geodes	Port height/port base	[ ]
Circular	n/a	geodes	Not used	[ ]
Trapezoidal	θ	geodes	θ = repeated angle in trapezoid h = height of trapezoid a = length of top of trapezoid	[deg.]
	h	geodes2		[ft]
	a	geodes3		[ft]

These port geometry parameters are fed into both the USEVAPMCHX and USCONDMCHX subroutines where they are then entered into the MCHXgeom subroutine where the remaining geometry psuedoconstants are calculated.

The majority of calculations and correlations in the literature are provided for circular geometries only, which presents a problem with microchannel heat exchangers since they can be any number of shapes. This requires that the non-circular ports be converted into circular equivalent diameters. ACMCHX requires three separate (and different) diameters for use in geometry calculations and correlations (Heun and Dunn, 1995). The hydraulic diameter, D_h, defined as four times the area of the port divided by the perimeter of the port, is needed to define the port geometry and is used in the calculation of the subsequent geometries. The next diameter, is the equivalent diameter, D_{eq}, and it is defined as the diameter of a circle that would give the identical free flow area as the non-circular geometry. The equivalent diameter is used in the geometry calculations for volume, mass flux, etc. The last diameter is the effective diameter, D_{eff}, which is defined as the average of the inscribed and circumscribed circles for the given port geometry. The effective diameter is used in heat transfer and pressure drop correlations.

The previous port parameters are used to calculate the equivalent and effective diameters which are different for each port geometry. The equations for calculating the equivalent diameter are listed below.

$$D_{eq} = kshape \cdot D_h \qquad (C.8)$$

Table C.2 kshape equations

Port geometry	Program form	Description	Units
Triangular	kshape	$$kshape = \frac{1}{\sqrt{\pi}} \cdot \left[\frac{1 + \cos(\theta)}{\sin(\theta)}\right] \cdot \left[\frac{\sin(\theta)}{\cos(\theta)}\right]^{0.5}$$	[ ]
Rectangular	kshape	$$kshape = \frac{1 + \frac{b}{a}}{\sqrt{\pi \cdot \frac{b}{a}}}$$	[ ]
Circular	kshape	$$kshape = 1$$	[ ]
Trapezoidal	kshape	$$kshape = \frac{\sqrt{4 \cdot h \cdot \left[\frac{a + \frac{h}{\tan(\theta)}}{\pi}\right]}}{D_h}$$	[ ]

Kshape is just the ratio of the equivalent diameter to the hydraulic diameter. The effective diameter is calculated using a similar ratio, DeffRat, which is simply the ratio of the effective diameter to the hydraulic diameter. Most manufacturers use the hydraulic diameter to characterize their microchannel ports, hence, the reason for formulating these equations as function of the hydraulic diameter. Equation C.13 shows the calculation for the effective diameter.

$$D_{eff} = DeffRat \cdot D_h$$

(C.9)

Table C.3 DeffRat equations

Port geometry	Program form	Description	Units
Triangular	DeffRat	$$\text{DeffRat} = 0.5 \cdot \left[\frac{D_{circs} + D_{insc}}{D_h} \right]$$	[ ]
	Dcircs	$$D_{circs} = (1 + \cos(\theta)) \cdot \frac{\dfrac{D_h}{\sin(\theta)}}{\cos\left[2 \cdot \theta - \dfrac{\pi}{2} \right]}$$	[ft]
	Dinsc	$$D_{insc} = (1 + \cos(\theta)) \cdot \frac{D_h}{\sin(\theta)} \cdot \tan(0.5 \cdot \theta)$$	[ft]
Rectangular	DeffRat	$$\text{DeffRat} = 2/3 + \frac{11}{24} \cdot \frac{b}{a} \cdot \left[2 - \frac{b}{a} \right]$$	[ ]
Circular	DeffRat	DeffRat =1	[ ]
Trapezoidal	DeffRat	$$\text{DeffRat} = 0.5 \cdot \left[\frac{D_{circs} + D_{insc}}{D_h} \right]$$	[ ]
	Dcircs	$$D_{circs} = \frac{a + 2 \cdot \dfrac{h}{\tan(\theta)}}{\cos(\theta - \phi)}$$	[ft]
	Dinsc	$$D_{insc} = \left[a + 2 \cdot \frac{h}{\tan(\theta)} \right] \cdot \tan(0.5 \cdot \theta)$$	[ft]
	phi	$$\phi = \arctan\left[\frac{\left(\dfrac{a}{a + 2 \cdot \dfrac{h}{\tan(\theta)}} \right) \cdot \cos(\theta) - \cos(\pi - \theta)}{\sin(\pi - \theta) - \left(\dfrac{a}{a + 2 \cdot \dfrac{h}{\tan(\theta)}} \right) \cdot \sin(\theta)} \right]$$	[rad]

87

The effective diameter is defined as the average of the inscribed and circumscribed circles about a certain port geometry. For the rectangular geometry, it is easy enough to reduce the equations for calculating DeffRat by canceling out similar terms, but for the triangular and trapezoidal geometries, the caclulations are considerably more complicated and contain a great deal of geometric manipulations.

The geometry equation for Lweb calculates the length of the web exposed to the refrigerant and is used in the web efficiency calculation in the overall conductance equations.

Table C.4 Lweb equations

Port geometry	Program form	Description	Units
Triangular	Lweb	$Lweb = 0.5 \cdot (1 + \cos(\theta)) \cdot \dfrac{D_h}{\sin(\theta) \cdot \cos(\theta)}$	[ft]
Rectangular	Lweb	$Lweb = D_h \cdot \left[\dfrac{1 + \dfrac{b}{a}}{2} \right]$	[ft]
Circular	Lweb	$Lweb = D_h \cdot 2 / 3$	[ft]
Trapezoidal	Lweb	$Lweb = \dfrac{h}{\sin(\theta)}$	[ft]

The next two port geometry dependent equations calculate H, the horizontal tube width, and b_t, the thickness of the tube. Figure C.1 shows these and other important microchannel geometry parameters.
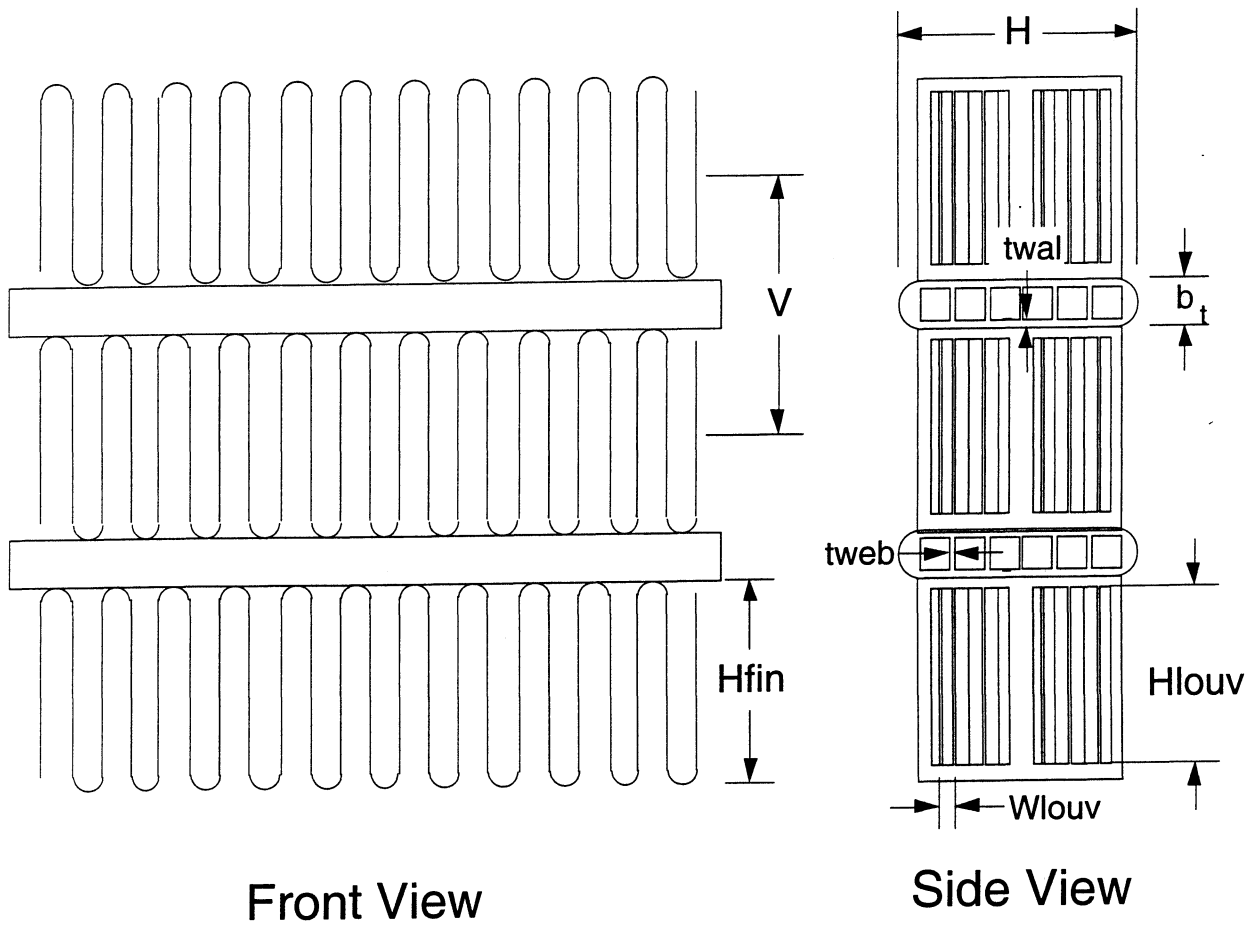
Figure C.1 Important geometry parameters for microchannel heat exchangers

The horizontal tube distance, H, is calculated as follows:

Table C.5 Horizontal tube distance equations

Port geometry	Program form	Description	Units
Triangular	Htubedist	$H = 2 \cdot twall + \left[\dfrac{Nports + 1}{2}\right] \cdot D_h \cdot \left[\dfrac{1 + \cos(\theta)}{\sin(\theta)}\right] + (Nports - 1) \cdot \dfrac{tweb}{\sin(\theta)}$	[ft]
Rectangular	Htubedist	$H = 2 \cdot twall + (Nports - 1) \cdot tweb + Nports \cdot \dfrac{D_h}{2} \cdot \left[\dfrac{\frac{b}{a} + 1}{b \cdot a}\right]$	[ft]
Circular	Htubedist	$H = 2 \cdot twall + (Nports - 1) \cdot tweb + Nports \cdot D_h$	[ft]
Trapezoidal	Htubedist	$H = 2 \cdot twall + \left[\dfrac{Nports + 1}{2}\right] \cdot \left[2 \cdot a + 2 \cdot \dfrac{H}{\tan(\theta)}\right] + (Nports - 1) \cdot \dfrac{tweb}{\sin(\theta)}$	[ft]

The tube thickness, b_t, is calculated as follows:

Table C.6 Tube thickness equations

Port geometry	Program form	Description	Units
Triangular	b_t	$b_t = 2 \cdot twall + \dfrac{D_h}{2} \cdot \left[\dfrac{1 + \cos(\theta)}{\cos(\theta)}\right]$	[ft]
Rectangular	b_t	$b_t = \dfrac{D_h}{2} \cdot \left[\dfrac{b}{a} + 1\right] + 2 \cdot twall$	[ft]
Circular	b_t	$b_t = D_h + 2 \cdot twall$	[ft]
Trapezoidal	b_t	$b_t = 2 \cdot twall + h$	[ft]

The last port geometry dependent equation calculates the ratio of the microchannel web surface area to the total refrigerant-side surface area. This calculation is used later in the web efficiency calculation for the refrigerant-side resistance.

Table C.7 Web surface area to total refrigerant-side surface area equations

Port geometry	Program form	Description	Units
Triangular	SweboverSref	$\dfrac{S_{web}}{S_{ref}} = \dfrac{1}{1 + \cos(\theta)}$	[ ]
Rectangular	SweboverSref	$\dfrac{S_{web}}{S_{ref}} = \dfrac{\dfrac{b}{a}}{1 + \dfrac{b}{a}}$	[ ]
Circular	SweboverSref	$\dfrac{S_{web}}{S_{ref}} = 1 / 2$	[ ]
Trapezoidal	SweboverSref	$\dfrac{S_{web}}{S_{ref}} = \dfrac{2 \cdot \dfrac{h}{\sin(\theta)}}{2 \cdot a + 2 \cdot \dfrac{h}{\tan(\theta)} + 2 \cdot \dfrac{h}{\sin(\theta)}}$	[ ]

The following calculations are general equations that apply to all port geometries. V is the vertical tube distance and it defines a vertical height that an individual microchannel tube and its associated fin takes up.

$$V = Hfin + b_t$$

(C.10)

91

The remaining equations calculate the various air-side and refrigerant-side areas and there associated ratios. The microchannel heat exchanger frontal area is calculated using the vertical tube spacing, the number of microchannel tubes, Ntubes, and the header to header length, Tubelen.

$$A_{front} = Ntubes \cdot V \cdot Tubelen$$

(C.11)

The refrigerant-side area is calculated by the following equation:

$$A_{ref} = Nports \cdot Ntubes \cdot Tubelen \cdot \pi \cdot kshape^2 \cdot D_h$$

(C.12)

CF, the ratio of the total air-side surface area to the total refrigerant-side area, is calculated as follows:

$$CF = \frac{S_{atp}}{S_{rtp}}$$

(C.13)

Where S_{atp} is the air-side surface density and S_{rtp} is the refrigerant-side surface density, and they are calculated as follows:

$$S_{atp} = 2 \cdot Tubelen \cdot \left[\frac{(Ntubes + 1) \cdot FinDns \cdot Hfin \cdot H + Ntubes \cdot (b_t + H)}{Volext} \right]$$

(C.14)

FinDns is the fin density and it has units of fins per ft

VolExt is the external heat exchanger volume and it has units of ft^3

$$S_{rtp} = \frac{\pi \cdot Nports \cdot Ntubes \cdot kshape^2 \cdot D_h \cdot Tubelen}{Volext}$$

(C.15)

92

$$Volext = V \cdot Ntubes \cdot H \cdot Tubelen$$

(C.16)

The total air-side surface area is then simply:

$$A_{air} = CF \cdot A_{ref}$$

(C.17)

The ratio of S_{fin}, the total fin surface area, to S_{air}, the total air-side surface area including both the tube and fin surfaces, is:

$$\frac{S_{fin}}{S_{air}} = \frac{1}{1 + Ntubes \cdot \left[\dfrac{b_t + H}{(Ntubes + 1) \cdot FinDns \cdot Hfin \cdot H} \right]}$$

(C.18)

The air-side free flow area ratio, σ, is used in calculating the air-side free flow area as well as the air-side hydraulic diameter.

$$\sigma = (Ntubes + 1) \cdot \left[\frac{1 - FinDns \cdot Finth}{Ntubes \cdot \left(1 + \dfrac{b_t}{Hfin} \right)} \right]$$

(C.19)

Where Finth is the fin thickness with units of ft

The free flow air-side area is calculated by:

$$A_{airff} = \sigma \cdot A_{front}$$

(C.20)

Finally, the air-side hydraulic diameter is calculated as follows:

93

$$D_{hair} = 4 \cdot \frac{\sigma}{S_{atp}}$$

(C.21)

C.4 Air-side correlations

C.4.1 Air-side heat transfer correlation

The air-side heat transfer coefficient was calculated internally within the RAIRMCHX function that was called from both the USCONDAIR and USEVAPAIR overall conductance subroutines. The correlation selected for the model was proposed by Chang and Wang (1997). It was selected because it covered the widest array of geometries and was one of the most recently published louvered fin air-side heat transfer coefficient correlations. Future work may investigate the effectiveness of other correlations.

The Chang and Wang correlation was defined in terms of the dimensionless heat transfer coefficient, the j-factor:

$$j = Re_{Wlouv}^{-0.49} \cdot \left[\frac{\theta_{louv}}{90} \right]^{0.27} \cdot \left[\frac{1}{FinDns \cdot Wlouv} \right]^{-0.14} \cdot \left[\frac{Hfin}{Wlouv} \right]^{-0.29}$$

$$\cdot \left[\frac{H}{Wlouv} \right]^{-0.23} \cdot \left[\frac{Hlouv}{Wlouv} \right]^{0.68} \cdot \left[\frac{V}{Wlouv} \right]^{-0.28} \cdot \left[\frac{Finth}{Wlouv} \right]^{-0.05}$$

(C.22)

Where:

j = Colburn j-factor dimensionless air-side heat transfer coefficient

(jH in ACMCHX) [ ]

Wlouv = louver width (Hlouvdist in ACMCHX) [ft]

Re_{Wlouv} = Reynolds number based on the louver width

(Ren in ACMCHX) [ ]

θ_{louv} = louver angle (ThetaLo in ACMCHX) [deg.]

FinDns = fin density (FinDns in ACMCHX) [fins per ft]

Hfin = fin height (Hfin in ACMCHX) [ft]

H = horizontal tube distance, hence horizontal fin distance

94

(htubedist in ACMCHX) [ft]

Hlouv = vertical height of the louver (Hlouv in ACMCHX) [ft]

V = vertical tube distance (vtubedist in ACMCHX) [ft]

Finth = fin thickness (Finth in ACMCHX) [ft]

Restrictions:

$$100 < Re_{Wlouv} < 3000$$

C.4.2 Air-side pressure drop correlation

The air-side pressure drop was calculated within the function dpairMCHX. The friction factor correlation used in this function was from Davenport (1983). Again there is a significant amount of work that can be done in investigating alternative correlations in the future. Davenport's correlation is outlined below:

$$f = 0.494 \cdot Re_{Wlouv}^{-0.39} \cdot (0.5 \cdot \tan(\theta_{louv}))^{-0.33} \cdot \left[\frac{Hlouv}{Hfin} \right]^{1.1} \cdot (Hfin \cdot 304.8)^{0.46}$$

(C.23)

Restrictions:

$1000 < Re_{Dhair} < 4000$, where Re is the Reynolds number based on the air-side hydraulic diameter (this is not the same Reynolds number as is used in the correlation, which is based on the louver pitch of the fins)

Also note: the fin height dimension must be in mm in order for the correlation to give the correct friction factor, hence the reason for 304.8 conversion factor

C.5 Refrigerant-side correlations

C.5.1 Single-phase heat transfer correlations

The single-phase refrigerant-side heat transfer coefficient correlation was taken from Heun and Dunn's model (1995). The coefficient was correlated in the nondimensional Nu, or the Nusselt number:

$$Nutot = \left(Nul^{10} + term^{-5}\right)^{0.1}$$

(C.24)

Where:

$$term = \frac{\exp\left[\dfrac{2200 - Re}{365}\right]}{Nul \cdot Nul} + \frac{1}{Nut \cdot Nut}$$

(C.25)

$$Nut = 6.3 + \frac{0.079 \cdot \sqrt{\dfrac{ff}{8}} \cdot Re \cdot Pr}{\left(1 + Pr^{(4/5)}\right)^{(5/6)}}$$

(C.26)

Nul is the laminar constant heat flux boundary condition

$\quad$ = 3.00 for triangular ports

$\quad$ = 3.61 for rectangular ports

$\quad$ = 4.36 for circular ports

$\quad$ = 3.00 for trapezoidal ports

C.5.2 Two-phase heat transfer correlations

The same two-phase heat transfer correlations (with the appropriate microchannel port diameter correction) are used in ACMCHX as those that were utilized in RACMOD: Dobson's correlation for condensing heat transfer (1994) and Wattlet's correlation for evaporating heat transfer (1998). The implementation of these two correlations are outlined in Bridge's thesis and therefore will not be outlined here for the sake of brevity.

C.5.3 Pressure drop correlations

Again, the same correlations as used in RACMOD were implemented in ACMCHX for both the single-phase and two-phase refrigerant-side pressure drop: the Souza correlation for two-phase flow (1995) and the Colebrook correlation for single-phase flow (1939).

C.5.4 Charge inventory correlations

ACMCHX uses the same void fraction correlation as RACMOD which was the Hughmark correlation (Rice, 1987).

C.6 Surface efficiency

C.6.1 Air-side surface efficiency

The surface efficiency corrects the heat transfer for how efficiently the fin surface conducts the heat to or from the microchannel tube. The surface efficiency is simply an area-weighted fin efficiency defined by:

$$\eta_{air} = 1 - \frac{S_{fin}}{S_{air}} \cdot (1 - \eta_{fin})$$

(C.27)

Where:

$$\eta_{fin} = \frac{\tanh(mL)}{mL}$$

(C.28)

$$mL = \sqrt{2 \cdot \frac{h_{air}}{Kfin \cdot Finth} \cdot \frac{Hfin}{2}}$$

(C.29)

h_{air} = air-side heat transfer coefficent [Btu/hr-ft^2-F]

Kfin = fin thermal conductivity [Btu/hr-F-ft]

97

C.6.2 Refigerant-side surface efficiency

Similarly, the surface efficiency for the refrigerant-side is an area-weighted web efficiency defined by:

$$\eta_{ref} = 1 - \frac{S_{web}}{S_{ref}} \cdot (1 - \eta_{web})$$

(C.30)

Where:

$$\eta_{web} = \frac{\tanh(mL)}{mL}$$

(C.31)

$$mL = \sqrt{2 \cdot \frac{h_{ref}}{K_{tube} \cdot t_{web}}} \cdot \frac{L_{web}}{2}$$

(C.32)

h_{ref} = refrigerant-side heat transfer coefficent [Btu/hr-ft^2-F]

Ktube = tube thermal conductivity [Btu/hr-F-ft]

References

Bridges, B.D. and C.W. Bullard, "Simulation of Room Air Conditioner Performance." *University of Illinois at Urbana-Champaign*, ACRC TR-79, 1995.

Chang, Y.J. and C.C. Wang, "A Generalized Heat Transfer Correlation for Louver Fin Geometry." *Int. J. Heat Mass Transfer*, vol. 40, no. 3, pp. 533-544, 1997.

Colebrook C. F., "Turbulent flow in pipes, with particular reference to the transition region between the smooth and rough pipe laws." *Institution of Civ. Eng.*, vol. 11, paper no.5204, 1939.

Davenport, C.J., "Correlations for Heat Transfer and Flow Friction Characteristics of Louvered Fin." *AIChE Symposium Series, Heat Transfer-Seattle*, pp. 19-27, 1983.

Dobson, M.K. and J.C. Chato, "Condensation in Smooth Horizontal Tubes," *Journal of Heat Transfer*, 120:2, pp. 193-213, 1998.

Heun, M.K. and W.E. Dunn, "Principles of Refrigerant Circuiting with Application to Microchannel Condensers: Part I-Problem Formulation and the Effects of Port Diameter and Port Shape," *ASHRAE Transactions*, 102:2, pp. 373-381,1996.

Heun, M.K. and W.E. Dunn, "Principles of Refrigerant Circuiting with Application to Microchannel Condensers: Part II-The Pressure-Drop Effect and the Cross-Flow Heat Exchanger Effect," *ASHRAE Transactions*, 102:2, pp. 382-393, 1996.

Rice, C.K., "The Effect of Void Fraction Correlation and Heat Flux Assumption on Refrigerant Charge Inventory Predictions." *ASHRAE Transactions*, vol. 93, part 1, pp. 341-367, 1987.

Souza, A.L. and M.M. Pimenta, "Prediction of Pressure Drop During Horizontal Two-Phase Flow of Pure and Mixed Refrigerants," *ASME Conf. Cavitation and Multiphase Flow*, S. Carolina, FED Vol. 210, pp. 161-71, 1995.

Wattelet, J.P., J.C. Chato, A.L. Souza, and B.R. Christoffersen, "Evaporative Characteristics of R-12, R-134a, and MP-39 at Low Mass Fluxes," *ASHRAE Transactions*, 100:1, pp. 603-615, 1994.

Appendix D

ACMCHX simulation data

D.1 Dry point comparison data

Table D.1 Dry indoor/low outdoor ambient temperature system simulation runs

	Corresp. Exp. Data set	80/68 (10-3-98)	80/68 (10-28-98)	80/71 (10-1-98)	80/74 (10-6-98)	80/75 (10-23-98)	80/81 (10-23-98)
COP	[ ]	4.9542	4.9457	4.7075	4.4908	4.4394	4.0355
EER	[Btu/hr-W]	16.9039	16.8749	16.0620	15.3225	15.1472	13.7692
qEvap	[Btu/hr]	27577	27555	27192	26924	26724	26304
degsubcool	[F]	9.7	9.8	10.7	11.5	11.8	13
degsup	[F]	10	10	10	10	10	10
tsatincomp	[F]	39.8	39.8	40	40.5	40.4	41.7
tsatoutcomp	[F]	81.4	81.6	84.8	88.2	89.1	96.2
w	[lbm/hr]	331	331	330	330.6	329.2	333.1
PwrComp	[W]	1340.4	1343.9	1398.7	1459.8	1478.5	1623.8
Acond	[ft^2]	107.793	107.793	107.793	107.793	107.793	107.793
Aevap	[ft^2]	32.001	32.001	32.001	32.001	32.001	32.001
a2phEdry	[ft^2]	30.483	30.482	30.461	30.439	30.431	30.378
a2phEwet	[ft^2]	0	0	0	0	0	0
esupC	[ ]	0.773	0.773	0.779	0.784	0.786	0.794
e2phC	[ ]	0.865	0.865	0.866	0.867	0.867	0.87
esubC	[ ]	0.714	0.718	0.777	0.819	0.835	0.884
e2phE	[ ]	0.845	0.845	0.845	0.846	0.845	0.846
e2phEwet	[ ]	0.75	0.75	0.75	0.75	0.75	0.75
esupE	[ ]	0.58	0.58	0.578	0.578	0.576	0.576
fsupC	[ ]	0.111	0.111	0.118	0.125	0.128	0.142
f2phC	[ ]	0.806	0.805	0.783	0.762	0.753	0.71
fsubC	[ ]	0.083	0.084	0.099	0.114	0.12	0.148
f2phE	[ ]	0.953	0.953	0.952	0.951	0.951	0.949
fsupE	[ ]	0.047	0.047	0.048	0.049	0.049	0.051
h0	[Btu/lbm]	137.1	137.2	138.2	139.2	139.6	141.6
h1	[Btu/lbm]	135.7	135.8	136.7	137.6	137.9	139.9
h2i	[Btu/lbm]	121.2	121.2	121.3	121.3	121.3	121.2
h2o	[Btu/lbm]	42.8	42.9	44.1	45.4	45.8	48.6
h3	[Btu/lbm]	39.2	39.2	40.1	41.1	41.4	43.6
h4	[Btu/lbm]	39.2	39.2	40.1	41.1	41.4	43.6
h5	[Btu/lbm]	39.2	39.2	40.1	41.1	41.4	43.6
h7i	[Btu/lbm]	39.2	39.2	40.1	41.1	41.4	43.6
h7o	[Btu/lbm]	119.7	119.7	119.7	119.8	119.8	119.8
h9	[Btu/lbm]	122.5	122.5	122.5	122.5	122.5	122.6
h10	[Btu/lbm]	124.4	124.4	124.8	125.1	125.3	125.9
MtotC	[lbm]	2.121	2.124	2.162	2.197	2.212	2.273
MtotE	[lbm]	0.354	0.354	0.349	0.344	0.342	0.334
MsupC	[lbm]	0.026	0.026	0.029	0.032	0.033	0.04
M2phC	[lbm]	1.222	1.221	1.202	1.184	1.176	1.138
MsubC	[lbm]	0.325	0.329	0.386	0.438	0.461	0.558
M2phE	[lbm]	0.281	0.281	0.279	0.277	0.276	0.273
MsupE	[lbm]	0.002	0.002	0.002	0.002	0.002	0.002
Maccum	[lbm]	0	0	0	0	0	0

Mcaptube	[lbm]	0.021	0.021	0.021	0.02	0.02	0.02
Mcomp	[lbm]	0.137	0.137	0.137	0.137	0.136	0.138
MdisLine	[lbm]	0.062	0.062	0.065	0.068	0.068	0.074
MliqLine	[lbm]	1.24	1.239	1.231	1.22	1.218	1.195
MsuctLine	[lbm]	0.082	0.082	0.083	0.083	0.083	0.085
Mrefoil	[lbm]	0.492	0.49	0.466	0.446	0.436	0.403
p0	[psia]	255.6	256.4	268.5	281.6	285.4	315.2
p1	[psia]	255.5	256.3	268.4	281.5	285.3	315.1
p2i	[psia]	255.4	256.1	268.2	281.3	285.2	314.9
p2avg	[psia]	255.3	256.1	268.2	281.3	285.1	314.9
p2o	[psia]	255.2	256	268.1	281.2	285.1	314.8
p3i	[psia]	255.2	255.9	268	281.2	285	314.8
p4	[psia]	255.1	255.9	268	281.1	285	314.7
p5	[psia]	253.7	254.5	266.6	279.7	·283.6	313.3
p7ii	[psia]	139.2	139.2	139.7	140.7	140.5	143.7
p7avg	[psia]	138.7	138.8	139.2	140.2	140	143.2
p7o	[psia]	138.2	138.3	138.7	139.7	139.5	142.7
p9	[psia]	138	138.1	138.5	139.5	139.3	142.5
p10	[psia]	132.7	132.7	133.2	134.2	134	137.1
qCond	[Btu/hr]	31953	31949	31870	31905	31795	32058
qspray	[Btu/hr]	0	0	0	0	0	0
qsupC	[Btu/hr]	4794	4812	5087	5395	5481	6211
q2phC	[Btu/hr]	25965	25935	25459	25077	24849	24184
qsubC	[Btu/hr]	1194	1203	1324	1432	1466	1663
q2phE	[Btu/hr]	26661	26639	26278	26007	25811	25375
q2phEdry	[Btu/hr]	26661	26639	26278	26007	25811	25375
q2phEwet	[Btu/hr]	0	0	0	0	0	0
q2phEwetlat	[Btu/hr]	0	0	0	0	0	0
q2phEwetsns	[Btu/hr]	0	0	0	0	0	0
qsupE	[Btu/hr]	916	916	914	917	913	929
t0	[F]	133	133.4	139.1	144.8	146.8	158.9
t1o	[F]	127.9	128.2	133.7	139.2	141.1	152.9
t2i	[F]	81.4	81.6	84.8	88.1	89.1	96.1
t2avg	[F]	81.3	81.6	84.7	88.1	89	96.1
t2o	[F]	81.3	81.5	84.7	88.1	89	96.1
t3i	[F]	71.6	71.7	74	76.6	77.2	83.1
t4	[F]	71.6	71.7	74	76.6	77.2	83.1
t5	[F]	71.6	71.8	74	76.6	77.2	83.1
t7i	[F]	42.6	42.6	42.8	43.3	43.2	44.5
t7avg	[F]	42.4	42.4	42.6	43.1	43	44.3
t7o	[F]	42.2	42.2	42.4	42.8	42.8	44.1
t9	[F]	52.2	52.2	52.4	52.8	52.8	54.1
t10	[F]	57.8	57.9	59.4	61	61.4	65
tafanoutC	[F]	79.7	79.9	83	86.1	87	93.8
tasupoutC	[F]	83.6	83.8	86.8	90	90.9	97.9
ta2phoutC	[F]	79.5	79.7	82.9	86.2	87.2	94.2
tasuboutC	[F]	73	73.2	75.8	78.7	79.4	85.6
taoutC	[F]	79.4	79.6	82.7	85.8	86.7	93.5
TainE	[F]	80.1	80.1	79.8	79.9	79.5	80.3
TainEwet	[F]	48.2	48.2	48.4	48.7	48.6	49.8
ta2phoutE	[F]	48.2	48.2	48.4	48.7	48.6	49.8
tasupoutE	[F]	58.1	58.1	58.2	58.5	58.3	59.4
taoutE	[F]	48.7	48.7	48.8	49.2	49.1	50.3
tafanoutE	[F]	49.3	49.3	49.4	49.8	49.7	50.9
usupC	[Btu/hr-ft^2-F]	16.8	16.8	16.1	15.5	15.2	14.3
u2phC	[Btu/hr-ft^2-F]	50.7	50.7	50.6	50.5	50.5	50.2

usubC	[Btu/hr-ft^2-F]	26	26	25.8	25.6	25.5	25
u2phE	[Btu/hr-ft^2-F]	51.2	51.2	51.2	51.2	51.2	51.3
u2phEwet	[Btu/hr-ft^2-F]	51.2	51.2	51.2	51.2	51.2	51.3
usupE	[Btu/hr-ft^2-F]	30.2	30.2	30.1	30.1	30.1	30.2
TubeLenC	[ft]	6.28	6.28	6.28	6.28	6.28	6.28
TubeLenE	[ft]	3.68	3.68	3.68	3.68	3.68	3.68
Vcond	[ft^3]	0.059	0.059	0.059	0.059	0.059	0.059
VolextC	[ft^3]	0.9825	0.9825	0.9825	0.9825	0.9825	0.9825
VolextE	[ft^3]	0.2917	0.2917	0.2917	0.2917	0.2917	0.2917
x2o	[ ]	0	0	0	0	0	0
x4	[ ]	0	0	0	0	0	0
x5	[ ]	0	0	0	0	0	0
x7i	[ ]	0.117	0.118	0.126	0.136	0.139	0.16
x7o	[ ]	1	1	1	1	1	1
MWR	[lbm]	0	0	0	0	0	0
tfinEi	[F]	44.5	44.5	44.7	45.2	45.1	46.5
tfinEo	[F]	44.1	44.1	44.3	44.8	44.7	46.1
wairEi	[lbm H2O/lbm of air]	0.00472	0.0044	0.0046	0.0046	0.00531	0.006
wairEo	[lbm H2O/lbm of air]	0.005	0.004	0.005	0.005	0.005	0.006
wfinEi	[lbm H2O/lbm of air]	0.00638	0.00639	0.00644	0.00655	0.00653	0.00689
wfinEo	[lbm H2O/lbm of air]	0.00638	0.00639	0.00644	0.00655	0.00653	0.00689
Tindoor	[F]	80.1	80.1	79.8	79.9	79.5	80.3
Toutdoor	[F]	67.7	67.9	70.9	74	74.9	81.4
RhaiC	[ ]	0.405	0.405	0.405	0.405	0.405	0.405
RhaiE	[ ]	0.211	0.197	0.208	0.207	0.242	0.266
vdotaCmeas	[cfm]	2600	2600	2600	2600	2600	2600
vdotaE	[cfm]	800	800	800	800	800	800
PwrFanE	[W]	120.9	119.2	122.6	124.2	114.5	113.2
PwrFanC	[W]	145.7	145.7	145.6	145.5	145.5	145.3
Mtotal	[lbm]	4.8583	4.8583	4.8583	4.8583	4.8583	4.8583
NportsC	[ports/tube]	19	19	19	19	19	19
porgeoC	[]	1	1	1	1	1	1
NportsE	[ports/tube]	19	19	19	19	19	19
porgeoE	[]	1	1	1	1	1	1
geodesC	[ ]	62.69	62.69	62.69	62.69	62.69	62.69
geodesE	[ ]	62.69	62.69	62.69	62.69	62.69	62.69
NtubesC	[ ]	79	79	79	79	79	79
NtubesE	[ ]	40	40	40	40	40	40
twebC	[ft]	0.00112	0.00112	0.00112	0.00112	0.00112	0.00112
twallC	[ft]	0.00138	0.00138	0.00138	0.00138	0.00138	0.00138
HfinC	[ft]	0.026	0.026	0.026	0.026	0.026	0.026
twebE	[ft]	0.00112	0.00112	0.00112	0.00112	0.00112	0.00112
twallE	[ft]	0.00138	0.00138	0.00138	0.00138	0.00138	0.00138
HfinE	[ft]	0.026	0.026	0.026	0.026	0.026	0.026
Lcap	[in]	19	19	19	19	19	19
Dcap	[in]	0.128	0.128	0.128	0.128	0.128	0.128
Dh_tC	[ft]	0.00219	0.00219	0.00219	0.00219	0.00219	0.00219
Dh_tE	[ft]	0.00219	0.00219	0.00219	0.00219	0.00219	0.00219
Dh_airC	[ft]	0.00639	0.00639	0.00639	0.00639	0.00639	0.00639
Dh_airE	[ft]	0.0064	0.0064	0.0064	0.0064	0.0064	0.0064
AfrontC	[ft^2]	16	16	16	16	16	16
AfrontE	[ft^2]	4.75	4.75	4.75	4.75	4.75	4.75
DeqinC	[ft]	0.00282	0.00282	0.00282	0.00282	0.00282	0.00282

DeqinE	[ft]	0.00282	0.00282	0.00282	0.00282	0.00282	0.00282
HtubeDistC	[ft]	0.0614	0.0614	0.0614	0.0614	0.0614	0.0614
HtubeDistE	[ft]	0.0614	0.0614	0.0614	0.0614	0.0614	0.0614
VtubeDistC	[ft]	0.03224	0.03224	0.03224	0.03224	0.03224	0.03224
VtubeDistE	[ft]	0.03224	0.03224	0.03224	0.03224	0.03224	0.03224
FinThC	[ft]	0.000417	0.000417	0.000417	0.000417	0.000417	0.000417
FinThE	[ft]	0.000417	0.000417	0.000417	0.000417	0.000417	0.000417
taEwet	[F]	0.8	-11.7	-4.8	-7.8	19	33
AairE	[ft^2]	135.654	135.654	135.654	135.654	135.654	135.654
hairE	[Btu/hr-ft^2-F]	14.06	14.06	14.06	14.06	14.06	14.06
hreftpE	[Btu/hr-ft^2-F]	430.41	430.4	430.02	430.88	429.97	433.8
seffEw	[ ]	0.98	0.98	0.98	0.98	0.98	0.98
Tshell	[F]	90.3	90.5	93.3	96.1	97	102.9
dpC	[psia]	0.4	0.4	0.3	0.3	0.3	0.3
dpE	[psia]	1.2	1.2	1.2	1.2	1.2	1.2
ThetaLoC	[deg]	27	27	27	27	27	27
HlouvC	[ft]	0.02167	0.02167	0.02167	0.02167	0.02167	0.02167
HlouvdistC	[ft]	0.004583	0.004583	0.004583	0.004583	0.004583	0.004583
ThetaLoE	[deg]	27	27	27	27	27	27
HlouvE	[ft]	0.02167	0.02167	0.02167	0.02167	0.02167	0.02167
HlouvdistE	[ft]	0.004583	0.004583	0.004583	0.004583	0.004583	0.004583
DeffC	[ft]	0.0033	0.0033	0.0033	0.0033	0.0033	0.0033
DeffE	[ft]	0.0033	0.0033	0.0033	0.0033	0.0033	0.0033
VheadCin	[ft^3]	0.00779	0.00779	0.00779	0.00779	0.00779	0.00779
VheadCout	[ft^3]	0.00779	0.00779	0.00779	0.00779	0.00779	0.00779
VheadEin	[ft^3]	0.00395	0.00395	0.00395	0.00395	0.00395	0.00395
VheadEout	[ft^3]	0.00395	0.00395	0.00395	0.00395	0.00395	0.00395
MheadCin	[lbm]	0.03068	0.03078	0.03213	0.03369	0.03409	0.0375
MheadCout	[lbm]	0.51749	0.51725	0.51364	0.50939	0.50819	0.49891
MheadEin	[lbm]	0.06261	0.06239	0.0591	0.05619	0.05507	0.05014
MheadEout	[lbm]	0.00889	0.00889	0.00892	0.00898	0.00897	0.00918
DheadC	[ft]	0.06242	0.06242	0.06242	0.06242	0.06242	0.06242
DheadE	[ft]	0.06242	0.06242	0.06242	0.06242	0.06242	0.06242
etaisenComp	[ ]	0.542	0.543	0.555	0.564	0.565	0.574
AairC	[ft^2]	452.245	452.245	452.245	452.245	452.245	452.245
hairC	[Btu/hr-ft^2-F]	13.85	13.85	13.84	13.84	13.83	13.82
hreftpC	[Btu/hr-ft^2-F]	481.5	481.02	473.71	466.52	464.03	449.46
NlouvC	[ ]	10	10	10	10	10	10
NlouvE	[ ]	10	10	10	10	10	10
dPairC	[psia]	0.0011453	0.0011452	0.001143	0.0011408	0.0011402	0.0011356
dPairE	[psia]	0.0011316	0.0011316	0.0011324	0.0011328	0.0011334	0.0011336
eta_fanC	[ ]	0.18	0.18	0.18	0.18	0.18	0.18
Le	[ ]	0.821	0.821	0.821	0.821	0.822	0.822
hD	[1/hr-ft^2-lbm of air]	66.14	66.15	66.15	66.15	66.1	66.1
ttubeEi	[F]	44.44	44.46	44.65	45.12	45.02	46.42
ttubeEo	[F]	44	44.02	44.22	44.68	44.58	45.97
NCht	[ ]	8	8	8	8	8	8
DCht	[ft]	0.01583	0.01583	0.01583	0.01583	0.01583	0.01583
LCht	[ft]	3.33	3.33	3.33	3.33	3.33	3.33
UlossCht	[Btu/hr-ft2-F]	0	0	0	0	0	0
pdCht	[psia]	0.04	0.04	0.04	0.04	0.04	0.04
qlossCht	[Btu/hr]	0	0	0	0	0	0
MCht	[lbm]	0.3481	0.34794	0.34551	0.34265	0.34185	0.3356
VCht	[ft^3]	0.00524	0.00524	0.00524	0.00524	0.00524	0.00524

Table D.2 Dry indoor/medium outdoor ambient temperature system simulation runs

	Corresp. Exp. Data set	80/82 (10-8-98)	80/82 (10-23-98)	80/90 (10-24-98)	80/94 (10-26-98)	80/95 (10-2-98)	80/95 (10-24-98)
COP	[ ]	3.9392	3.9651	3.4185	3.2029	3.1226	3.1162
EER	[Btu/hr-W]	13.4404	13.5289	11.6640	10.9284	10.6543	10.6326
qEvap	[Btu/hr]	26143	26242	25239	24841	24696	24676
degsubcool	[F]	13.2	13.2	15	15.8	16	16.1
degsup	[F]	10	10	10	10	10	10
tsatincomp	[F]	41.7	42	42.9	43.5	43.6	43.7
tsatoutcomp	[F]	97.1	97.4	106.3	110.3	111.5	112
w	[lbm/hr]	332.1	333.9	333	333.3	333.1	333.5
PwrComp	[W]	1643.8	1650.5	1868	1975.3	2009.3	2022.1
Acond	[ft^2]	107.793	107.793	107.793	107.793	107.793	107.793
Aevap	[ft^2]	32.001	32.001	32.001	32.001	32.001	32.001
a2phEdry	[ft^2]	30.371	30.369	30.291	30.255	30.243	30.238
a2phEwet	[ft^2]	0	0	0	0	0	0
esupC	[ ]	0.795	0.795	0.803	0.805	0.806	0.806
e2phC	[ ]	0.87	0.87	0.872	0.873	0.873	0.873
esubC	[ ]	0.894	0.89	0.943	0.958	0.962	0.962
e2phE	[ ]	0.846	0.846	0.847	0.847	0.847	0.847
e2phEwet	[ ]	0.75	0.75	0.75	0.75	0.75	0.75
esupE	[ ]	0.576	0.577	0.573	0.572	0.571	0.572
fsupC	[ ]	0.145	0.144	0.169	0.18	0.184	0.185
f2phC	[ ]	0.701	0.703	0.627	0.592	0.58	0.577
fsubC	[ ]	0.154	0.153	0.204	0.228	0.236	0.238
f2phE	[ ]	0.949	0.949	0.947	0.945	0.945	0.945
fsupE	[ ]	0.051	0.051	0.053	0.055	0.055	0.055
h0	[Btu/lbm]	142	142	145.1	146.6	147	147.2
h1	[Btu/lbm]	140.2	140.2	143.1	144.5	144.9	145
h2i	[Btu/lbm]	121.2	121.2	121	120.9	120.9	120.8
h2o	[Btu/lbm]	49	49.1	52.8	54.5	55	55.2
h3	[Btu/lbm]	43.9	44.1	46.9	48.2	48.6	48.8
h4	[Btu/lbm]	43.9	44.1	46.9	48.2	48.6	48.8
h5	[Btu/lbm]	43.9	44.1	46.9	48.2	48.6	48.8
h7i	[Btu/lbm]	43.9	44.1	46.9	48.2	48.6	48.8
h7o	[Btu/lbm]	119.8	119.8	119.9	119.9	119.9	119.9
h9	[Btu/lbm]	122.6	122.6	122.7	122.7	122.7	122.8
h10	[Btu/lbm]	126	126.1	127	127.3	127.4	127.5
MtotC	[lbm]	2.284	2.282	2.371	2.406	2.418	2.421
MtotE	[lbm]	0.333	0.333	0.322	0.319	0.317	0.317
MsupC	[lbm]	0.042	0.042	0.055	0.061	0.063	0.064
M2phC	[lbm]	1.127	1.13	1.04	0.995	0.979	0.976
MsubC	[lbm]	0.58	0.575	0.749	0.827	0.854	0.859
M2phE	[lbm]	0.272	0.272	0.267	0.265	0.265	0.264
MsupE	[lbm]	0.002	0.002	0.002	0.002	0.002	0.002
Maccum	[lbm]	0	0	0	0	0	0
Mcaptube	[lbm]	0.02	0.02	0.02	0.02	0.02	0.02
Mcomp	[lbm]	0.137	0.138	0.138	0.138	0.138	0.138
MdisLine	[lbm]	0.075	0.076	0.084	0.087	0.088	0.089
MliqLine	[lbm]	1.193	1.191	1.161	1.146	1.142	1.14
MsuctLine	[lbm]	0.085	0.086	0.087	0.088	0.088	0.088
Mrefoil	[lbm]	0.396	0.398	0.35	0.333	0.327	0.326
p0	[psia]	319	320.5	361.9	381.6	387.8	390.1
p1	[psia]	319	320.4	361.8	381.6	387.7	390.1
p2i	[psia]	318.8	320.3	361.7	381.4	387.6	389.9
p2avg	[psia]	318.8	320.2	361.6	381.4	387.5	389.9

p2o	[psia]	318.7	320.1	361.6	381.3	387.5	389.8
p3i	[psia]	318.7	320.1	361.5	381.3	387.4	389.8
p4	[psia]	318.6	320.1	361.5	381.2	387.4	389.7
p5	[psia]	317.2	318.6	360	379.8	385.9	388.3
p7ii	[psia]	143.6	144.3	146.4	147.7	147.9	148.2
p7avg	[psia]	143.1	143.8	145.9	147.2	147.4	147.7
p7o	[psia]	142.6	143.3	145.4	146.7	146.9	147.2
p9	[psia]	142.4	143.1	145.2	146.5	146.7	147
p10	[psia]	137.1	137.7	139.9	141.2	141.5	141.8
qCond	[Btu/hr]	31985	32117	32046	32084	32072	32105
qspray	[Btu/hr]	0	0	0	0	0	0
qsupC	[Btu/hr]	6301	6345	7360	7853	8005	8068
q2phC	[Btu/hr]	23994	24075	22716	22132	21926	21882
qsubC	[Btu/hr]	1690	1697	1969	2099	2141	2156
q2phE	[Btu/hr]	25216	25309	24305	23904	23759	23737
q2phEdry	[Btu/hr]	25216	25309	24305	23904	23759	23737
q2phEwet	[Btu/hr]	0	0	0	0	0	0
q2phEwetlat	[Btu/hr]	0	0	0	0	0	0
q2phEwetsns	[Btu/hr]	0	0	0	0	0	0
qsupE	[Btu/hr]	927	933	934	938	937	939
t0	[F]	160.7	161	178	185.7	188.1	188.9
t1o	[F]	154.6	154.9	171.2	178.5	180.8	181.6
t2i	[F]	97	97.4	106.3	110.3	111.5	112
t2avg	[F]	97	97.3	106.3	110.3	111.5	111.9
t2o	[F]	97	97.3	106.3	110.3	111.5	111.9
t3i	[F]	83.8	84.1	91.3	94.5	95.4	95.8
t4	[F]	83.8	84.1	91.3	94.5	95.4	95.8
t5	[F]	83.8	84.1	91.3	94.5	95.4	95.8
t7i	[F]	44.5	44.8	45.6	46.1	46.3	46.4
t7avg	[F]	44.3	44.5	45.4	45.9	46.1	46.2
t7o	[F]	44.1	44.3	45.2	45.7	45.8	46
t9	[F]	54.1	54.3	55.2	55.7	55.8	56
t10	[F]	65.4	65.6	69.6	71.4	72	72.2
tafanoutC	[F]	94.5	94.9	103	106.5	107.5	107.9
tasupoutC	[F]	98.6	99.1	107.1	110.6	111.6	112.1
ta2phoutC	[F]	95.1	95.4	104.2	108.2	109.4	109.8
tasuboutC	[F]	86.3	86.7	94.1	97.3	98.3	98.7
taoutC	[F]	94.2	94.6	102.6	106.1	107.2	107.6
TainE	[F]	80.1	80.5	80.1	80.1	80	80.1
TainEwet	[F]	49.8	50.1	50.7	51.2	51.2	51.4
ta2phoutE	[F]	49.8	50.1	50.7	51.2	51.2	51.4
tasupoutE	[F]	59.3	59.6	60.1	60.4	60.5	60.6
taoutE	[F]	50.3	50.6	51.2	51.7	51.8	51.9
tafanoutE	[F]	50.8	51.2	51.8	52.3	52.3	52.4
usupC	[Btu/hr-ft^2-F]	14.1	14.2	12.5	11.9	11.7	11.7
u2phC	[Btu/hr-ft^2-F]	50.2	50.2	49.9	49.8	49.7	49.7
usubC	[Btu/hr-ft^2-F]	24.9	24.9	24.3	24	23.9	23.8
u2phE	[Btu/hr-ft^2-F]	51.3	51.3	51.3	51.3	51.3	51.3
u2phEwet	[Btu/hr-ft^2-F]	51.3	51.3	51.3	51.3	51.3	51.3
usupE	[Btu/hr-ft^2-F]	30.2	30.2	30.2	30.2	30.2	30.2
TubeLenC	[ft]	6.28	6.28	6.28	6.28	6.28	6.28
TubeLenE	[ft]	3.68	3.68	3.68	3.68	3.68	3.68
Vcond	[ft^3]	0.059	0.059	0.059	0.059	0.059	0.059
VolextC	[ft^3]	0.9825	0.9825	0.9825	0.9825	0.9825	0.9825
VolextE	[ft^3]	0.2917	0.2917	0.2917	0.2917	0.2917	0.2917
x2o	[ ]	0	0	0	0	0	0

105

x4	[ ]	0	0	0	0	0	0
x5	[ ]	0	0	0	0	0	0
x7i	[ ]	0.163	0.163	0.192	0.205	0.209	0.21
x7o	[ ]	1	1	1	1	1	1
MWR	[lbm]	0	0	0	0	0	0
tfinEi	[F]	46.5	46.8	47.7	48.2	48.4	48.5
tfinEo	[F]	46	46.3	47.3	47.8	47.9	48
wairEi	[lbm H2O/lbm of air]	0.00467	0.00553	0.00503	0.00503	0.00533	0.00517
wairEo	[lbm H2O/lbm of air]	0.005	0.006	0.005	0.005	0.005	0.005
wfinEi	[lbm H2O/lbm of air]	0.00688	0.00696	0.00721	0.00736	0.00739	0.00742
wfinEo	[lbm H2O/lbm of air]	0.00688	0.00696	0.00721	0.00736	0.00739	0.00742
Tindoor	[F]	80.1	80.5	80.1	80.1	80	80.1
Toutdoor	[F]	82.2	82.5	90.4	93.8	94.8	95.2
RhaiC	[ ]	0.405	0.405	0.405	0.405	0.405	0.405
RhaiE	[ ]	0.209	0.244	0.225	0.225	0.239	0.231
vdotaCmeas	[cfm]	2600	2600	2600	2600	2600	2600
vdotaE	[cfm]	800	800	800	800	800	800
PwrFanE	[W]	124.5	115	116.7	116.5	124.1	116.5
PwrFanC	[W]	145.2	145.2	145	144.9	144.8	144.8
Mtotal	[lbm]	4.8583	4.8583	4.8583	4.8583	4.8583	4.8583
NportsC	[ports/tube]	19	19	19	19	19	19
porgeoC	[]	1	1	1	1	1	1
NportsE	[ports/tube]	19	19	19	19	19	19
porgeoE	[]	1	1	1	1	1	1
geodesC	[ ]	62.69	62.69	62.69	62.69	62.69	62.69
geodesE	[ ]	62.69	62.69	62.69	62.69	62.69	62.69
NtubesC	[ ]	79	79	79	79	79	79
NtubesE	[ ]	40	40	40	40	40	40
twebC	[ft]	0.00112	0.00112	0.00112	0.00112	0.00112	0.00112
twallC	[ft]	0.00138	0.00138	0.00138	0.00138	0.00138	0.00138
HfinC	[ft]	0.026	0.026	0.026	0.026	0.026	0.026
twebE	[ft]	0.00112	0.00112	0.00112	0.00112	0.00112	0.00112
twallE	[ft]	0.00138	0.00138	0.00138	0.00138	0.00138	0.00138
HfinE	[ft]	0.026	0.026	0.026	0.026	0.026	0.026
Lcap	[in]	19	19	19	19	19	19
Dcap	[in]	0.128	0.128	0.128	0.128	0.128	0.128
Dh_tC	[ft]	0.00219	0.00219	0.00219	0.00219	0.00219	0.00219
Dh_tE	[ft]	0.00219	0.00219	0.00219	0.00219	0.00219	0.00219
Dh_airC	[ft]	0.00639	0.00639	0.00639	0.00639	0.00639	0.00639
Dh_airE	[ft]	0.0064	0.0064	0.0064	0.0064	0.0064	0.0064
AfrontC	[ft^2]	16	16	16	16	16	16
AfrontE	[ft^2]	4.75	4.75	4.75	4.75	4.75	4.75
DeqinC	[ft]	0.00282	0.00282	0.00282	0.00282	0.00282	0.00282
DeqinE	[ft]	0.00282	0.00282	0.00282	0.00282	0.00282	0.00282
HtubeDistC	[ft]	0.0614	0.0614	0.0614	0.0614	0.0614	0.0614
HtubeDistE	[ft]	0.0614	0.0614	0.0614	0.0614	0.0614	0.0614
VtubeDistC	[ft]	0.03224	0.03224	0.03224	0.03224	0.03224	0.03224
VtubeDistE	[ft]	0.03224	0.03224	0.03224	0.03224	0.03224	0.03224
FinThC	[ft]	0.000417	0.000417	0.000417	0.000417	0.000417	0.000417
FinThE	[ft]	0.000417	0.000417	0.000417	0.000417	0.000417	0.000417
taEwet	[F]	-12.5	16.5	-6.4	-9.6	0.3	-6.1
AairE	[ft^2]	135.654	135.654	135.654	135.654	135.654	135.654
hairE	[Btu/hr-ft^2-F]	14.06	14.06	14.06	14.05	14.05	14.05

hreftpE	[Btu/hr-ft^2-F]	433.21	434.58	434.95	435.63	435.55	435.92
seffEw	[ ]	0.98	0.98	0.98	0.98	0.98	0.98
Tshell	[F]	103.8	103.9	112.2	116	117.1	117.5
dpC	[psia]	0.3	0.3	0.3	0.3	0.3	0.3
dpE	[psia]	1.2	1.2	1.2	1.2	1.2	1.2
ThetaLoC	[deg]	27	27	27	27	27	27
HlouvC	[ft]	0.02167	0.02167	0.02167	0.02167	0.02167	0.02167
HlouvdistC	[ft]	0.004583	0.004583	0.004583	0.004583	0.004583	0.004583
ThetaLoE	[deg]	27	27	27	27	27	27
HlouvE	[ft]	0.02167	0.02167	0.02167	0.02167	0.02167	0.02167
HlouvdistE	[ft]	0.004583	0.004583	0.004583	0.004583	0.004583	0.004583
DeffC	[ft]	0.0033	0.0033	0.0033	0.0033	0.0033	0.0033
DeffE	[ft]	0.0033	0.0033	0.0033	0.0033	0.0033	0.0033
VheadCin	[ft^3]	0.00779	0.00779	0.00779	0.00779	0.00779	0.00779
VheadCout	[ft^3]	0.00779	0.00779	0.00779	0.00779	0.00779	0.00779
VheadEin	[ft^3]	0.00395	0.00395	0.00395	0.00395	0.00395	0.00395
VheadEout	[ft^3]	0.00395	0.00395	0.00395	0.00395	0.00395	0.00395
MheadCin	[lbm]	0.03795	0.03814	0.04272	0.04492	0.04556	0.04582
MheadCout	[lbm]	0.49774	0.49719	0.48449	0.47853	0.47671	0.47598
MheadEin	[lbm]	0.04935	0.04942	0.04374	0.04172	0.04111	0.04095
MheadEout	[lbm]	0.00917	0.00922	0.00935	0.00943	0.00945	0.00947
DheadC	[ft]	0.06242	0.06242	0.06242	0.06242	0.06242	0.06242
DheadE	[ft]	0.06242	0.06242	0.06242	0.06242	0.06242	0.06242
etaisenComp	[ ]	0.574	0.575	0.571	0.566	0.564	0.563
AairC	[ft^2]	452.245	452.245	452.245	452.245	452.245	452.245
hairC	[Btu/hr-ft^2-F]	13.82	13.82	13.8	13.79	13.79	13.79
hreftpC	[Btu/hr-ft^2-F]	447.27	447.02	427.13	418.47	415.76	414.87
NlouvC	[ ]	10	10	10	10	10	10
NlouvE	[ ]	10	10	10	10	10	10
dPairC	[psia]	0.0011351	0.0011349	0.0011295	0.0011272	0.0011265	0.0011262
dPairE	[psia]	0.0011339	0.0011335	0.0011353	0.001136	0.0011363	0.0011362
eta_fanC	[ ]	0.18	0.18	0.18	0.18	0.18	0.18
Le	[ ]	0.821	0.821	0.821	0.821	0.821	0.821
hD	[1/hr-ft^2-lbm of air]	66.17	66.17	66.17	66.17	66.14	66.17
ttubeEi	[F]	46.39	46.69	47.63	48.17	48.28	48.4
ttubeEo	[F]	45.93	46.24	47.16	47.7	47.81	47.93
NCht	[ ]	8	8	8	8	8	8
DCht	[ft]	0.01583	0.01583	0.01583	0.01583	0.01583	0.01583
LCht	[ft]	3.33	3.33	3.33	3.33	3.33	3.33
UlossCht	[Btu/hr-ft2-F]	0	0	0	0	0	0
pdCht	[psia]	0.04	0.04	0.04	0.04	0.04	0.04
qlossCht	[Btu/hr]	0	0	0	0	0	0
MCht	[lbm]	0.33482	0.33445	0.3259	0.3219	0.32067	0.32018
VCht	[ft^3]	0.00524	0.00524	0.00524	0.00524	0.00524	0.00524

Table D.3 Dry indoor/high outdoor ambient temperature system simulation runs

	Corresp. Exp. Data set	80/96 (10-26-98)	80/104 (10-3-98)	80/106 (10-24-98)	80/111 (10-25-98)	80/118 (10-4-98)	80/118 (10-25-98)
COP	[ ]	3.0468	2.5569	2.4599	2.1601	1.7001	1.7030
EER	[Btu/hr-W]	10.3957	8.7243	8.3931	7.3704	5.8006	5.8105
qEvap	[Btu/hr]	24562	23525	23313	22626	21506	21616
degsubcool	[F]	16.4	19	19.8	22.9	31.1	31.4
degsup	[F]	10	10	10	10	10	10
tsatincomp	[F]	43.9	45.2	45.6	46.5	48	48.3
tsatoutcomp	[F]	113.4	123.6	126.1	134	148.8	149.3
w	[lbm/hr]	334	333.9	334.3	334.3	332.6	334.7
PwrComp	[W]	2063.3	2379.5	2465.9	2752.2	3366.5	3388.9
Acond	[ft^2]	107.793	107.793	107.793	107.793	107.793	107.793
Aevap	[ft^2]	32.001	32.001	32.001	32.001	32.001	32.001
a2phEdry	[ft^2]	30.225	30.12	30.092	30.013	29.89	29.89
a2phEwet	[ft^2]	0	0	0	0	0	0
esupC	[ ]	0.806	0.805	0.804	0.795	0.769	0.768
e2phC	[ ]	0.874	0.875	0.875	0.876	0.875	0.875
esubC	[ ]	0.965	0.984	0.987	0.993	0.997	0.996
e2phE	[ ]	0.847	0.847	0.848	0.848	0.848	0.848
e2phEwet	[ ]	0.75	0.75	0.75	0.75	0.75	0.75
esupE	[ ]	0.571	0.567	0.566	0.564	0.557	0.559
fsupC	[ ]	0.188	0.218	0.224	0.242	0.25	0.25
f2phC	[ ]	0.565	0.463	0.438	0.355	0.219	0.216
fsubC	[ ]	0.247	0.319	0.338	0.402	0.531	0.534
f2phE	[ ]	0.944	0.941	0.94	0.938	0.934	0.934
fsupE	[ ]	0.056	0.059	0.06	0.062	0.066	0.066
h0	[Btu/lbm]	147.7	151.6	152.6	155.8	162.2	162.2
h1	[Btu/lbm]	145.5	149.1	150	152.9	158.7	158.7
h2i	[Btu/lbm]	120.8	120.2	120.1	119.5	118.2	118.2
h2o	[Btu/lbm]	55.9	60.3	61.5	65.3	73.4	73.8
h3	[Btu/lbm]	49.2	52.4	53.2	55.3	58.4	58.5
h4	[Btu/lbm]	49.2	52.4	53.2	55.3	58.4	58.5
h5	[Btu/lbm]	49.2	52.4	53.2	55.3	58.4	58.5
h7i	[Btu/lbm]	49.2	52.4	53.2	55.3	58.4	58.5
h7o	[Btu/lbm]	120	120	120	120.1	120.2	120.2
h9	[Btu/lbm]	122.8	122.9	122.9	123	123	123.1
h10	[Btu/lbm]	127.6	128.5	128.7	129.2	129.9	129.9
MtotC	[lbm]	2.432	2.516	2.535	2.594	2.698	2.698
MtotE	[lbm]	0.316	0.308	0.306	0.302	0.296	0.297
MsupC	[lbm]	0.067	0.087	0.092	0.109	0.132	0.133
M2phC	[lbm]	0.959	0.811	0.772	0.639	0.399	0.394
MsubC	[lbm]	0.886	1.107	1.162	1.346	1.681	1.684
M2phE	[lbm]	0.264	0.259	0.258	0.255	0.252	0.252
MsupE	[lbm]	0.002	0.003	0.003	0.003	0.003	0.003
Maccum	[lbm]	0	0	0	0	0	0
Mcaptube	[lbm]	0.02	0.02	0.02	0.02	0.02	0.02
Mcomp	[lbm]	0.138	0.138	0.138	0.138	0.136	0.137
MdisLine	[lbm]	0.09	0.1	0.103	0.111	0.127	0.128
MliqLine	[lbm]	1.135	1.098	1.088	1.059	1.001	0.999
MsuctLine	[lbm]	0.088	0.09	0.091	0.092	0.094	0.095
Mrefoil	[lbm]	0.32	0.281	0.272	0.247	0.205	0.206
p0	[psia]	397.6	453.2	468	516.5	617.8	621.6
p1	[psia]	397.5	453.1	468	516.5	617.8	621.5
p2i	[psia]	397.4	453	467.9	516.4	617.7	621.4

p2avg	[psia]	397.3	453	467.8	516.3	617.7	621.4
p2o	[psia]	397.3	452.9	467.8	516.3	617.7	621.4
p3i	[psia]	397.2	452.9	467.7	516.2	617.6	621.3
p4	[psia]	397.2	452.8	467.7	516.2	617.5	621.2
p5	[psia]	395.7	451.3	466.2	514.7	616	619.7
p7ii	[psia]	148.8	151.7	152.6	154.9	158.4	159.3
p7avg	[psia]	148.3	151.2	152.1	154.4	157.9	158.8
p7o	[psia]	147.8	150.7	151.6	153.9	157.4	158.3
p9	[psia]	147.6	150.5	151.4	153.7	157.2	158
p10	[psia]	142.3	145.3	146.2	148.5	152.2	153
qCond	[Btu/hr]	32154	32290	32382	32643	33351	33538
qspray	[Btu/hr]	0	0	0	0	0	0
qsupC	[Btu/hr]	8258	9640	10011	11174	13442	13551
q2phC	[Btu/hr]	21688	20000	19580	18127	14906	14875
qsubC	[Btu/hr]	2208	2650	2791	3342	5003	5112
q2phE	[Btu/hr]	23620	22576	22359	21666	20547	20648
q2phEdry	[Btu/hr]	23620	22576	22359	21666	20547	20648
q2phEwet	[Btu/hr]	0	0	0	0	0	0
q2phEwetlat	[Btu/hr]	0	0	0	0	0	0
q2phEwetsns	[Btu/hr]	0	0	0	0	0	0
qsupE	[Btu/hr]	942	949	953	960	960	967
t0	[F]	191.7	212	217	233.2	264.5	264.9
t1o	[F]	184.2	203.5	208.3	223.6	252.9	253.4
t2i	[F]	113.4	123.5	126.1	134	148.8	149.3
t2avg	[F]	113.4	123.5	126.1	134	148.8	149.3
t2o	[F]	113.4	123.5	126.1	134	148.8	149.3
t3i	[F]	97	104.5	106.3	111.1	117.7	117.9
t4	[F]	97	104.5	106.3	111.1	117.7	117.9
t5	[F]	97	104.5	106.3	111.1	117.7	117.9
t7i	[F]	46.6	47.8	48.1	49	50.4	50.7
t7avg	[F]	46.4	47.6	47.9	48.8	50.2	50.5
t7o	[F]	46.2	47.4	47.7	48.6	50	50.4
t9	[F]	56.2	57.4	57.7	58.6	60	60.4
t10	[F]	72.8	77	77.9	80.6	84.4	84.6
tafanoutC	[F]	109.1	117.2	119.1	124.2	131.5	131.8
tasupoutC	[F]	113.3	121.5	123.5	129.2	139.2	139.6
ta2phoutC	[F]	111.2	121.1	123.6	131.1	144.9	145.4
tasuboutC	[F]	99.9	107.5	109.2	114.2	121.4	121.6
taoutC	[F]	108.8	116.9	118.7	123.8	131	131.3
TainE	[F]	80.2	80	80.1	80.1	80	80.5
TainEwet	[F]	51.6	52.5	52.8	53.6	54.7	55.1
ta2phoutE	[F]	51.6	52.5	52.8	53.6	54.7	55.1
tasupoutE	[F]	60.8	61.5	61.8	62.4	63.3	63.6
taoutE	[F]	52.1	53.1	53.4	54.1	55.3	55.6
tafanoutE	[F]	52.7	53.6	54	54.7	55.9	56.2
usupC	[Btu/hr-ft^2-F]	11.5	10	9.7	8.9	8.2	8.2
u2phC	[Btu/hr-ft^2-F]	49.6	49.3	49.2	48.8	48.1	48.1
usubC	[Btu/hr-ft^2-F]	23.7	22.9	22.8	22.2	21.1	21.1
u2phE	[Btu/hr-ft^2-F]	51.3	51.3	51.3	51.3	51.3	51.3
u2phEwet	[Btu/hr-ft^2-F]	51.3	51.3	51.3	51.3	51.3	51.3
usupE	[Btu/hr-ft^2-F]	30.2	30.2	30.2	30.2	30.2	30.3
TubeLenC	[ft]	6.28	6.28	6.28	6.28	6.28	6.28
TubeLenE	[ft]	3.68	3.68	3.68	3.68	3.68	3.68
Vcond	[ft^3]	0.059	0.059	0.059	0.059	0.059	0.059
VolextC	[ft^3]	0.9825	0.9825	0.9825	0.9825	0.9825	0.9825
VolextE	[ft^3]	0.2917	0.2917	0.2917	0.2917	0.2917	0.2917

x2o	[ ]	0	0	0	0	0	0
x4	[ ]	0	0	0	0	0	0
x5	[ ]	0	0	0	0	0	0
x7i	[ ]	0.215	0.246	0.253	0.274	0.305	0.305
x7o	[ ]	1	1	1	1	1	1
MWR	[lbm]	0	0	0	0	0	0
tfinEi	[F]	48.7	50	50.3	51.3	52.7	53.1
tfinEo	[F]	48.3	49.5	49.9	50.8	52.2	52.6
wairEi	[lbm H2O/lbm of air]	0.00512	0.00587	0.00573	0.00603	0.00677	0.00661
wairEo	[lbm H2O/lbm of air]	0.005	0.006	0.006	0.006	0.007	0.007
wfinEi	[lbm H2O/lbm of air]	0.00749	0.00785	0.00796	0.00825	0.00871	0.00882
wfinEo	[lbm H2O/lbm of air]	0.00749	0.00785	0.00796	0.00825	0.00871	0.00882
Tindoor	[F]	80.2	80	80.1	80.1	80	80.5
Toutdoor	[F]	96.4	104.2	106	110.9	117.6	117.8
RhaiC	[ ]	0.405	0.405	0.405	0.405	0.405	0.405
RhaiE	[ ]	0.228	0.263	0.256	0.269	0.303	0.291
vdotaCmeas	[cfm]	2600	2600	2600	2600	2600	2600
vdotaE	[cfm]	800	800	800	800	800	800
PwrFanE	[W]	116.4	124	118.9	118.5	124	117.9
PwrFanC	[W]	144.8	144.5	144.5	144.3	144.1	144.1
Mtotal	[lbm]	4.8583	4.8583	4.8583	4.8583	4.8583	4.8583
NportsC	[ports/tube]	19	19	19	19	19	19
porgeoC	[]	1	1	1	1	1	1
NportsE	[ports/tube]	19	19	19	19	19	19
porgeoE	[]	1	1	1	1	1	1
geodesC	[ ]	62.69	62.69	62.69	62.69	62.69	62.69
geodesE	[ ]	62.69	62.69	62.69	62.69	62.69	62.69
NtubesC	[ ]	79	79	79	79	79	79
NtubesE	[ ]	40	40	40	40	40	40
twebC	[ft]	0.00112	0.00112	0.00112	0.00112	0.00112	0.00112
twallC	[ft]	0.00138	0.00138	0.00138	0.00138	0.00138	0.00138
HfinC	[ft]	0.026	0.026	0.026	0.026	0.026	0.026
twebE	[ft]	0.00112	0.00112	0.00112	0.00112	0.00112	0.00112
twallE	[ft]	0.00138	0.00138	0.00138	0.00138	0.00138	0.00138
HfinE	[ft]	0.026	0.026	0.026	0.026	0.026	0.026
Lcap	[in]	19	19	19	19	19	19
Dcap	[in]	0.128	0.128	0.128	0.128	0.128	0.128
Dh_tC	[ft]	0.00219	0.00219	0.00219	0.00219	0.00219	0.00219
Dh_tE	[ft]	0.00219	0.00219	0.00219	0.00219	0.00219	0.00219
Dh_airC	[ft]	0.00639	0.00639	0.00639	0.00639	0.00639	0.00639
Dh_airE	[ft]	0.0064	0.0064	0.0064	0.0064	0.0064	0.0064
AfrontC	[ft^2]	16	16	16	16	16	16
AfrontE	[ft^2]	4.75	4.75	4.75	4.75	4.75	4.75
DeqinC	[ft]	0.00282	0.00282	0.00282	0.00282	0.00282	0.00282
DeqinE	[ft]	0.00282	0.00282	0.00282	0.00282	0.00282	0.00282
HtubeDistC	[ft]	0.0614	0.0614	0.0614	0.0614	0.0614	0.0614
HtubeDistE	[ft]	0.0614	0.0614	0.0614	0.0614	0.0614	0.0614
VtubeDistC	[ft]	0.03224	0.03224	0.03224	0.03224	0.03224	0.03224
VtubeDistE	[ft]	0.03224	0.03224	0.03224	0.03224	0.03224	0.03224
FinThC	[ft]	0.000417	0.000417	0.000417	0.000417	0.000417	0.000417
FinThE	[ft]	0.000417	0.000417	0.000417	0.000417	0.000417	0.000417
taEwet	[F]	-9.5	8.7	1.9	5.7	19.3	12.5
AairE	[ft^2]	135.654	135.654	135.654	135.654	135.654	135.654

hairE	[Btu/hr-ft^2-F]	14.05	14.05	14.05	14.05	14.05	14.05
hreftpE	[Btu/hr-ft^2-F]	436.44	437.05	437.49	437.54	435.7	437.27
seffEw	[ ]	0.98	0.98	0.98	0.98	0.98	0.98
Tshell	[F]	118.8	128.7	131.2	139.1	154.3	154.5
dpC	[psia]	0.3	0.3	0.3	0.2	0.2	0.2
dpE	[psia]	1.2	1.2	1.2	1.2	1.2	1.2
ThetaLoC	[deg]	27	27	27	27	27	27
HlouvC	[ft]	0.02167	0.02167	0.02167	0.02167	0.02167	0.02167
HlouvdistC	[ft]	0.004583	0.004583	0.004583	0.004583	0.004583	0.004583
ThetaLoE	[deg]	27	27	27	27	27	27
HlouvE	[ft]	0.02167	0.02167	0.02167	0.02167	0.02167	0.02167
HlouvdistE	[ft]	0.004583	0.004583	0.004583	0.004583	0.004583	0.004583
DeffC	[ft]	0.0033	0.0033	0.0033	0.0033	0.0033	0.0033
DeffE	[ft]	0.0033	0.0033	0.0033	0.0033	0.0033	0.0033
VheadCin	[ft^3]	0.00779	0.00779	0.00779	0.00779	0.00779	0.00779
VheadCout	[ft^3]	0.00779	0.00779	0.00779	0.00779	0.00779	0.00779
VheadEin	[ft^3]	0.00395	0.00395	0.00395	0.00395	0.00395	0.00395
VheadEout	[ft^3]	0.00395	0.00395	0.00395	0.00395	0.00395	0.00395
MheadCin	[lbm]	0.04665	0.05266	0.05426	0.05919	0.06958	0.07004
MheadCout	[lbm]	0.4738	0.4583	0.45432	0.44186	0.41772	0.41682
MheadEin	[lbm]	0.04036	0.03651	0.03578	0.03386	0.03148	0.03164
MheadEout	[lbm]	0.00951	0.0097	0.00975	0.00989	0.01012	0.01021
DheadC	[ft]	0.06242	0.06242	0.06242	0.06242	0.06242	0.06242
DheadE	[ft]	0.06242	0.06242	0.06242	0.06242	0.06242	0.06242
etaisenComp	[ ]	0.561	0.539	0.533	0.511	0.468	0.468
AairC	[ft^2]	452.245	452.245	452.245	452.245	452.245	452.245
hairC	[Btu/hr-ft^2-F]	13.79	13.77	13.77	13.76	13.75	13.75
hreftpC	[Btu/hr-ft^2-F]	411.85	389.75	384.31	366.97	331.41	330.56
NlouvC	[ ]	10	10	10	10	10	10
NlouvE	[ ]	10	10	10	10	10	10
dPairC	[psia]	0.0011255	0.0011203	0.0011192	0.001116	0.0011118	0.0011117
dPairE	[psia]	0.0011364	0.0011382	0.0011385	0.0011396	0.0011415	0.001141
eta_fanC	[ ]	0.18	0.18	0.18	0.18	0.18	0.18
Le	[ ]	0.821	0.821	0.821	0.821	0.821	0.821
hD	[1/hr-ft^2-lbm of air]	66.17	66.14	66.13	66.17	66.15	66.17
ttubeEi	[F]	48.66	49.89	50.28	51.22	52.66	53.02
ttubeEo	[F]	48.18	49.41	49.79	50.72	52.15	52.5
NCht	[ ]	8	8	8	8	8	8
DCht	[ft]	0.01583	0.01583	0.01583	0.01583	0.01583	0.01583
LCht	[ft]	3.33	3.33	3.33	3.33	3.33	3.33
UlossCht	[Btu/hr-ft2-F]	0	0	0	0	0	0
pdCht	[psia]	0.04	0.04	0.04	0.04	0.04	0.04
qlossCht	[Btu/hr]	0	0	0	0	0	0
MCht	[lbm]	0.31872	0.30829	0.30561	0.29723	0.28099	0.28038
VCht	[ft^3]	0.00524	0.00524	0.00524	0.00524	0.00524	0.00524

Table D.4 Wet indoor system simulation runs

	Corresp. Exp. Data set	80/70 (10-6-98)	80/75 (10-7-98)	80/82 (10-7-98)	80/95 (10-9-98)	80/105 (10-9-98)	80/118 (10-12-98)
COP	[ ]	5.3357	4.9445	4.4553	3.5602	2.8716	2.0108
EER	[Btu/hr-W]	18.2056	16.8707	15.2015	12.1474	9.7981	6.8608
qEvap	[Btu/hr]	31205	30677	29819	28045	26329	23893
degsubcool	[F]	3.5	6.3	9.3	13.5	16.7	25.2
degsup	[F]	10	10	10	10	10	10
tsatincomp	[F]	48.1	48.5	48.9	49.9	50.8	52.3
tsatoutcomp	[F]	85.1	90.6	97.5	111.1	123.3	143.9
w	[lbm/hr]	389.2	387.7	384.4	380.1	375.9	369.4
PwrComp	[W]	1390.8	1489.5	1632.1	1973.2	2346.9	3137.5
Acond	[ft^2]	107.793	107.793	107.793	107.793	107.793	107.793
Aevap	[ft^2]	32.001	32.001	32.001	32.001	32.001	32.001
a2phEdry	[ft^2]	0	0	0	0	0	0
a2phEwet	[ft^2]	29.536	29.509	29.483	29.366	29.285	29.131
esupC	[ ]	0.745	0.757	0.772	0.793	0.803	0.783
e2phC	[ ]	0.867	0.869	0.871	0.874	0.877	0.878
esubC	[ ]	0.56	0.489	0.62	0.844	0.937	0.988
e2phE	[ ]	0.1	0.1	0.1	0.1	0.1	0.1
e2phEwet	[ ]	0.849	0.849	0.849	0.849	0.849	0.85
esupE	[ ]	0.57	0.568	0.565	0.559	0.554	0.546
fsupC	[ ]	0.098	0.107	0.119	0.151	0.185	0.238
f2phC	[ ]	0.879	0.846	0.798	0.689	0.568	0.319
fsubC	[ ]	0.023	0.048	0.083	0.16	0.247	0.443
f2phE	[ ]	0.923	0.922	0.921	0.918	0.915	0.91
fsupE	[ ]	0.077	0.078	0.079	0.082	0.085	0.09
h0	[Btu/lbm]	135.9	137.5	139.6	144.2	148.8	157.2
h1	[Btu/lbm]	134.8	136.3	138.3	142.6	146.8	154.5
h2i	[Btu/lbm]	121.3	121.3	121.2	120.9	120.3	118.7
h2o	[Btu/lbm]	44.2	46.4	49.2	54.8	60.2	70.5
h3	[Btu/lbm]	42.9	44	45.6	49.4	53.2	58.7
h4	[Btu/lbm]	42.9	44	45.6	49.4	53.2	58.7
h5	[Btu/lbm]	42.9	44	45.6	49.4	53.2	58.7
h7i	[Btu/lbm]	42.9	44	45.6	49.4	53.2	58.7
h7o	[Btu/lbm]	120.2	120.2	120.2	120.3	120.3	120.4
h9	[Btu/lbm]	123.1	123.1	123.1	123.2	123.3	123.3
h10	[Btu/lbm]	124.2	124.8	125.5	126.8	127.9	129.3
MtotC	[lbm]	1.979	2.051	2.14	2.297	2.423	2.606
MtotE	[lbm]	0.355	0.349	0.341	0.325	0.313	0.299
MsupC	[lbm]	0.024	0.029	0.035	0.053	0.075	0.121
M2phC	[lbm]	1.326	1.303	1.264	1.146	0.982	0.576
MsubC	[lbm]	0.088	0.182	0.309	0.577	0.856	1.419
M2phE	[lbm]	0.276	0.273	0.27	0.263	0.257	0.249
MsupE	[lbm]	0.004	0.004	0.004	0.004	0.004	0.004
Maccum	[lbm]	0	0	0	0	0	0
Mcaptube	[lbm]	0.02	0.02	0.02	0.02	0.02	0.02
Mcomp	[lbm]	0.162	0.161	0.159	0.157	0.155	0.151
MdisLine	[lbm]	0.067	0.071	0.077	0.09	0.102	0.124
MliqLine	[lbm]	1.217	1.203	1.183	1.139	1.094	1.013
MsuctLine	[lbm]	0.095	0.096	0.096	0.098	0.099	0.101
Mrefoil	[lbm]	0.621	0.569	0.508	0.413	0.345	0.259
p0	[psia]	269.5	291.5	320.9	385.6	451.4	582.6
p1	[psia]	269.4	291.4	320.8	385.6	451.4	582.5
p2i	[psia]	269.3	291.2	320.7	385.4	451.2	582.4
p2avg	[psia]	269.2	291.1	320.6	385.3	451.1	582.4

112

p2o	[psia]	269	291	320.5	385.3	451.1	582.4
p3i	[psia]	269	291	320.5	385.2	451	582.3
p4	[psia]	269	291	320.4	385.2	451	582.2
p5	[psia]	267.1	289.1	318.5	383.3	449.1	580.3
p7ii	[psia]	160.3	161.3	162	164.5	166.8	170.5
p7avg	[psia]	159.8	160.8	161.5	164	166.3	170
p7o	[psia]	159.2	160.2	161	163.5	165.8	169.4
p9	[psia]	158.8	159.8	160.6	163.1	165.4	169.1
p10	[psia]	152.5	153.6	154.4	157.1	159.5	163.5
qCond	[Btu/hr]	35770	35777	35638	35407	35196	35421
qspray	[Btu/hr]	0	0	0	0	0	0
qsupC	[Btu/hr]	5280	5815	6553	8245	9992	13249
q2phC	[Btu/hr]	29984	29041	27700	25095	22578	17813
qsubC	[Btu/hr]	506	922	1384	2067	2625	4359
q2phE	[Btu/hr]	30074	29548	28699	26934	25226	22803
q2phEdry	[Btu/hr]	0	0	0	0	0	0
q2phEwet	[Btu/hr]	30074	29548	28699	26934	25226	22803
q2phEwetlat	[Btu/hr]	10163	9856	9302	8414	7287	5834
q2phEwetsns	[Btu/hr]	19911	19692	19397	18521	17940	16969
qsupE	[Btu/hr]	1131	1129	1120	1110	1102	1090
t0	[F]	131.3	140.5	152.8	178.1	202.2	244.7
t1o	[F]	127.5	136.5	148.3	172.7	195.7	236
t2i	[F]	85	90.5	97.4	111.1	123.2	143.9
t2avg	[F]	85	90.5	97.4	111.1	123.2	143.9
t2o	[F]	85	90.5	97.4	111	123.2	143.9
t3i	[F]	81.5	84.2	88.1	97.5	106.5	118.6
t4	[F]	81.5	84.2	88.1	97.5	106.5	118.6
t5	[F]	81.5	84.2	88.1	97.5	106.5	118.6
t7i	[F]	51.1	51.5	51.8	52.7	53.6	54.9
t7avg	[F]	50.9	51.3	51.6	52.5	53.4	54.7
t7o	[F]	50.7	51.1	51.4	52.3	53.2	54.6
t9	[F]	60.7	61.1	61.4	62.3	63.2	64.6
t10	[F]	63	65.3	68.1	73.7	78.5	84.8
tafanoutC	[F]	83.9	89.4	96.1	108.9	119.5	132.9
tasupoutC	[F]	90.3	96.1	103.1	116.1	126.6	140.6
ta2phoutC	[F]	83.1	88.6	95.5	109	121	140.7
tasuboutC	[F]	78.6	83	88.7	100	109.6	122.3
taoutC	[F]	83.7	89.1	95.8	108.6	119.2	132.5
TainE	[F]	80.1	80.2	80.1	79.9	80	80.1
TainEwet	[F]	80.1	80.2	80.1	79.9	80	80.1
ta2phoutE	[F]	55.5	55.8	56.1	56.8	57.6	58.7
tasupoutE	[F]	63.4	63.7	63.9	64.5	65.1	66.2
taoutE	[F]	56.1	56.4	56.7	57.5	58.2	59.4
tafanoutE	[F]	56.7	57	57.3	58	58.8	60
usupC	[Btu/hr-ft^2-F]	23.2	22.3	20.7	17.4	14.4	10.3
u2phC	[Btu/hr-ft^2-F]	50.8	50.6	50.4	49.9	49.4	48.5
usubC	[Btu/hr-ft^2-F]	25.5	25.2	24.7	23.8	22.9	21.3
u2phE	[Btu/hr-ft^2-F]	51.8	51.8	51.7	51.7	51.7	51.6
u2phEwet	[Btu/hr-ft^2-F]	51.8	51.8	51.7	51.7	51.7	51.6
usupE	[Btu/hr-ft^2-F]	31.8	31.8	31.7	31.6	31.5	31.4
TubeLenC	[ft]	6.28	6.28	6.28	6.28	6.28	6.28
TubeLenE	[ft]	3.68	3.68	3.68	3.68	3.68	3.68
Vcond	[ft^3]	0.059	0.059	0.059	0.059	0.059	0.059
VolextC	[ft^3]	0.9825	0.9825	0.9825	0.9825	0.9825	0.9825
VolextE	[ft^3]	0.2917	0.2917	0.2917	0.2917	0.2917	0.2917
x2o	[ ]	0	0	0	0	0	0

x4	[ ]	0	0	0	0	0	0
x5	[ ]	0	0	0	0	0	0
x7i	[ ]	0.128	0.139	0.156	0.196	0.236	0.294
x7o	[ ]	1	1	1	1	1	1
MWR	[lbm]	9.69	9.4	8.87	8.02	6.95	5.56
tfinEi	[F]	55.9	56.2	56.4	57.1	57.8	58.8
tfinEo	[F]	51.9	52.3	52.6	53.5	54.3	55.7
wairEi	[lbm H2O/lbm of air]	0.01178	0.01182	0.01176	0.01182	0.01179	0.01185
wairEo	[lbm H2O/lbm of air]	0.009	0.009	0.009	0.009	0.01	0.01
wfinEi	[lbm H2O/lbm of air]	0.00981	0.00992	0.00999	0.01025	0.01049	0.01089
wfinEo	[lbm H2O/lbm of air]	0.00845	0.00857	0.00866	0.00896	0.00924	0.00971
Tindoor	[F]	80.1	80.2	80.1	79.9	80	80.1
Toutdoor	[F]	70.5	75.8	82.4	95	105.4	118.3
RhaiC	[ ]	0.405	0.405	0.405	0.405	0.405	0.405
RhaiE	[ ]	0.521	0.521	0.52	0.526	0.523	0.524
vdotaCmeas	[cfm]	2600	2600	2600	2600	2600	2600
vdotaE	[cfm]	800	800	800	800	800	800
PwrFanE	[W]	149.6	152.6	150.5	148.9	145.2	134.2
PwrFanC	[W]	145.6	145.4	145.2	144.8	144.5	144.1
Mtotal	[lbm]	4.8583	4.8583	4.8583	4.8583	4.8583	4.8583
NportsC	[ports/tube]	19	19	19	19	19	19
porgeoC	[]	1	1	1	1	1	1
NportsE	[ports/tube]	19	19	19	19	19	19
porgeoE	[]	1	1	1	1	1	1
geodesC	[ ]	62.69	62.69	62.69	62.69	62.69	62.69
geodesE	[ ]	62.69	62.69	62.69	62.69	62.69	62.69
NtubesC	[ ]	79	79	79	79	79	79
NtubesE	[ ]	40	40	40	40	40	40
twebC	[ft]	0.00112	0.00112	0.00112	0.00112	0.00112	0.00112
twallC	[ft]	0.00138	0.00138	0.00138	0.00138	0.00138	0.00138
HfinC	[ft]	0.026	0.026	0.026	0.026	0.026	0.026
twebE	[ft]	0.00112	0.00112	0.00112	0.00112	0.00112	0.00112
twallE	[ft]	0.00138	0.00138	0.00138	0.00138	0.00138	0.00138
HfinE	[ft]	0.026	0.026	0.026	0.026	0.026	0.026
Lcap	[in]	19	19	19	19	19	19
Dcap	[in]	0.128	0.128	0.128	0.128	0.128	0.128
Dh_tC	[ft]	0.00219	0.00219	0.00219	0.00219	0.00219	0.00219
Dh_tE	[ft]	0.00219	0.00219	0.00219	0.00219	0.00219	0.00219
Dh_airC	[ft]	0.00639	0.00639	0.00639	0.00639	0.00639	0.00639
Dh_airE	[ft]	0.0064	0.0064	0.0064	0.0064	0.0064	0.0064
AfrontC	[ft^2]	16	16	16	16	16	16
AfrontE	[ft^2]	4.75	4.75	4.75	4.75	4.75	4.75
DeqinC	[ft]	0.00282	0.00282	0.00282	0.00282	0.00282	0.00282
DeqinE	[ft]	0.00282	0.00282	0.00282	0.00282	0.00282	0.00282
HtubeDistC	[ft]	0.0614	0.0614	0.0614	0.0614	0.0614	0.0614
HtubeDistE	[ft]	0.0614	0.0614	0.0614	0.0614	0.0614	0.0614
VtubeDistC	[ft]	0.03224	0.03224	0.03224	0.03224	0.03224	0.03224
VtubeDistE	[ft]	0.03224	0.03224	0.03224	0.03224	0.03224	0.03224
FinThC	[ft]	0.000417	0.000417	0.000417	0.000417	0.000417	0.000417
FinThE	[ft]	0.000417	0.000417	0.000417	0.000417	0.000417	0.000417
taEwet	[F]	126.4	124.5	121.2	115.9	109.5	101.4
AairE	[ft^2]	135.654	135.654	135.654	135.654	135.654	135.654
hairE	[Btu/hr-ft^2-F]	14.04	14.04	14.04	14.04	14.04	14.04

hreftpE	[Btu/hr-ft^2-F]	477.74	476.87	474.65	472.52	470.28	465.59
seffEw	[ ]	0.98	0.98	0.98	0.98	0.98	0.98
Tshell	[F]	89.5	94	100	112.3	124	144.6
dpC	[psia]	0.4	0.4	0.4	0.3	0.3	0.3
dpE	[psia]	1.5	1.5	1.4	1.4	1.4	1.4
ThetaLoC	[deg]	27	27	27	27	27	27
HlouvC	[ft]	0.02167	0.02167	0.02167	0.02167	0.02167	0.02167
HlouvdistC	[ft]	0.004583	0.004583	0.004583	0.004583	0.004583	0.004583
ThetaLoE	[deg]	27	27	27	27	27	27
HlouvE	[ft]	0.02167	0.02167	0.02167	0.02167	0.02167	0.02167
HlouvdistE	[ft]	0.004583	0.004583	0.004583	0.004583	0.004583	0.004583
DeffC	[ft]	0.0033	0.0033	0.0033	0.0033	0.0033	0.0033
DeffE	[ft]	0.0033	0.0033	0.0033	0.0033	0.0033	0.0033
VheadCin	[ft^3]	0.00779	0.00779	0.00779	0.00779	0.00779	0.00779
VheadCout	[ft^3]	0.00779	0.00779	0.00779	0.00779	0.00779	0.00779
VheadEin	[ft^3]	0.00395	0.00395	0.00395	0.00395	0.00395	0.00395
VheadEout	[ft^3]	0.00395	0.00395	0.00395	0.00395	0.00395	0.00395
MheadCin	[lbm]	0.03274	0.03533	0.03878	0.04611	0.05337	0.06714
MheadCout	[lbm]	0.50804	0.5021	0.49393	0.47533	0.45673	0.42289
MheadEin	[lbm]	0.0654	0.06169	0.0567	0.04766	0.04122	0.03484
MheadEout	[lbm]	0.01027	0.01034	0.01039	0.01056	0.01071	0.01095
DheadC	[ft]	0.06242	0.06242	0.06242	0.06242	0.06242	0.06242
DheadE	[ft]	0.06242	0.06242	0.06242	0.06242	0.06242	0.06242
etaisenComp	[ ]	0.528	0.554	0.574	0.578	0.558	0.502
AairC	[ft^2]	452.245	452.245	452.245	452.245	452.245	452.245
hairC	[Btu/hr-ft^2-F]	13.84	13.83	13.82	13.79	13.77	13.74
hreftpC	[Btu/hr-ft^2-F]	488.84	476.19	459.94	428.62	400.88	352.83
NlouvC	[ ]	10	10	10	10	10	10
NlouvE	[ ]	10	10	10	10	10	10
dPairC	[psia]	0.0011433	0.0011395	0.0011349	0.0011264	0.0011196	0.0011113
dPairE	[psia]	0.0011425	0.0011428	0.0011434	0.0011449	0.0011458	0.0011474
eta_fanC	[ ]	0.18	0.18	0.18	0.18	0.18	0.18
Le	[ ]	0.82	0.82	0.82	0.82	0.82	0.82
hD	[1/hr-ft^2-lbm of air]	65.38	65.38	65.38	65.37	65.36	65.34
ttubeEi	[F]	55.34	55.65	55.84	56.57	57.2	58.26
ttubeEo	[F]	51.82	52.19	52.48	53.41	54.25	55.59
NCht	[ ]	8	8	8	8	8	8
DCht	[ft]	0.01583	0.01583	0.01583	0.01583	0.01583	0.01583
LCht	[ft]	3.33	3.33	3.33	3.33	3.33	3.33
UlossCht	[Btu/hr-ft2-F]	0	0	0	0	0	0
pdCht	[psia]	0.05	0.05	0.05	0.05	0.05	0.05
qlossCht	[Btu/hr]	0	0	0	0	0	0
MCht	[lbm]	0.34174	0.33775	0.33226	0.31974	0.30723	0.28447
VCht	[ft^3]	0.00524	0.00524	0.00524	0.00524	0.00524	0.00524

Table D.5 Dry indoor/low outdoor ambient temperature evaporator submodel simulation runs

	Corresp. Exp. Data set	80/68 (10-3-98)	80/68 (10-28-98)	80/71 (10-1-98)	80/74 (10-6-98)	80/75 (10-23-98)	80/81 (10-23-98)
qEvap	[Btu/hr]	27923	27398	27455	26975	27531	27206
degsup	[F]	32.2	38.5	34.6	37.4	15.4	11.5
w	[lbm/hr]	322.9	310.7	317.4	313	342.6	351.3
Aevap	[ft^2]	32.001	32.001	32.001	32.001	32.001	32.001
a2phEdry	[ft^2]	25.738	23.698	24.9	23.818	29.423	30.101
a2phEwet	[ft^2]	0	0	0	0	0	0
e2phE	[ ]	0.846	0.846	0.846	0.846	0.846	0.847
e2phEwet	[ ]	0.75	0.75	0.75	0.75	0.75	0.75
esupE	[ ]	0.768	0.876	0.82	0.869	· 0.53	0.571
f2phE	[ ]	0.804	0.741	0.778	0.744	0.919	0.941
fsupE	[ ]	0.196	0.259	0.222	0.256	0.081	0.059
h7i	[Btu/lbm]	41.4	41.1	42	42.9	43.5	45.5
h7o	[Btu/lbm]	119.5	119.3	119.4	119.4	119.7	119.8
h9	[Btu/lbm]	127.9	129.3	128.5	129.1	123.9	122.9
MtotE	[lbm]	0.286	0.266	0.276	0.262	0.315	0.317
M2phE	[lbm]	0.225	0.206	0.216	0.205	0.258	0.262
MsupE	[lbm]	0.007	0.009	0.008	0.009	0.003	0.002
p7ii	[psia]	129.1	124.5	127.6	126	136.9	140.8
p7avg	[psia]	128.7	124.1	127.1	125.6	136.4	140.3
p7o	[psia]	128.2	123.7	126.7	125.2	135.9	139.7
p9	[psia]	127.3	122.5	125.7	124.1	135.5	139.4
q2phE	[Btu/hr]	25187	24302	24579	23930	26091	26089
q2phEdry	[Btu/hr]	25187	24302	24579	23930	26091	26089
q2phEwet	[Btu/hr]	0	0	0	0	0	0
q2phEwetlat	[Btu/hr]	0	0	0	0	0	0
q2phEwetsns	[Btu/hr]	0	0	0	0	0	0
qsupE	[Btu/hr]	2736	3097	2877	3044	1440	1117
t7i	[F]	38.2	36.1	37.5	36.8	41.6	43.3
t7avg	[F]	38	35.9	37.3	36.6	41.4	43.1
t7o	[F]	37.8	35.7	37.1	36.4	41.2	42.8
t9	[F]	70	74.2	71.8	73.8	56.6	54.3
TainE	[F]	80.1	80.1	79.8	79.9	79.5	80.3
TainEwet	[F]	44.5	42.7	43.8	43.3	47.3	48.8
ta2phoutE	[F]	44.5	42.7	43.8	43.3	47.3	48.8
tasupoutE	[F]	64.2	66.5	65	66.3	59.2	58.9
taoutE	[F]	48.3	48.9	48.6	49.2	48.2	49.4
tafanoutE	[F]	48.9	49.5	49.1	49.7	48.8	49.9
u2phE	[Btu/hr-ft^2-F]	51.4	51.3	51.4	51.4	51.5	51.6
u2phEwet	[Btu/hr-ft^2-F]	51.4	51.3	51.4	51.4	51.5	51.6
usupE	[Btu/hr-ft^2-F]	30	29.7	29.9	29.7	30.5	30.8
TubeLenE	[ft]	3.68	3.68	3.68	3.68	3.68	3.68
VolextE	[ft^3]	0.2917	0.2917	0.2917	0.2917	0.2917	0.2917
x7i	[ ]	0.157	0.16	0.165	0.177	0.168	0.184
x7o	[ ]	1	1	1	1	1	1
MWR	[lbm]	0	0	0	0	0	0
tfinEi	[F]	39.9	37.7	39.2	38.4	43.5	45.2
tfinEo	[F]	39.5	37.4	38.8	38.1	43.1	44.8
wairEi	[lbm H2O/lbm of air]	0.00472	0.0044	0.0046	0.0046	0.00531	0.006
wairEo	[lbm H2O/lbm of air]	0.005	0.004	0.005	0.005	0.005	0.006
wfinEi	[lbm H2O/lbm	0.00533	0.00489	0.00518	0.00503	0.00613	0.00655

	of air]						
wfinEo	[lbm H2O/lbm of air]	0.00533	0.00489	0.00518	0.00503	0.00613	0.00655
Tindoor	[F]	80.1	80.1	79.8	79.9	79.5	80.3
RhaiE	[ ]	0.211	0.197	0.208	0.207	0.242	0.266
vdotaE	[cfm]	800	800	800	800	800	800
PwrFanE	[W]	120.9	119.2	122.6	124.2	114.5	113.2
NportsE	[ports/tube]	19	19	19	19	19	19
porgeoE	[]	1	1	1	1	1	1
geodesE	[ ]	62.69	62.69	62.69	62.69	62.69	62.69
NtubesE	[ ]	40	40	40	40	40	40
twebE	[ft]	0.00112	0.00112	0.00112	0.00112	0.00112	0.00112
twallE	[ft]	0.00138	0.00138	0.00138	0.00138	0.00138	0.00138
HfinE	[ft]	0.026	0.026	0.026	0.026	·0.026	0.026
Dh_tE	[ft]	0.00219	0.00219	0.00219	0.00219	0.00219	0.00219
Dh_airE	[ft]	0.0064	0.0064	0.0064	0.0064	0.0064	0.0064
AfrontE	[ft^2]	4.75	4.75	4.75	4.75	4.75	4.75
DeqinE	[ft]	0.00282	0.00282	0.00282	0.00282	0.00282	0.00282
HtubeDistE	[ft]	0.0614	0.0614	0.0614	0.0614	0.0614	0.0614
VtubeDistE	[ft]	0.03224	0.03224	0.03224	0.03224	0.03224	0.03224
FinThE	[ft]	0.000417	0.000417	0.000417	0.000417	0.000417	0.000417
taEwet	[F]	27.6	28.1	27.6	31.6	27.8	40.3
AairE	[ft^2]	135.654	135.654	135.654	135.654	135.654	135.654
hairE	[Btu/hr-ft^2-F]	14.06	14.06	14.06	14.06	14.06	14.06
hreftpE	[Btu/hr-ft^2-F]	442.36	437.98	440.27	440.27	450.7	450.7
seffEw	[ ]	0.98	0.98	0.98	0.98	0.98	0.98
dpE	[psia]	1.8	2	1.9	2	1.4	1.4
ThetaLoE	[deg]	27	27	27	27	27	27
HlouvE	[ft]	0.02167	0.02167	0.02167	0.02167	0.02167	0.02167
HlouvdistE	[ft]	0.004583	0.004583	0.004583	0.004583	0.004583	0.004583
DeffE	[ft]	0.0033	0.0033	0.0033	0.0033	0.0033	0.0033
VheadEin	[ft^3]	0.00395	0.00395	0.00395	0.00395	0.00395	0.00395
VheadEout	[ft^3]	0.00395	0.00395	0.00395	0.00395	0.00395	0.00395
MheadEin	[lbm]	0.04641	0.04422	0.04406	0.04099	0.04615	0.04615
MheadEout	[lbm]	0.00785	0.00748	0.00772	0.00759	0.00863	0.00863
DheadE	[ft]	0.06242	0.06242	0.06242	0.06242	0.06242	0.06242
NlouvE	[ ]	10	10	10	10	10	10
dPairE	[psia]	0.001131	0.0011318	0.001132	0.0011327	0.0011321	0.0011321
Le	[ ]	0.83	0.831	0.831	0.831	0.831	0.831
hD	[1/hr-ft^2-lbm of air]	65.78	65.78	65.78	65.78	65.78	65.78
ttubeEi	[F]	39.78	37.58	39.05	38.32	43.39	43.39
ttubeEo	[F]	39.4	37.22	38.67	37.95	42.96	42.96

Table D.6 Dry indoor/medium outdoor ambient temperature evaporator submodel simulation runs

	Corresp. Exp. Data set	80/82 (10-8-98)	80/82 (10-23-98)	80/90 (10-24-98)	80/94 (10-26-98)	80/95 (10-2-98)	80/95 (10-24-98)
qEvap	[Btu/hr]	26249	27240	25900	25208	25464	25235
degsup	[F]	37.9	22.6	34.2	35.3	30.8	34.2
w	[lbm/hr]	311	339.6	317.3	312.9	321.1	316.6
Aevap	[ft^2]	32.001	32.001	32.001	32.001	32.001	32.001
a2phEdry	[ft^2]	23.262	27.807	24.3	23.612	25.2	23.985
a2phEwet	[ft^2]	0	0	0	0	0	0
e2phE	[ ]	0.847	0.847	0.847	0.847	0.847	0.847
e2phEwet	[ ]	0.75	0.75	0.75	0.75	· 0.75	0.75
esupE	[ ]	0.888	0.583	0.843	0.872	0.793	0.854
f2phE	[ ]	0.727	0.869	0.759	0.738	0.787	0.75
fsupE	[ ]	0.273	0.131	0.241	0.262	0.213	0.25
h7i	[Btu/lbm]	44.9	45.6	46.9	48.3	48.6	48.9
h7o	[Btu/lbm]	119.4	119.7	119.5	119.5	119.6	119.6
h9	[Btu/lbm]	129.3	125.8	128.6	128.9	127.9	128.6
MtotE	[lbm]	0.253	0.295	0.259	0.251	0.265	0.253
M2phE	[lbm]	0.198	0.24	0.206	0.199	0.214	0.202
MsupE	[lbm]	0.009	0.005	0.009	0.009	0.008	0.009
p7ii	[psia]	127.1	137.3	131.8	132	135.7	133.2
p7avg	[psia]	126.7	136.8	131.4	131.6	135.3	132.8
p7o	[psia]	126.3	136.3	131	131.2	134.9	132.4
p9	[psia]	125.1	135.7	129.9	130.1	133.9	131.3
q2phE	[Btu/hr]	23176	25161	23032	22293	22820	22370
q2phEdry	[Btu/hr]	23176	25161	23032	22293	22820	22370
q2phEwet	[Btu/hr]	0	0	0	0	0	0
q2phEwetlat	[Btu/hr]	0	0	0	0	0	0
q2phEwetsns	[Btu/hr]	0	0	0	0	0	0
qsupE	[Btu/hr]	3072	2079	2868	2914	2644	2865
t7i	[F]	37.3	41.8	39.4	39.5	41.1	40
t7avg	[F]	37.1	41.6	39.2	39.3	40.9	39.8
t7o	[F]	36.9	41.4	39	39.1	40.7	39.7
t9	[F]	74.9	64	73.3	74.5	71.6	73.8
TainE	[F]	80.1	80.5	80.1	80.1	80	80.1
TainEwet	[F]	43.7	47.5	45.5	45.6	46.9	46
ta2phoutE	[F]	43.7	47.5	45.5	45.6	46.9	46
tasupoutE	[F]	67.3	62.4	66.5	67.4	65.8	67
taoutE	[F]	50.1	49.5	50.5	51.3	50.9	51.3
tafanoutE	[F]	50.7	50.1	51.1	51.9	51.5	51.8
u2phE	[Btu/hr-ft^2-F]	51.4	51.5	51.4	51.3	51.4	51.4
u2phEwet	[Btu/hr-ft^2-F]	51.4	51.5	51.4	51.3	51.4	51.4
usupE	[Btu/hr-ft^2-F]	29.7	30.4	29.8	29.6	29.9	29.7
TubeLenE	[ft]	3.68	3.68	3.68	3.68	3.68	3.68
VolextE	[ft^3]	0.2917	0.2917	0.2917	0.2917	0.2917	0.2917
x7i	[ ]	0.197	0.19	0.212	0.227	0.225	0.232
x7o	[ ]	1	1	1	1	1	1
MWR	[lbm]	0	0	0	0	0	0
tfinEi	[F]	39	43.7	41.2	41.3	43	41.8
tfinEo	[F]	38.6	43.2	40.8	40.9	42.6	41.4
wairEi	[lbm H2O/lbm of air]	0.00467	0.00553	0.00503	0.00503	0.00533	0.00517
wairEo	[lbm H2O/lbm of air]	0.005	0.006	0.005	0.005	0.005	0.005

wfinEi	[lbm H2O/lbm of air]	0.00514	0.00617	0.0056	0.00563	0.00601	0.00575
wfinEo	[lbm H2O/lbm of air]	0.00514	0.00617	0.0056	0.00563	0.00601	0.00575
Tindoor	[F]	80.1	80.5	80.1	80.1	80	80.1
RhaiE	[ ]	0.209	0.244	0.225	0.225	0.239	0.231
vdotaE	[cfm]	800	800	800	800	800	800
PwrFanE	[W]	124.5	115	116.7	116.5	124.1	116.5
NportsE	[ports/tube]	19	19	19	19	19	19
porgeoE	[]	1	1	1	1	1	1
geodesE	[ ]	62.69	62.69	62.69	62.69	62.69	62.69
NtubesE	[ ]	40	40	40	40	40	40
twebE	[ft]	0.00112	0.00112	0.00112	0.00112	0.00112	0.00112
twallE	[ft]	0.00138	0.00138	0.00138	0.00138	0.00138	0.00138
HfinE	[ft]	0.026	0.026	0.026	0.026	0.026	0.026
Dh_tE	[ft]	0.00219	0.00219	0.00219	0.00219	0.00219	0.00219
Dh_airE	[ft]	0.0064	0.0064	0.0064	0.0064	0.0064	0.0064
AfrontE	[ft^2]	4.75	4.75	4.75	4.75	4.75	4.75
DeqinE	[ft]	0.00282	0.00282	0.00282	0.00282	0.00282	0.00282
HtubeDistE	[ft]	0.0614	0.0614	0.0614	0.0614	0.0614	0.0614
VtubeDistE	[ft]	0.03224	0.03224	0.03224	0.03224	0.03224	0.03224
FinThE	[ft]	0.000417	0.000417	0.000417	0.000417	0.000417	0.000417
taEwet	[F]	31.5	34.5	32.1	31.5	32	33.1
AairE	[ft^2]	135.654	135.654	135.654	135.654	135.654	135.654
hairE	[Btu/hr-ft^2-F]	14.06	14.06	14.06	14.06	14.06	14.06
hreftpE	[Btu/hr-ft^2-F]	439.98	452.26	441.8	439.36	441.82	441.96
seffEw	[ ]	0.98	0.98	0.98	0.98	0.98	0.98
dpE	[psia]	2	1.6	1.9	1.9	1.8	1.9
ThetaLoE	[deg]	27	27	27	27	27	27
HlouvE	[ft]	0.02167	0.02167	0.02167	0.02167	0.02167	0.02167
HlouvdistE	[ft]	0.004583	0.004583	0.004583	0.004583	0.004583	0.004583
DeffE	[ft]	0.0033	0.0033	0.0033	0.0033	0.0033	0.0033
VheadEin	[ft^3]	0.00395	0.00395	0.00395	0.00395	0.00395	0.00395
VheadEout	[ft^3]	0.00395	0.00395	0.00395	0.00395	0.00395	0.00395
MheadEin	[lbm]	0.03774	0.04166	0.03647	0.03451	0.03567	0.03411
MheadEout	[lbm]	0.00765	0.00852	0.00799	0.00799	0.00828	0.00807
DheadE	[ft]	0.06242	0.06242	0.06242	0.06242	0.06242	0.06242
NlouvE	[ ]	10	10	10	10	10	10
dPairE	[psia]	0.0011337	0.0011319	0.0011343	0.0011354	0.0011351	0.0011354
Le	[ ]	0.83	0.83	0.83	0.83	0.83	0.83
hD	[1/hr-ft^2-lbm of air]	65.76	65.76	65.76	65.76	65.78	65.76
ttubeEi	[F]	38.86	43.57	41.07	41.18	42.88	41.73
ttubeEo	[F]	38.48	43.14	40.67	40.78	42.46	41.32

Table D.7 Dry indoor/high outdoor ambient temperature evaporator submodel simulation runs

	Corresp. Exp. Data set	80/96 (10-26-98)	80/104 (10-3-98)	80/106 (10-24-98)	80/111 (10-25-98)	80/118 (10-4-98)	80/118 (10-25-98)
qEvap	[Btu/hr]	24887	24304	23710	22876	22216	21970
degsup	[F]	35.2	28.7	32.4	31.7	25.8	29.9
w	[lbm/hr]	313	324	316.6	314.8	323.3	316.4
Aevap	[ft^2]	32.001	32.001	32.001	32.001	32.001	32.001
a2phEdry	[ft^2]	23.457	25.377	23.805	23.644	25.449	23.813
a2phEwet	[ft^2]	0	0	0	0	0	0
e2phE	[ ]	0.847	0.848	0.848	0.848	0.848	0.848
e2phEwet	[ ]	0.75	0.75	0.75	0.75	0.75	0.75
esupE	[ ]	0.876	0.777	0.857	0.862	·0.766	0.851
f2phE	[ ]	0.733	0.793	0.744	0.739	0.795	0.744
fsupE	[ ]	0.267	0.207	0.256	0.261	0.205	0.256
h7i	[Btu/lbm]	49.4	52.5	53.5	55.6	58.3	58.6
h7o	[Btu/lbm]	119.6	119.8	119.7	119.8	119.9	119.9
h9	[Btu/lbm]	128.9	127.5	128.4	128.3	127	128
MtotE	[lbm]	0.248	0.261	0.245	0.242	0.256	0.242
M2phE	[lbm]	0.197	0.212	0.197	0.195	0.21	0.195
MsupE	[lbm]	0.01	0.008	0.01	0.01	0.008	0.01
p7ii	[psia]	132.9	140.3	138.2	140.8	148.1	145.8
p7avg	[psia]	132.5	139.9	137.8	140.4	147.6	145.4
p7o	[psia]	132.1	139.5	137.4	140	147.2	145
p9	[psia]	131	138.6	136.3	139	146.4	144
q2phE	[Btu/hr]	21974	21794	20960	20191	19917	19395
q2phEdry	[Btu/hr]	21974	21794	20960	20191	19917	19395
q2phEwet	[Btu/hr]	0	0	0	0	0	0
q2phEwetlat	[Btu/hr]	0	0	0	0	0	0
q2phEwetsns	[Btu/hr]	0	0	0	0	0	0
qsupE	[Btu/hr]	2914	2510	2750	2686	2298	2575
t7i	[F]	39.9	43.1	42.2	43.3	46.3	45.4
t7avg	[F]	39.7	42.9	42	43.1	46.1	45.2
t7o	[F]	39.5	42.7	41.9	43	46	45
t9	[F]	74.8	71.4	74.3	74.6	71.8	74.9
TainE	[F]	80.2	80	80.1	80.1	80	80.5
TainEwet	[F]	45.9	48.6	47.8	48.8	51.3	50.6
ta2phoutE	[F]	45.9	48.6	47.8	48.8	51.3	50.6
tasupoutE	[F]	67.7	66.1	67.8	68.3	67.1	68.9
taoutE	[F]	51.7	52.2	52.9	53.9	54.5	55.3
tafanoutE	[F]	52.3	52.8	53.5	54.4	55.1	55.8
u2phE	[Btu/hr-ft^2-F]	51.3	51.4	51.3	51.3	51.3	51.3
u2phEwet	[Btu/hr-ft^2-F]	51.3	51.4	51.3	51.3	51.3	51.3
usupE	[Btu/hr-ft^2-F]	29.6	29.9	29.7	29.6	29.9	29.7
TubeLenE	[ft]	3.68	3.68	3.68	3.68	3.68	3.68
VolextE	[ft^3]	0.2917	0.2917	0.2917	0.2917	0.2917	0.2917
x7i	[ ]	0.237	0.261	0.275	0.295	0.316	0.322
x7o	[ ]	1	1	1	1	1	1
MWR	[lbm]	0	0	0	0	0	0
tfinEi	[F]	41.7	45.1	44.1	45.3	48.4	47.5
tfinEo	[F]	41.3	44.6	43.7	44.9	48	47
wairEi	[lbm H2O/lbm of air]	0.00512	0.00587	0.00573	0.00603	0.00677	0.00661
wairEo	[lbm H2O/lbm of air]	0.005	0.006	0.006	0.006	0.007	0.007
wfinEi	[lbm H2O/lbm	0.00572	0.00652	0.00629	0.00657	0.00741	0.00714

120

	of air]						
wfinEo	[lbm H2O/lbm of air]	0.00572	0.00652	0.00629	0.00657	0.00741	0.00714
Tindoor	[F]	80.2	80	80.1	80.1	80	80.5
RhaiE	[ ]	0.228	0.263	0.256	0.269	0.303	0.291
vdotaE	[cfm]	800	800	800	800	800	800
PwrFanE	[W]	116.4	124	118.9	118.5	124	117.9
NportsE	[ports/tube]	19	19	19	19	19	19
porgeoE	[]	1	1	1	1	1	1
geodesE	[ ]	62.69	62.69	62.69	62.69	62.69	62.69
NtubesE	[ ]	40	40	40	40	40	40
twebE	[ft]	0.00112	0.00112	0.00112	0.00112	0.00112	0.00112
twallE	[ft]	0.00138	0.00138	0.00138	0.00138	0.00138	0.00138
HfinE	[ft]	0.026	0.026	0.026	0.026	·0.026	0.026
Dh_tE	[ft]	0.00219	0.00219	0.00219	0.00219	0.00219	0.00219
Dh_airE	[ft]	0.0064	0.0064	0.0064	0.0064	0.0064	0.0064
AfrontE	[ft^2]	4.75	4.75	4.75	4.75	4.75	4.75
DeqinE	[ft]	0.00282	0.00282	0.00282	0.00282	0.00282	0.00282
HtubeDistE	[ft]	0.0614	0.0614	0.0614	0.0614	0.0614	0.0614
VtubeDistE	[ft]	0.03224	0.03224	0.03224	0.03224	0.03224	0.03224
FinThE	[ft]	0.000417	0.000417	0.000417	0.000417	0.000417	0.000417
taEwet	[F]	32	37.6	38.8	41.3	44.6	45.8
AairE	[ft^2]	135.654	135.654	135.654	135.654	135.654	135.654
hairE	[Btu/hr-ft^2-F]	14.05	14.05	14.05	14.05	14.05	14.05
hreftpE	[Btu/hr-ft^2-F]	439.77	443.55	441.09	438.56	440.14	437.56
seffEw	[ ]	0.98	0.98	0.98	0.98	0.98	0.98
dpE	[psia]	1.9	1.8	1.9	1.9	1.7	1.8
ThetaLoE	[deg]	27	27	27	27	27	27
HlouvE	[ft]	0.02167	0.02167	0.02167	0.02167	0.02167	0.02167
HlouvdistE	[ft]	0.004583	0.004583	0.004583	0.004583	0.004583	0.004583
DeffE	[ft]	0.0033	0.0033	0.0033	0.0033	0.0033	0.0033
VheadEin	[ft^3]	0.00395	0.00395	0.00395	0.00395	0.00395	0.00395
VheadEout	[ft^3]	0.00395	0.00395	0.00395	0.00395	0.00395	0.00395
MheadEin	[lbm]	0.03339	0.03219	0.03033	0.02898	0.02857	0.02771
MheadEout	[lbm]	0.00804	0.00861	0.00841	0.00859	0.00914	0.00893
DheadE	[ft]	0.06242	0.06242	0.06242	0.06242	0.06242	0.06242
NlouvE	[ ]	10	10	10	10	10	10
dPairE	[psia]	0.0011358	0.001137	0.0011378	0.0011392	0.0011404	0.0011404
Le	[ ]	0.83	0.83	0.83	0.83	0.83	0.83
hD	[1/hr-ft^2-lbm of air]	65.76	65.78	65.76	65.76	65.78	65.76
ttubeEi	[F]	41.61	44.97	44.04	45.2	48.36	47.38
ttubeEo	[F]	41.2	44.53	43.6	44.76	47.89	46.92

Table D.8 Wet indoor evaporator submodel simulation runs

	Corresp. Exp. Data set	80/70 (10-6-98)	80/75 (10-7-98)	80/82 (10-7-98)	80/95 (10-9-98)	80/105 (10-9-98)	80/118 (10-12-98)
qEvap	[Btu/hr]	31856	31503	30848	29480	27715	24994
degsup	[F]	29	28.1	27.1	22.7	24.3	22.4
w	[lbm/hr]	377.2	381.7	381.7	386	375	368.3
Aevap	[ft^2]	32.001	32.001	32.001	32.001	32.001	32.001
a2phEdry	[ft^2]	0	0	0	0	0	0
a2phEwet	[ft^2]	22.127	22.452	22.805	24.539	23.312	23.651
e2phE	[ ]	0.1	0.1	0.1	0.1	0.1	0.1
e2phEwet	[ ]	0.85	0.851	0.851	0.851	0.851	0.851
esupE	[ ]	0.866	0.851	0.838	0.756	·0.819	0.805
f2phE	[ ]	0.691	0.702	0.713	0.767	0.728	0.739
fsupE	[ ]	0.309	0.298	0.287	0.233	0.272	0.261
h7i	[Btu/lbm]	43.5	45.2	46.7	50.2	53.1	58.8
h7o	[Btu/lbm]	119.9	120	120	120.1	120.1	120.3
h9	[Btu/lbm]	127.9	127.7	127.5	126.5	127	126.6
MtotE	[lbm]	0.273	0.27	0.269	0.276	0.259	0.253
M2phE	[lbm]	0.198	0.199	0.201	0.213	0.2	0.198
MsupE	[lbm]	0.012	0.012	0.012	0.01	0.012	0.012
p7ii	[psia]	148.1	149.8	151.3	156.9	157.6	163.1
p7avg	[psia]	147.6	149.3	150.8	156.4	157.2	162.7
p7o	[psia]	147.2	148.9	150.4	155.9	156.7	162.2
p9	[psia]	145.6	147.3	148.9	154.7	155.4	161
q2phE	[Btu/hr]	28838	28538	27977	27009	25139	22639
q2phEdry	[Btu/hr]	0	0	0	0	0	0
q2phEwet	[Btu/hr]	28838	28538	27977	27009	25139	22639
q2phEwetlat	[Btu/hr]	11429	11187	10730	9831	8959	7358
q2phEwetsns	[Btu/hr]	17410	17351	17247	17178	16179	15281
qsupE	[Btu/hr]	3017	2965	2871	2472	2577	2355
t7i	[F]	46.3	47	47.6	49.8	50.1	52.2
t7avg	[F]	46.1	46.8	47.4	49.6	49.9	52
t7o	[F]	46	46.6	47.2	49.4	49.7	51.9
t9	[F]	75	74.7	74.3	72.1	74.1	74.2
TainE	[F]	80.1	80.2	80.1	79.9	80	80.1
TainEwet	[F]	80.1	80.2	80.1	79.9	80	80.1
ta2phoutE	[F]	51.4	52	52.5	54.3	54.6	56.4
tasupoutE	[F]	68.9	68.9	68.7	67.8	69.1	69.7
taoutE	[F]	56.8	57	57.1	57.4	58.5	59.9
tafanoutE	[F]	57.4	57.6	57.7	58	59.1	60.4
u2phE	[Btu/hr-ft^2-F]	52	52	52	52	51.9	51.8
u2phEwet	[Btu/hr-ft^2-F]	52	52	52	52	51.9	51.8
usupE	[Btu/hr-ft^2-F]	31.5	31.6	31.6	31.7	31.4	31.3
TubeLenE	[ft]	3.68	3.68	3.68	3.68	3.68	3.68
VolextE	[ft^3]	0.2917	0.2917	0.2917	0.2917	0.2917	0.2917
x7i	[ ]	0.152	0.168	0.183	0.214	0.246	0.304
x7o	[ ]	1	1	1	1	1	1
MWR	[lbm]	10.9	10.67	10.23	9.37	8.54	7.02
tfinEi	[F]	52.2	52.8	53.2	54.8	55.1	56.7
tfinEo	[F]	47.1	47.8	48.4	50.6	50.9	52.9
wairEi	[lbm H2O/lbm of air]	0.01178	0.01182	0.01176	0.01182	0.01179	0.01185
wairEo	[lbm H2O/lbm of air]	0.007	0.008	0.008	0.008	0.008	0.009
wfinEi	[lbm H2O/lbm	0.00855	0.00872	0.00886	0.00942	0.00951	0.0101

	of air]						
wfinEo	[lbm H2O/lbm of air]	0.00705	0.00723	0.0074	0.00803	0.00812	0.00878
Tindoor	[F]	80.1	80.2	80.1	79.9	80	80.1
RhaiE	[ ]	0.521	0.521	0.52	0.526	0.523	0.524
vdotaE	[cfm]	800	800	800	800	800	800
PwrFanE	[W]	149.6	152.6	150.5	148.9	145.2	134.2
NportsE	[ports/tube]	19	19	19	19	19	19
porgeoE	[]	1	1	1	1	1	1
geodesE	[ ]	62.69	62.69	62.69	62.69	62.69	62.69
NtubesE	[ ]	40	40	40	40	40	40
twebE	[ft]	0.00112	0.00112	0.00112	0.00112	0.00112	0.00112
twallE	[ft]	0.00138	0.00138	0.00138	0.00138	0.00138	0.00138
HfinE	[ft]	0.026	0.026	0.026	0.026	·0.026	0.026
Dh_tE	[ft]	0.00219	0.00219	0.00219	0.00219	0.00219	0.00219
Dh_airE	[ft]	0.0064	0.0064	0.0064	0.0064	0.0064	0.0064
AfrontE	[ft^2]	4.75	4.75	4.75	4.75	4.75	4.75
DeqinE	[ft]	0.00282	0.00282	0.00282	0.00282	0.00282	0.00282
HtubeDistE	[ft]	0.0614	0.0614	0.0614	0.0614	0.0614	0.0614
VtubeDistE	[ft]	0.03224	0.03224	0.03224	0.03224	0.03224	0.03224
FinThE	[ft]	0.000417	0.000417	0.000417	0.000417	0.000417	0.000417
taEwet	[F]	161.9	158.3	152.8	138.3	134.9	120.8
AairE	[ft^2]	135.654	135.654	135.654	135.654	135.654	135.654
hairE	[Btu/hr-ft^2-F]	14.04	14.04	14.04	14.04	14.04	14.04
hreftpE	[Btu/hr-ft^2-F]	496.48	499.57	498.13	495.33	488.97	480.16
seffEw	[ ]	0.98	0.98	0.98	0.98	0.98	0.98
dpE	[psia]	2.5	2.5	2.4	2.2	2.2	2.1
ThetaLoE	[deg]	27	27	27	27	27	27
HlouvE	[ft]	0.02167	0.02167	0.02167	0.02167	0.02167	0.02167
HlouvdistE	[ft]	0.004583	0.004583	0.004583	0.004583	0.004583	0.004583
DeffE	[ft]	0.0033	0.0033	0.0033	0.0033	0.0033	0.0033
VheadEin	[ft^3]	0.00395	0.00395	0.00395	0.00395	0.00395	0.00395
VheadEout	[ft^3]	0.00395	0.00395	0.00395	0.00395	0.00395	0.00395
MheadEin	[lbm]	0.05367	0.04976	0.04683	0.04237	0.03776	0.03247
MheadEout	[lbm]	0.00905	0.00918	0.0093	0.00973	0.00975	0.01015
DheadE	[ft]	0.06242	0.06242	0.06242	0.06242	0.06242	0.06242
NlouvE	[ ]	10	10	10	10	10	10
dPairE	[psia]	0.0011435	0.0011436	0.001144	0.0011449	0.0011463	0.001148
Le	[ ]	0.82	0.82	0.82	0.82	0.82	0.82
hD	[1/hr-ft^2-lbm of air]	65.38	65.37	65.37	65.37	65.36	65.34
ttubeEi	[F]	51.53	52.07	52.51	54.22	54.48	56.15
ttubeEo	[F]	47	47.69	48.28	50.46	50.77	52.86

Table D.9 Dry indoor/low outdoor ambient temperature condenser submodel simulation runs

	Corresp. Exp. Data set	80/68 (10-3-98)	80/68 (10-28-98)	80/71 (10-1-98)	80/74 (10-6-98)	80/75 (10-23-98)	80/81 (10-23-98)
degsubcool	[F]	17	15.3	17.4	17.3	18.7	19.2
w	[lbm/hr]	322.9	310.7	317.4	313	342.6	351.3
PwrComp	[W]	1384	1361.9	1443.1	1498.9	1549.2	1705.5
Acond	[ft^2]	107.793	107.793	107.793	107.793	107.793	107.793
esupC	[ ]	0.779	0.8	0.78	0.786	0.761	0.761
e2phC	[ ]	0.865	0.865	0.865	0.866	0.867	0.869
esubC	[ ]	0.988	0.976	0.992	0.992	0.991	0.99
fsupC	[ ]	0.123	0.135	0.132	0.142	0.122	0.13
f2phC	[ ]	0.613	0.651	0.585	0.571	·0.572	0.552
fsubC	[ ]	0.264	0.214	0.284	0.287	0.306	0.318
h0	[Btu/lbm]	137.3	137.6	138.5	139.7	139.2	141.1
h1	[Btu/lbm]	140	140.4	140.7	141.6	140.7	141.8
h2i	[Btu/lbm]	121.3	121.3	121.3	121.3	121.3	121.2
h2o	[Btu/lbm]	44.2	43.7	45.6	46.8	47.7	50.6
h3	[Btu/lbm]	37.9	38	39.1	40.2	40.6	43.1
h4	[Btu/lbm]	37.9	38	39.1	40.2	40.6	43.1
MtotC	[lbm]	2.558	2.424	2.597	2.59	2.653	2.664
MsupC	[lbm]	0.029	0.031	0.033	0.037	0.033	0.039
M2phC	[lbm]	0.945	1.002	0.915	0.906	0.905	0.893
MsubC	[lbm]	1.035	0.841	1.103	1.104	1.173	1.195
p0	[psia]	269.1	264.1	282.9	295.4	305.1	336.3
p1	[psia]	269	264	282.8	295.3	305	336.2
p2i	[psia]	268.9	263.9	282.7	295.2	304.9	336.1
p2avg	[psia]	268.8	263.8	282.6	295.1	304.8	336
p2o	[psia]	268.7	263.7	282.6	295.1	304.7	336
p3i	[psia]	268.7	263.7	282.5	295	304.7	335.9
p4	[psia]	268.6	263.6	282.4	295	304.6	335.8
qCond	[Btu/hr]	32966	31831	32269	31728	34275	34654
qsupC	[Btu/hr]	6037	5962	6170	6361	6641	7239
q2phC	[Btu/hr]	24889	24103	24034	23320	25206	24804
qsubC	[Btu/hr]	2040	1766	2065	2047	2428	2611
t0	[F]	136	136	142.7	148.9	148.7	160.5
t1o	[F]	145.5	146.4	150.5	155.7	153.9	162.7
t2i	[F]	84.9	83.6	88.4	91.5	93.8	100.9
t2avg	[F]	84.9	83.6	88.4	91.5	93.8	100.8
t2o	[F]	84.9	83.6	88.4	91.5	93.8	100.8
t3i	[F]	67.9	68.3	71	74.1	75.1	81.6
t4	[F]	67.9	68.3	71	74.1	75.1	81.6
tafanoutC	[F]	80.1	79.9	83.1	86.1	87.9	94.7
tasupoutC	[F]	85.7	84.1	88.2	90.6	95.1	102.3
ta2phoutC	[F]	82.6	81.5	86.1	89.1	91.3	98.3
tasuboutC	[F]	70.5	70.9	73.6	76.6	77.8	84.5
taoutC	[F]	79.8	79.6	82.8	85.8	87.6	94.4
usupC	[Btu/hr-ft^2-F]	14.4	13	13.2	12.2	15.6	15.5
u2phC	[Btu/hr-ft^2-F]	50.6	50.6	50.5	50.4	50.4	50.2
usubC	[Btu/hr-ft^2-F]	26	26	25.7	25.5	25.4	24.9
TubeLenC	[ft]	6.28	6.28	6.28	6.28	6.28	6.28
Vcond	[ft^3]	0.059	0.059	0.059	0.059	0.059	0.059
VolextC	[ft^3]	0.9825	0.9825	0.9825	0.9825	0.9825	0.9825
x2o	[ ]	0	0	0	0	0	0
x4	[ ]	0	0	0	0	0	0
Toutdoor	[F]	67.7	67.9	70.9	74	74.9	81.4

RhaiC	[ ]	0.405	0.405	0.405	0.405	0.405	0.405
vdotaCmeas	[cfm]	2600	2600	2600	2600	2600	2600
PwrFanC	[W]	145.7	145.7	145.6	145.5	145.5	145.3
NportsC	[ports/tube]	19	19	19	19	19	19
porgeoC	[]	1	1	1	1	1	1
geodesC	[ ]	62.69	62.69	62.69	62.69	62.69	62.69
NtubesC	[ ]	79	79	79	79	79	79
twebC	[ft]	0.00112	0.00112	0.00112	0.00112	0.00112	0.00112
twallC	[ft]	0.00138	0.00138	0.00138	0.00138	0.00138	0.00138
HfinC	[ft]	0.026	0.026	0.026	0.026	0.026	0.026
Dh_tC	[ft]	0.00219	0.00219	0.00219	0.00219	0.00219	0.00219
Dh_airC	[ft]	0.00639	0.00639	0.00639	0.00639	0.00639	0.00639
AfrontC	[ft^2]	16	16	16	16	16	16
DeqinC	[ft]	0.00282	0.00282	0.00282	0.00282	0.00282	0.00282
HtubeDistC	[ft]	0.0614	0.0614	0.0614	0.0614	0.0614	0.0614
VtubeDistC	[ft]	0.03224	0.03224	0.03224	0.03224	0.03224	0.03224
FinThC	[ft]	0.000417	0.000417	0.000417	0.000417	0.000417	0.000417
dpC	[psia]	0.3	0.3	0.3	0.3	0.3	0.3
ThetaLoC	[deg]	27	27	27	27	27	27
HlouvC	[ft]	0.02167	0.02167	0.02167	0.02167	0.02167	0.02167
HlouvdistC	[ft]	0.004583	0.004583	0.004583	0.004583	0.004583	0.004583
DeffC	[ft]	0.0033	0.0033	0.0033	0.0033	0.0033	0.0033
DeffE	[ft]	0.0033	0.0033	0.0033	0.0033	0.0033	0.0033
VheadCin	[ft^3]	0.00779	0.00779	0.00779	0.00779	0.00779	0.00779
VheadCout	[ft^3]	0.00779	0.00779	0.00779	0.00779	0.00779	0.00779
MheadCin	[lbm]	0.03144	0.03071	0.03306	0.03444	0.03595	0.03974
MheadCout	[lbm]	0.51757	0.5182	0.51316	0.50866	0.50631	0.49639
DheadC	[ft]	0.06242	0.06242	0.06242	0.06242	0.06242	0.06242
AairC	[ft^2]	452.245	452.245	452.245	452.245	452.245	452.245
hairC	[Btu/hr-ft^2-F]	13.85	13.85	13.84	13.84	13.83	13.82
hreftpC	[Btu/hr-ft^2-F]	471.37	470.79	462.13	454.19	457.18	443.86
NlouvC	[ ]	10	10	10	10	10	10
dPairC	[psia]	0.0011453	0.0011452	0.001143	0.0011408	0.0011402	0.0011356
eta_fanC	[ ]	0.18	0.18	0.18	0.18	0.18	0.18
NCht	[ ]	8	8	8	8	8	8
DCht	[ft]	0.01583	0.01583	0.01583	0.01583	0.01583	0.01583
LCht	[ft]	3.33	3.33	3.33	3.33	3.33	3.33
UlossCht	[Btu/hr-ft2-F]	0	0	0	0	0	0
pdCht	[psia]	0.03	0.03	0.03	0.03	0.04	0.04
qlossCht	[Btu/hr]	0	0	0	0	0	0
MCht	[lbm]	0.34816	0.34858	0.34519	0.34217	0.34058	0.33391
VCht	[ft^3]	0.00524	0.00524	0.00524	0.00524	0.00524	0.00524

Table D.10 Dry indoor/medium outdoor ambient temperature condenser submodel simulation runs

	Corresp. Exp. Data set	80/82 (10-8-98)	80/82 (10-23-98)	80/90 (10-24-98)	80/94 (10-26-98)	80/95 (10-2-98)	80/95 (10-24-98)
degsubcool	[F]	17.6	19.1	20.5	20.8	22.6	21.7
w	[lbm/hr]	311	339.6	317.3	312.9	321.1	316.6
PwrComp	[W]	1676	1725.2	1957.7	2064.4	2148.7	2132.6
Acond	[ft^2]	107.793	107.793	107.793	107.793	107.793	107.793
esupC	[ ]	0.797	0.769	0.783	0.793	0.776	0.784
e2phC	[ ]	0.869	0.869	0.871	0.872	0.872	0.872
esubC	[ ]	0.992	0.992	0.996	0.996	0.998	0.997
fsupC	[ ]	0.168	0.141	0.182	0.202	·0.193	0.2
f2phC	[ ]	0.54	0.536	0.447	0.425	0.395	0.407
fsubC	[ ]	0.293	0.323	0.37	0.373	0.412	0.393
h0	[Btu/lbm]	142.8	141.9	146.3	148.1	148.5	148.7
h1	[Btu/lbm]	144	142.6	146.3	148.3	148.1	148.2
h2i	[Btu/lbm]	121.2	121.2	120.9	120.7	120.6	120.6
h2o	[Btu/lbm]	50.2	51	54.8	56.4	57.6	57.4
h3	[Btu/lbm]	43.4	43.6	46.7	48	48.5	48.6
h4	[Btu/lbm]	43.4	43.6	46.7	48	48.5	48.6
MtotC	[lbm]	2.568	2.663	2.696	2.666	2.747	2.703
MsupC	[lbm]	0.049	0.043	0.062	0.071	0.071	0.073
M2phC	[lbm]	0.883	0.874	0.758	0.729	0.683	0.703
MsubC	[lbm]	1.101	1.212	1.35	1.344	1.473	1.406
p0	[psia]	332.1	340.6	385.1	404.4	419	416.3
p1	[psia]	332	340.5	385	404.4	418.9	416.3
p2i	[psia]	331.9	340.4	384.9	404.3	418.8	416.2
p2avg	[psia]	331.8	340.3	384.9	404.3	418.8	416.2
p2o	[psia]	331.8	340.3	384.8	404.2	418.7	416.1
p3i	[psia]	331.7	340.2	384.7	404.1	418.6	416
p4	[psia]	331.7	340.1	384.7	404.1	418.6	416
qCond	[Btu/hr]	31286	33640	31613	31382	32006	31540
qsupC	[Btu/hr]	7095	7285	8061	8641	8849	8748
q2phC	[Btu/hr]	22081	23841	20965	20118	20223	20014
qsubC	[Btu/hr]	2110	2514	2587	2623	2935	2778
t0	[F]	165.4	163.9	185.2	193.9	197.1	197.5
t1o	[F]	169.8	166.2	185.2	194.8	196	196
t2i	[F]	99.9	101.8	111	114.7	117.4	116.9
t2avg	[F]	99.9	101.8	111	114.7	117.4	116.9
t2o	[F]	99.9	101.8	111	114.7	117.4	116.9
t3i	[F]	82.4	82.7	90.5	93.9	94.9	95.3
t4	[F]	82.4	82.7	90.5	93.9	94.9	95.3
tafanoutC	[F]	94.3	95.5	102.8	106.2	107.5	107.7
tasupoutC	[F]	98.1	102	107.3	110.2	112.5	112.1
ta2phoutC	[F]	97.6	99.3	108.3	112	114.5	114.2
tasuboutC	[F]	84.9	85.4	93.1	96.5	97.5	97.9
taoutC	[F]	94	95.2	102.5	105.9	107.1	107.4
usupC	[Btu/hr-ft^2-F]	10.8	13.8	10.1	9.2	9.6	9.3
u2phC	[Btu/hr-ft^2-F]	50.1	50.1	49.7	49.5	49.5	49.5
usubC	[Btu/hr-ft^2-F]	24.9	24.8	24.1	23.8	23.6	23.6
TubeLenC	[ft]	6.28	6.28	6.28	6.28	6.28	6.28
Vcond	[ft^3]	0.059	0.059	0.059	0.059	0.059	0.059
VolextC	[ft^3]	0.9825	0.9825	0.9825	0.9825	0.9825	0.9825
x2o	[ ]	0	0	0	0	0	0
x4	[ ]	0	0	0	0	0	0

126

Toutdoor	[F]	82.2	82.5	90.4	93.8	94.8	95.2
RhaiC	[ ]	0.405	0.405	0.405	0.405	0.405	0.405
vdotaCmeas	[cfm]	2600	2600	2600	2600	2600	2600
PwrFanC	[W]	145.2	145.2	145	144.9	144.8	144.8
NportsC	[ports/tube]	19	19	19	19	19	19
porgeoC	[]	1	1	1	1	1	1
geodesC	[ ]	62.69	62.69	62.69	62.69	62.69	62.69
NtubesC	[ ]	79	79	79	79	79	79
twebC	[ft]	0.00112	0.00112	0.00112	0.00112	0.00112	0.00112
twallC	[ft]	0.00138	0.00138	0.00138	0.00138	0.00138	0.00138
HfinC	[ft]	0.026	0.026	0.026	0.026	0.026	0.026
Dh_tC	[ft]	0.00219	0.00219	0.00219	0.00219	0.00219	0.00219
Dh_airC	[ft]	0.00639	0.00639	0.00639	0.00639	0.00639	0.00639
AfrontC	[ft^2]	16	16	16	16	16	16
DeqinC	[ft]	0.00282	0.00282	0.00282	0.00282	0.00282	0.00282
HtubeDistC	[ft]	0.0614	0.0614	0.0614	0.0614	0.0614	0.0614
VtubeDistC	[ft]	0.03224	0.03224	0.03224	0.03224	0.03224	0.03224
FinThC	[ft]	0.000417	0.000417	0.000417	0.000417	0.000417	0.000417
dpC	[psia]	0.3	0.3	0.3	0.3	0.3	0.3
ThetaLoC	[deg]	27	27	27	27	27	27
HlouvC	[ft]	0.02167	0.02167	0.02167	0.02167	0.02167	0.02167
HlouvdistC	[ft]	0.004583	0.004583	0.004583	0.004583	0.004583	0.004583
DeffC	[ft]	0.0033	0.0033	0.0033	0.0033	0.0033	0.0033
DeffE	[ft]	0.0033	0.0033	0.0033	0.0033	0.0033	0.0033
VheadCin	[ft^3]	0.00779	0.00779	0.00779	0.00779	0.00779	0.00779
VheadCout	[ft^3]	0.00779	0.00779	0.00779	0.00779	0.00779	0.00779
MheadCin	[lbm]	0.03852	0.04009	0.04472	0.04653	0.04845	0.04807
MheadCout	[lbm]	0.49652	0.49479	0.48139	0.4753	0.47222	0.47228
DheadC	[ft]	0.06242	0.06242	0.06242	0.06242	0.06242	0.06242
AairC	[ft^2]	452.245	452.245	452.245	452.245	452.245	452.245
hairC	[Btu/hr-ft^2-F]	13.82	13.82	13.8	13.79	13.79	13.79
hreftpC	[Btu/hr-ft^2-F]	435.14	438.73	412.78	403.5	399.76	399.63
NlouvC	[ ]	10	10	10	10	10	10
dPairC	[psia]	0.0011351	0.0011349	0.0011295	0.0011272	0.0011265	0.0011262
eta_fanC	[ ]	0.18	0.18	0.18	0.18	0.18	0.18
NCht	[ ]	8	8	8	8	8	8
DCht	[ft]	0.01583	0.01583	0.01583	0.01583	0.01583	0.01583
LCht	[ft]	3.33	3.33	3.33	3.33	3.33	3.33
UlossCht	[Btu/hr-ft2-F]	0	0	0	0	0	0
pdCht	[psia]	0.03	0.04	0.03	0.03	0.03	0.03
qlossCht	[Btu/hr]	0	0	0	0	0	0
MCht	[lbm]	0.334	0.33283	0.32382	0.31972	0.31765	0.31769
VCht	[ft^3]	0.00524	0.00524	0.00524	0.00524	0.00524	0.00524

Table D.11 Dry indoor/high outdoor ambient temperature condenser submodel simulation runs

	Corresp. Exp. Data set	80/96 (10-26-98)	80/104 (10-3-98)	80/106 (10-24-98)	80/111 (10-25-98)	80/118 (10-4-98)	80/118 (10-25-98)
degsubcool	[F]	21.4	23.9	24.2	25.5	27.1	27.1
w	[lbm/hr]	313	324	316.6	314.8	323.3	316.4
PwrComp	[W]	2161.3	2507.5	2583.6	2820.6	3171.7	3177.4
Acond	[ft^2]	107.793	107.793	107.793	107.793	107.793	107.793
esupC	[ ]	0.793	0.785	0.791	0.797	0.796	0.802
e2phC	[ ]	0.872	0.874	0.874	0.875	0.876	0.876
esubC	[ ]	0.997	0.997	0.997	0.997	0.996	0.997
fsupC	[ ]	0.211	0.225	0.237	0.248	0.259	0.257
f2phC	[ ]	0.405	0.348	0.33	0.294	0.259	0.253
fsubC	[ ]	0.385	0.426	0.433	0.457	0.482	0.49
h0	[Btu/lbm]	149.4	153	154.5	157.6	161.1	161.9
h1	[Btu/lbm]	149.3	151.7	153.3	156.4	159	160.1
h2i	[Btu/lbm]	120.6	119.9	119.8	119.3	118.6	118.6
h2o	[Btu/lbm]	57.8	62.5	63.5	66.5	71	71.1
h3	[Btu/lbm]	49.1	52.4	53.2	55.3	58.3	58.4
h4	[Btu/lbm]	49.1	52.4	53.2	55.3	58.3	58.4
MtotC	[lbm]	2.668	2.688	2.675	2.666	2.633	2.644
MsupC	[lbm]	0.077	0.094	0.101	0.112	0.129	0.127
M2phC	[lbm]	0.702	0.619	0.591	0.534	0.473	0.463
MsubC	[lbm]	1.37	1.466	1.477	1.521	1.543	1.566
p0	[psia]	421.5	480.3	493.3	532.5	589.2	590.3
p1	[psia]	421.5	480.3	493.3	532.5	589.2	590.3
p2i	[psia]	421.4	480.2	493.2	532.4	589.1	590.2
p2avg	[psia]	421.4	480.2	493.2	532.4	589.1	590.2
p2o	[psia]	421.3	480.2	493.2	532.4	589.1	590.2
p3i	[psia]	421.3	480.1	493.1	532.3	589	590.1
p4	[psia]	421.2	480	493	532.2	588.9	590
qCond	[Btu/hr]	31364	32180	31715	31818	32559	32197
qsupC	[Btu/hr]	9000	10299	10624	11665	13064	13147
q2phC	[Btu/hr]	19639	18616	17823	16618	15386	15025
qsubC	[Btu/hr]	2726	3265	3268	3536	4109	4025
t0	[F]	200.5	219.8	226.4	241.1	258.5	261.1
tlo	[F]	200.3	215.5	222.4	236.8	251.3	255.2
t2i	[F]	117.9	128.2	130.3	136.5	144.8	145
t2avg	[F]	117.9	128.1	130.3	136.5	144.8	145
t2o	[F]	117.9	128.1	130.3	136.5	144.8	145
t3i	[F]	96.5	104.3	106.1	111	117.7	117.9
t4	[F]	96.5	104.3	106.1	111	117.7	117.9
tafanoutC	[F]	108.9	117.2	118.9	124	131.1	131.2
tasupoutC	[F]	112.9	122.1	123.6	129.5	137.8	138.3
ta2phoutC	[F]	115.2	125.1	127.2	133.3	141.4	141.6
tasuboutC	[F]	99.1	107.2	109	114	121	121.1
taoutC	[F]	108.5	116.8	118.5	123.5	130.7	130.7
usupC	[Btu/hr-ft^2-F]	8.9	8.7	8.2	8	8.1	8.1
u2phC	[Btu/hr-ft^2-F]	49.4	49.1	48.9	48.6	48.3	48.2
usubC	[Btu/hr-ft^2-F]	23.6	22.8	22.6	22.1	21.3	21.3
TubeLenC	[ft]	6.28	6.28	6.28	6.28	6.28	6.28
Vcond	[ft^3]	0.059	0.059	0.059	0.059	0.059	0.059
VolextC	[ft^3]	0.9825	0.9825	0.9825	0.9825	0.9825	0.9825
x2o	[ ]	0	0	0	0	0	0
x4	[ ]	0	0	0	0	0	0
Toutdoor	[F]	96.4	104.2	106	110.9	117.6	117.8

RhaiC	[ ]	0.405	0.405	0.405	0.405	0.405	0.405
vdotaCmeas	[cfm]	2600	2600	2600	2600	2600	2600
PwrFanC	[W]	144.8	144.5	144.5	144.3	144.1	144.1
NportsC	[ports/tube]	19	19	19	19	19	19
porgeoC	[]	1	1	1	1	1	1
geodesC	[ ]	62.69	62.69	62.69	62.69	62.69	62.69
NtubesC	[ ]	79	79	79	79	79	79
twebC	[ft]	0.00112	0.00112	0.00112	0.00112	0.00112	0.00112
twallC	[ft]	0.00138	0.00138	0.00138	0.00138	0.00138	0.00138
HfinC	[ft]	0.026	0.026	0.026	0.026	0.026	0.026
Dh_tC	[ft]	0.00219	0.00219	0.00219	0.00219	0.00219	0.00219
Dh_airC	[ft]	0.00639	0.00639	0.00639	0.00639	0.00639	0.00639
AfrontC	[ft^2]	16	16	16	16	16	16
DeqinC	[ft]	0.00282	0.00282	0.00282	0.00282	0.00282	0.00282
HtubeDistC	[ft]	0.0614	0.0614	0.0614	0.0614	0.0614	0.0614
VtubeDistC	[ft]	0.03224	0.03224	0.03224	0.03224	0.03224	0.03224
FinThC	[ft]	0.000417	0.000417	0.000417	0.000417	0.000417	0.000417
dpC	[psia]	0.2	0.2	0.2	0.2	0.2	0.2
ThetaLoC	[deg]	27	27	27	27	27	27
HlouvC	[ft]	0.02167	0.02167	0.02167	0.02167	0.02167	0.02167
HlouvdistC	[ft]	0.004583	0.004583	0.004583	0.004583	0.004583	0.004583
DeffC	[ft]	0.0033	0.0033	0.0033	0.0033	0.0033	0.0033
DeffE	[ft]	0.0033	0.0033	0.0033	0.0033	0.0033	0.0033
VheadCin	[ft^3]	0.00779	0.00779	0.00779	0.00779	0.00779	0.00779
VheadCout	[ft^3]	0.00779	0.00779	0.00779	0.00779	0.00779	0.00779
MheadCin	[lbm]	0.04836	0.05508	0.0561	0.0597	0.06574	0.06531
MheadCout	[lbm]	0.47049	0.45425	0.45069	0.43928	0.42283	0.4224
DheadC	[ft]	0.06242	0.06242	0.06242	0.06242	0.06242	0.06242
AairC	[ft^2]	452.245	452.245	452.245	452.245	452.245	452.245
hairC	[Btu/hr-ft^2-F]	13.79	13.77	13.77	13.76	13.75	13.75
hreftpC	[Btu/hr-ft^2-F]	396.62	377.21	370.68	356.56	339.25	337.15
NlouvC	[ ]	10	10	10	10	10	10
dPairC	[psia]	0.0011255	0.0011203	0.0011192	0.001116	0.0011118	0.0011117
eta_fanC	[ ]	0.18	0.18	0.18	0.18	0.18	0.18
NCht	[ ]	8	8	8	8	8	8
DCht	[ft]	0.01583	0.01583	0.01583	0.01583	0.01583	0.01583
LCht	[ft]	3.33	3.33	3.33	3.33	3.33	3.33
UlossCht	[Btu/hr-ft2-F]	0	0	0	0	0	0
pdCht	[psia]	0.03	0.04	0.03	0.03	0.04	0.03
qlossCht	[Btu/hr]	0	0	0	0	0	0
MCht	[lbm]	0.31649	0.30556	0.30317	0.29549	0.28443	0.28414
VCht	[ft^3]	0.00524	0.00524	0.00524	0.00524	0.00524	0.00524

Table D.12 Wet indoor condenser submodel simulation runs

	Corresp. Exp. Data set	80/70 (10-6-98)	80/75 (10-7-98)	80/82 (10-7-98)	80/95 (10-9-98)	80/105 (10-9-98)	80/118 (10-12-98)
degsubcool	[F]	16.9	16.7	16.7	18.3	21	25.7
w	[lbm/hr]	377.2	381.7	381.7	386	375	368.3
PwrComp	[W]	1449.2	1551.9	1696.5	2062.5	2469.3	3157.6
Acond	[ft^2]	107.793	107.793	107.793	107.793	107.793	107.793
esupC	[ ]	0.755	0.758	0.769	0.781	0.788	0.782
e2phC	[ ]	0.866	0.868	0.87	0.874	0.876	0.878
esubC	[ ]	0.948	0.94	0.94	0.961	0.982	0.988
fsupC	[ ]	0.105	0.111	0.123	0.149	0.187	0.24
f2phC	[ ]	0.682	0.677	0.657	0.576	0.458	0.31
fsubC	[ ]	0.213	0.213	0.22	0.274	0.355	0.449
h0	[Btu/lbm]	136.7	138.1	140.2	144.6	149.7	157.4
h1	[Btu/lbm]	138.7	139.4	141	144.7	149.2	155
h2i	[Btu/lbm]	121.3	121.3	121.2	120.7	120	118.6
h2o	[Btu/lbm]	45.5	47.6	50.3	56.2	61.8	70.7
h3	[Btu/lbm]	39.2	41.3	43.8	48.8	53	58.7
h4	[Btu/lbm]	39.2	41.3	43.8	48.8	53	58.7
MtotC	[lbm]	2.447	2.441	2.449	2.528	2.608	2.611
MsupC	[lbm]	0.027	0.03	0.037	0.054	0.078	0.123
M2phC	[lbm]	1.045	1.056	1.052	0.967	0.8	0.561
MsubC	[lbm]	0.829	0.813	0.825	0.986	1.22	1.437
p0	[psia]	282.6	304.4	333.5	401.3	472.2	585.9
p1	[psia]	282.5	304.3	333.4	401.2	472.1	585.8
p2i	[psia]	282.3	304.1	333.2	401	471.9	585.7
p2avg	[psia]	282.3	304.1	333.2	401	471.9	585.7
p2o	[psia]	282.2	304	333.1	400.9	471.9	585.6
p3i	[psia]	282.1	303.9	333	400.9	471.8	585.5
p4	[psia]	282.1	303.9	333	400.8	471.7	585.5
qCond	[Btu/hr]	37544	37468	37102	37029	36092	35485
qsupC	[Btu/hr]	6582	6933	7577	9244	10949	13395
q2phC	[Btu/hr]	28576	28110	27054	24935	21824	17647
qsubC	[Btu/hr]	2386	2425	2471	2850	3319	4443
t0	[F]	136.3	145	156.8	181.6	207.9	245.8
t1o	[F]	143.4	149.5	159.7	182	206.2	237.8
t2i	[F]	88.3	93.6	100.2	114.1	126.8	144.3
t2avg	[F]	88.3	93.6	100.2	114.1	126.8	144.3
t2o	[F]	88.3	93.6	100.2	114.1	126.8	144.3
t3i	[F]	71.4	76.9	83.5	95.7	105.8	118.6
t4	[F]	71.4	76.9	83.5	95.7	105.8	118.6
tafanoutC	[F]	84.6	90	96.6	109.5	119.9	132.9
tasupoutC	[F]	93.6	99.1	105.6	118.9	128.3	140.7
ta2phoutC	[F]	85.9	91.3	97.9	111.7	124.1	141.1
tasuboutC	[F]	74.6	80	86.6	99	109.1	122.3
taoutC	[F]	84.3	89.7	96.4	109.3	119.6	132.6
usupC	[Btu/hr-ft^2-F]	20.8	20.6	19.4	17.2	13.4	10.2
u2phC	[Btu/hr-ft^2-F]	50.7	50.5	50.3	49.8	49.3	48.5
usubC	[Btu/hr-ft^2-F]	25.7	25.3	24.8	23.7	22.7	21.3
TubeLenC	[ft]	6.28	6.28	6.28	6.28	6.28	6.28
Vcond	[ft^3]	0.059	0.059	0.059	0.059	0.059	0.059
VolextC	[ft^3]	0.9825	0.9825	0.9825	0.9825	0.9825	0.9825
x2o	[ ]	0	0	0	0	0	0
x4	[ ]	0	0	0	0	0	0
Toutdoor	[F]	70.5	75.8	82.4	95	105.4	118.3

RhaiC	[ ]	0.405	0.405	0.405	0.405	0.405	0.405
vdotaCmeas	[cfm]	2600	2600	2600	2600	2600	2600
PwrFanC	[W]	145.6	145.4	145.2	144.8	144.5	144.1
NportsC	[ports/tube]	19	19	19	19	19	19
porgeoC	[]	1	1	1	1	1	1
geodesC	[ ]	62.69	62.69	62.69	62.69	62.69	62.69
NtubesC	[ ]	79	79	79	79	79	79
twebC	[ft]	0.00112	0.00112	0.00112	0.00112	0.00112	0.00112
twallC	[ft]	0.00138	0.00138	0.00138	0.00138	0.00138	0.00138
HfinC	[ft]	0.026	0.026	0.026	0.026	0.026	0.026
Dh_tC	[ft]	0.00219	0.00219	0.00219	0.00219	0.00219	0.00219
Dh_airC	[ft]	0.00639	0.00639	0.00639	0.00639	0.00639	0.00639
AfrontC	[ft^2]	16	16	16	16	16	16
DeqinC	[ft]	0.00282	0.00282	0.00282	0.00282	0.00282	0.00282
HtubeDistC	[ft]	0.0614	0.0614	0.0614	0.0614	0.0614	0.0614
VtubeDistC	[ft]	0.03224	0.03224	0.03224	0.03224	0.03224	0.03224
FinThC	[ft]	0.000417	0.000417	0.000417	0.000417	0.000417	0.000417
dpC	[psia]	0.4	0.4	0.4	0.3	0.3	0.3
ThetaLoC	[deg]	27	27	27	27	27	27
HlouvC	[ft]	0.02167	0.02167	0.02167	0.02167	0.02167	0.02167
HlouvdistC	[ft]	0.004583	0.004583	0.004583	0.004583	0.004583	0.004583
DeffC	[ft]	0.0033	0.0033	0.0033	0.0033	0.0033	0.0033
DeffE	[ft]	0.0033	0.0033	0.0033	0.0033	0.0033	0.0033
VheadCin	[ft^3]	0.00779	0.00779	0.00779	0.00779	0.00779	0.00779
VheadCout	[ft^3]	0.00779	0.00779	0.00779	0.00779	0.00779	0.00779
MheadCin	[lbm]	0.03352	0.0362	0.03958	0.04745	0.05513	0.06735
MheadCout	[lbm]	0.51296	0.50515	0.49539	0.47426	0.45414	0.42231
DheadC	[ft]	0.06242	0.06242	0.06242	0.06242	0.06242	0.06242
AairC	[ft^2]	452.245	452.245	452.245	452.245	452.245	452.245
hairC	[Btu/hr-ft^2-F]	13.84	13.83	13.82	13.79	13.77	13.74
hreftpC	[Btu/hr-ft^2-F]	478.37	467.76	453.03	423.41	392.87	351.43
NlouvC	[ ]	10	10	10	10	10	10
dPairC	[psia]	0.0011433	0.0011395	0.0011349	0.0011264	0.0011196	0.0011113
eta_fanC	[ ]	0.18	0.18	0.18	0.18	0.18	0.18
NCht	[ ]	8	8	8	8	8	8
DCht	[ft]	0.01583	0.01583	0.01583	0.01583	0.01583	0.01583
LCht	[ft]	3.33	3.33	3.33	3.33	3.33	3.33
UlossCht	[Btu/hr-ft2-F]	0	0	0	0	0	0
pdCht	[psia]	0.04	0.05	0.05	0.05	0.05	0.05
qlossCht	[Btu/hr]	0	0	0	0	0	0
MCht	[lbm]	0.34506	0.3398	0.33324	0.31902	0.30549	0.28407
VCht	[ft^3]	0.00524	0.00524	0.00524	0.00524	0.00524	0.00524

Table D.13 Final charge estimation simulation

	Corresp. Exp. Data set	80/82 (10-7-98)
Acond	[ft^2]	109.603
Aevap	[ft^2]	32.539
MtotC	[lbm]	2.349
MtotE	[lbm]	0.385
MsupC	[lbm]	0.052
M2phC	[lbm]	1.422
MsubC	[lbm]	0.337
M2phE	[lbm]	0.314
MsupE	[lbm]	0.004
Maccum	[lbm]	0
Mcaptube	[lbm]	0.02
Mcomp	[lbm]	0.159
MdisLine	[lbm]	0.078
MliqLine	[lbm]	1.181
MsuctLine	[lbm]	0.096
Mrefoil	[lbm]	0.506
TubeLenC	[ft]	6.22
TubeLenE	[ft]	3.65
Tindoor	[F]	80.1
Toutdoor	[F]	82.4
RhaiC	[ ]	0.405
RhaiE	[ ]	0.52
vdotaCmeas	[cfm]	2600
vdotaE	[cfm]	800
Mtotal	[lbm]	5.9096
NportsC	[ports/tube]	19
porgeoC	[]	4
NportsE	[ports/tube]	19
porgeoE	[]	4
geodesC	[ ]	75
geodesE	[ ]	75
NtubesC	[ ]	79
NtubesE	[ ]	40
twebC	[ft]	0.00112
twallC	[ft]	0.00138
HfinC	[ft]	0.026
twebE	[ft]	0.00112
twallE	[ft]	0.00138
HfinE	[ft]	0.026
Lcap	[in]	19
Dcap	[in]	0.128
Dh_tC	[ft]	0.00248
Dh_tE	[ft]	0.00248
Dh_airC	[ft]	0.00638
Dh_airE	[ft]	0.00639
AfrontC	[ft^2]	16
AfrontE	[ft^2]	4.75
DeqinC	[ft]	0.00304
DeqinE	[ft]	0.00304
HtubeDistC	[ft]	0.06185
HtubeDistE	[ft]	0.06185

132

VtubeDistC	[ft]	0.03257
VtubeDistE	[ft]	0.03257
FinThC	[ft]	0.000417
FinThE	[ft]	0.000417
AairE	[ft^2]	135.341
ThetaLoC	[deg]	27
HlouvC	[ft]	0.02167
HlouvdistC	[ft]	0.004583
ThetaLoE	[deg]	27
HlouvE	[ft]	0.02167
HlouvdistE	[ft]	0.004583
DeffC	[ft]	0.00333
DeffE	[ft]	0.00333
VheadCin	[ft^3]	0.00787
VheadCout	[ft^3]	0.00787
VheadEin	[ft^3]	0.00399
VheadEout	[ft^3]	0.00399
MheadCin	[lbm]	0.03946
MheadCout	[lbm]	0.49809
MheadEin	[lbm]	0.05636
MheadEout	[lbm]	0.0105
DheadC	[ft]	0.06242
DheadE	[ft]	0.06242
AairC	[ft^2]	451.204
NlouvC	[ ]	10
NlouvE	[ ]	10
NCht	[ ]	8
DCht	[ft]	0.01583
LCht	[ft]	3.33
MCht	[lbm]	0.33168
VCht	[ft^3]	0.00524
geodes2C	[ft]	0.00381
geodes3C	[ft]	0.00089
geodes2E	[ft]	0.00381
geodes3E	[ft]	0.00089
Vfilter	[ft^3]	0.0127
Mfilter	[lbm]	0.8